**INDIGENOUS NATURAL DYES FOR GRÄTZEL SOLAR CELLS: SEPIA MELANIN**

by

**Agnes Mbonyiryivuze**

submitted in accordance with requirements for
the degree of

**MASTER OF SCIENCE**

In the subject

**PHYSICS**

at the

University of South Africa

Supervisor: Prof. Malik Maaza

Co-supervisors: Prof.S. Mokhotjwa Dhlamini
Dr. Bonex Mwakikunga

November 2014

# DECLARATION

Student number: 54721873

I declare that **'INDIGENOUS NATURAL DYES FOR GRÄTZEL SOLAR CELLS: SEPIA MELANIN'** is my own work and that all sources that I have used or quoted have been indicated and acknowledged by means of complete references.

_____ _____

Signature Date

Mrs. Agnes MBONYIRYIVUZE

# DEDICATIONS

This thesis is dedicated to my husband Alex Ndacyayisenga, my sons Cyuzuzo Confiance and Iranzi Souvenir for your endless love, patience, encouragement and the support you gave me.

# ACKNOWLEDGEMENT

Above all, I would like to thank the Almighty God for the patience and the strength He provided throughout this course.

I would like to extend my gratitude to the Organization for Women in Science for the Developing World (OWSDW), SIDA (Swedish International Development Cooperation Agency) as well as The Academy of Sciences for the developing World (TWAS) for intellectual and material support. Thank you very much for funding me during conducting my research.

I am very thankful to my guide and supervisor, Prof. Malik Maaza (iThemba LABS), for the constant support, suggestions and motivation that I received from him during the period of my MSc work. I have been extremely lucky to have a supervisor who cared so much about my work, and who responded to my questions and queries so promptly. Your guidance is deeply appreciated.

I appreciate the guidance of my co-supervisors: Prof. S.Mokhotjwa Dhlamini (UNISA), and Dr. Bonex Mwakikunga (CSIR), for all your time, patience, guidance, encouragement, outstanding hard work, and for always being there when I needed you.

To my immediate, extended family and friends, for their encouragement and support:

Firstly, to my husband Alex, for all the love, encouragement and the support you gave. My sons Souvenir and Confiance, you are the reason I worked so hard. Thank you for the understanding when I was unable to spend time with you. I love you!

To my mother Joséphine, my mother in law Pudenciene, my brothers especially Dr. Jéreon Claude and his wife Marie Rose, brothers in law, and sisters for their belief in me and always inspiring me to greater things!

My gratitude also goes to Dr. Balla N'Gom, Dr. Lebogang Kotsedi and Dr. Zebib Nuru, for their advice and support. I would like to thank the MRD staff members for all the help, they rendered. I also thank Dr. B. Sone, Dr. Aline Simo and Dr. Franscious Riccardo Cummings (UWC) for the help received from them. I want to thank, Miss Juliet Sackey, Mr Isaiah Omollo, and Mr Sidiki Zongo. I am grateful for their support, advice and trust.

I would like to thank once again all the people who helped me in one way or another for the successful completion of my research work.

# LIST OF ABBREVIATIONS

LUMO: lowest unoccupied molecular orbital

IPCE: incident photon to current efficiency

CB: conducting band

DSSC: dye-sensitized solar cell

HOMO: highest occupied molecular orbit

CE: counter electrode

$TiO_2$: titanium dioxide

TCO: transparent conducting oxide

FTO: fluorine-doped tin oxide

ITO: indium tin oxide

WE: working electrode

UV: ultra-violet

IR: infrared

SEM: scanning electron microscopy

TEM: transmission electron microscopy

EDS: energy dispersive x-ray spectroscopy

XRD: x-ray diffraction

FTIR: Fourier transform infrared spectroscopy

HRTEM: high resolution transmission electron microscopy

DHI: 5, 6-dihydroxyindole

DHICA: 5, 6-dihydroxyindole-2-carboxylic acid

PDCA: pyrrole-2, 3-dicarboxylic acid

PTCA: pyrrole-2, 3, 5-tricarboxylic acid

# ABSTRACT

Dye-sensitized Solar Cells (DSSC), also known as Grätzel cells, have been identified as a cost-effective, easy-to-manufacture alternative to conventional solar cells. While mimicking natural photosynthesis, they are currently the most efficient third-generation solar technology available. Among others, their cost is dominated by the synthetic dye which consists of efficient Ruthenium based complexes due to their high and wide spectral absorbance. However, the severe toxicity, sophisticated preparation techniques as well as the elevated total cost of the sensitizing dye is of concern.

Consequently, the current global trend in the field focuses on the exploitation of alternative organic dyes such as natural dyes which have been studied intensively. The main attractive features of natural dyes are their availability, environmental friendly, less toxicity, less polluting and low in cost. This contribution reports on the possibility of using sepia melanin dye for such DSSC application in replacement of standard costly ruthenium dyes.

The sepia melanin polymer has interesting properties such as a considerable spectral absorbance width due to the high degree of conjugation of the molecule. This polymer is capable of absorbing light quantum, both at low and high energies ranging from the infrared to the UV region.

The comprehensive literature survey on Grätzel solar cells, its operating principle, as well as its sensitization by natural dyes focusing on sepia melanin has been provided in this master's dissertation. The obtained results in investigating the morphology, chemical composition, crystalline structure as well as optical properties of sepia melanin samples using Scanning Electron Microscopy (SEM), Transmission Electron Microscopy (TEM), Energy x-ray diffraction, X-ray Diffraction (XRD), Fourier Transform Infrared spectroscopy (FTIR), Raman spectroscopy, UV-VIS absorption spectroscopy as well as Photoluminescence (PL) for Grätzel solar cell application have been reported.

These results represent an important step forward in defining the structure of melanin. The results clearly show that sepia melanin can be used as natural dye to DSSC sensitization. It is promising for the realization of high cell performance, low-cost production, and non-toxicity. It should be emphasized here that natural dyes from food are better for human health than synthetic dyes.

# KEY WORDS

Dye sensitized solar cell (DSSC)

Melanin

Eumelanin

Sepia melanin

Sepia officinalis

Dye sensitizer

Natural dye

Solar energy

Titanium dioxide

# Table of contents

# TABLE OF FIGURES

# LIST OF TABLES

# CHAPTER ONE: INTRODUCTION

## 1.1. Background of the research

Energy is of greatest importance to just about every aspect of human life. From the beginning of the ninetieth century, the energy demand has gone up rapidly as a result of the increasing global population. For this reason, the fossil fuels being key energy sources of today are being reduced considerably. The inevitable permanent decline in the global oil production rate is expected to start within the next 10-20 years according to recent predictions (Swami, 2012; Kaushik M. and Kaushik, B., 2013).

The use of fossil fuels also has negative effects on the environment. An important role in climate variations is played by the increased concentration of greenhouse gases due to the combustion of fossil fuels. The combustion of fossil fuels in the past has already had harmful effects on the delicate balance of nature on our planet (Hagberg, 2009; Qin, 2010). Today, about 20 x $10^{12}$ Kg of carbon dioxide are released into the atmosphere every year, mainly by fossil fuels. Today's plants are unable to absorb this huge amount of extra $CO_2$. This results in the $CO_2$ concentration in the atmosphere adding considerably to the greenhouse effect. This will increase the global mean surface temperature (Halme, 2002; Swami, 2012; Hemmatzadeh and Mohammadi, 2013).

The consequences of this temperature change has already increased the frequency and severity of natural disasters and likely to have more devastating effects for humans and other life forms in all parts of Earth within the next decades. The next decades, there is worldwide power consumption which is expected to go up (Rodríguez, 2011; Grätzel, 2001a; Grätzel, 2001b). This increasing energy demand in the near future forces us to seek environmentally clean alternative energy resources (Powell, 2004).

Solar energy is expected to be a good candidate for a future renewable energy source. There is intense interest by physicists and engineers in the field of solar cells in order to produce the electricity directly from solar radiation. There is an urgency need of solar cells for:

- Renewable and sustainable power means of reducing global warming;
- The cost effective of the power supplies for the people far away from the main electricity grid; e.g. cattle stations and some home sites not in grid connected areas;

- Silent and non-polluting electricity: e.g. tourist sites, caravans and campers;
- Avoiding transmission losses and cost as the electricity can be produced near the end user;
- Low maintenance and long lasting sources of electricity suitable for places far away from both the main electricity grid and from people; e.g. satellites, remote site water pumping, outback telecommunications stations;
- Flexible and convenient and source of small amount of power e.g. calculator, watches and cameras.

There are many advantages that solar cell systems present over other energy techniques. Those advantages include their need for very little maintenance and operation without production of noise and green gas emission. However, the high cost and the low efficiency of solar cells since their considerable development in the last three decades is still a big challenge for the implementation of the solar cell technology (El-Agez et al., 2012).

Photovoltaic cells are one of the devices being used to capture solar energy and convert it into electrical energy. The majority of these photovoltaic systems are based on p-n junction of semiconductor and silicon based solar cells, and they are the most effective under this technology (Qin, 2010; Karmakar and Ruparelia, 2011). However, the performance of these silicon solar cells are greatly affected by their crystallinity which result into a high cost due to the energy intensive manufacturing process associated with purifying and processing the material (Subianto, 2006). Furthermore, silicon-based photovoltaic cells are very expensive due to the input it requires in terms of money and labor to extract silicon from sand and then purify silicon before growing the crystals (Srinivasan, 2012).

The dye-sensitized solar cell (DSSC) also known as Grätzel solar cell from the name of its inventor Prof. Michael Grätzel (O'Regan and Grätzel, 1991) provides a technically and economically credible alternative concept to the present day p–n junction photovoltaic devices. While for the conventional systems, the semiconductor serves both the task of light absorption and charge carrier transport, the DSSC separate the two functions. The sensitizer anchored to the wide band semiconductor surface absorbs light (Grätzel, 2003). DSSC are relatively new class of low-cost solar cells that belong to the group of thin film solar cells. They are very promising compared to silicon based solar cells because they are made from low-cost materials and do not need elaborate apparatus for their manufacture (Alfa et al., 2012). DSSC have received an increasing interest due to the simple fabrication process and relatively high conversion efficiency (Taya et al., 2013). The

developed state solid version of DSSC fabricated by a new two-process which raised their efficiency up to a record of 15% without sacrificing stability was recently published by Grätzel and co-workers at the Swiss Federal Institute of Technology (EPFL) (Burschka et al., 2013). The authors believe that this will open new era of DSSC development, featuring stability and efficiencies that equal or even surpass today's best thin-film photovoltaic devices.

DSSC contains several components: a transparent conducting oxide (TCO), a mesoporous semiconductor film, a dye sensitizer, an electrolyte or mediator solution with a redox couple as well as counter electrode (O'Regan and Grätzel, 1991; Srinivasan, 2012). To improve the overall efficiency of the DSSC, the optimization of each of the components of them is imperative. During the last decades, the investigations of all these components and a great number of researches have been done. An interesting progress has been made since the first report of dye-sensitized solar cell in 1991 (O'Regan and Grätzel, 1991) through the development of photoanode materials, sensitizers, electrolytes and counter electrode. However, there are still more to be done in this field.

The conversion of visible light power into electricity for DSSC is based on the sensitization of wide band gap semiconductors (O'Regan and Grätzel, 1991; Grätzel, 2003; Wongcharee et al., 2006). The performance of the cell mainly depends on a dye used as sensitizer. The absorption spectrum of the dye and the anchorage of the dye to the surface of $TiO_2$ are important parameters determining the efficiency of the cell. The power conversion efficiency; and the stability of the DSSC are mainly influenced by the sensitizer (Wongcharee, et al., 2006; Kuang et al., 2011).

Since the role of the absorption of visible light and the conversion of photon energy into electricity is played by the dye, much attention should be paid in the analysis of effective sensitizer (Andrade, 2010). Due to their intense charge transfer absorption in the whole visible range, transition metal coordination compounds (ruthenium polypyridyl complexes) are generally used as the effective sensitizers (Smestad and Grätzel, 1998; Grätzel, 2003). Even if ruthenium polypyridyl complexes have been the best so far, their synthesis process is complicated and costly. In addition, they are environment pollutant, limited in amount and high in cost. Therefore, natural dyes promises to be the best alternative as they can be used for the same purpose with acceptable efficiency (Sekar and Ghelot, 2010; Karmakar and Ruparelia, 2011; Alhamed et al., 2012).

Due to their cost, efficiency, availability, non-toxicity, complete biodegradation, natural dyes is a popular subject of research. The natural dyes found in flowers, vegetables, leaves and fruits that can be extracted by simple procedures have been extensively investigated as DSSC sensitizer (Hernandez-Martinez et al., 2011; Alhamed et al., 2012). Alhamed et al. reported homemade DSSC prepared using natural dyes extracted from raspberries, shami-berries, grapes, hibiscus, and chlorophyll (Alhamed et al., 2012). Lai et al. applied rhoeo spathacea in DSSC as a dye sensitizer (Lai et al., 2008). There are many examples of natural dyes that have been used as DSSC dye sensitizers and some of them are mentioned below.

The natural dye extracted from pomegranate and punica granatum has been used as DSSC sensitizers (Bahadur et al., 2012). The DSSC has been prepared using a combination of natural dyes (raspberries, hibiscus and chlorophyll) as photo-sensitizer (Alhamed et al., 2012). The DSSC sensitization has been done by the dye from extracted bracts of bougainvillea glabra and spectabilis betalain pigments (Hernandez-Martinez et al., 2011). Zhou et al. reported DSSC fabricated using twenty natural dyes, extracted from natural materials such as flowers, leaves, fruits, traditional chinese medicines, and beverages (Zhou et al., 2011). DSSC using flame of the forest (*butea monosperma*) was fabricated (Alfa et al., 2012). The natural dyes extracted from black berry, black grapes, red spinach leaves; malabar spinach buds and aurum leaves were used as DSSC sensitizers (Khan et al., 2012). Hemmatzadeh and Mohammadi fabricated a DSSC using a natural dye extracted from pastinaca sativa and beta vulgaris (Hemmatzadeh and Mohammadi, 2013).

There are many other natural dye sensitizers used, among them are: pomegranate leaves and mulberry fruit (Chang and Lo, 2010; Chang et al., 2011); red kola nut (*cola nitida*) (Aduloju, 2012); hibiscus (Shelke et al., 2013); grapes (Hemamali and Kumara, 2013); lawsonia intermits leaves, sumac/rhus fruits, and curcuma longa roots (Al-Bat'hi et al., 2013); the curcumin (Win et al., 2012); leaves of anethum graveolens, parsley, arugula, spinach oleracea, and green algae (Taya et al., 2013); walnuts, rhubarb, and pomegranate (El-Agez et al., 2012); red cabbage (Li et al., 2013); wormwood and purple cabbage (Chang et al., 2013), and natural dye extracted from rhododendron species flowers (Kim et al., 2013) .

Currently, the utilization of natural dyes as novel technological materials is encouraged compared to the use of synthetic dyes, which are not environment friendly, very expensive

and their preparation requires sophisticated technique (Smestad and Grätzel, 1998; Alhamed et al., 2012). In general, plants have been identified as main sources of natural dyes that have been used intensively for DSSC.

## 1.2. Problem statement

Currently, there are many investigations on natural dyes for novel application in addition to their foods, medical and textile application to be used as cost-effective, non-toxic and environmental friendliness sensitizers for DSSC (Zongo, 2012). Because of their cost effectiveness, environmental friendliness, and relative abundance, natural dye photosensitizer are used as an alternative to synthetic dyes (Alhamed et al., 2012). Even if dyes from plants have been used intensively as DSSC dye sensitizers, there are some challenges in their extraction such as the conservation; short life span; less stability as they degrade quickly, and their availability and possibly high variability because some appear according to the seasons (Zongo, 2012). Despite the presence of carboxylic acid group in the structure of dye from plant; they do not have the broad absorption band because most of them absorb more in visible range only. To maximize the absorption of more photons from the sun light for DSSC; it is better to have a black dye sensitizer having extremely high broadband absorption. It should absorb not only in visible range but also in ultraviolet and near-infrared regions (Walter et al., 2010).

This challenge can be handled by using natural dyes from other sources such as fauna from which sepia melanin was obtained. Melanins are well-known natural pigments used for the photoprotective role as a skin protector because of their strong UV absorbance and antioxidant properties (Kim et al., 2011). Melanin possesses a broad band absorbance in UV and visible range up to infrared. It also possesses the COOH and OH groups which would be free to bind to the surface of $TiO_2$ (Subianto, 2006; Magarelli, 2011). Moreover, melanin polymer has interesting properties such as a considerable spectral absorbance width due to the high degree of conjugation of the molecule (Kim et al., 2012). All these features make sepia melanin to be attractive for Grätzel cell application.

The efficiency of DSSC fabricated using natural dye can be further improved by the anchoring groups, such as COOH to be adsorbed onto the $TiO_2$ surface with a large electronic coupling. It was reported that there is possibility for a purified extract of the squid ink pigment which has melanin as the major component, to cause strong interactions with the hydroxyl groups of a $TiO_2$ (Lee et al., 2013). Therefore melanin can be an attractive

alternative to Ruthenium polypyridyl complexes containing a heavy metal, which is undesirable from environmental point of view and for which the synthesis process is complicated and costly for DSSC sensitization (O'Regan and Grätzel, 1991; Alhamed, 2012).

## 1.3. Aims and objectives

The aim of this research work is to make a literature survey on DSSC and its sensitization using indigenous natural dyes. More specifically, the focus will be on sepia melanin; the selected natural dyes extracted from fauna (*Sepia officinalis* cuttlefish).

The main objectives of the study are:

- To make comprehensive literature survey on Grätzel solar cells, its operating principle, as well as its sensitization by natural dyes focusing on sepia melanin.
- To investigate the morphology, chemical composition, crystalline structure as well as optical properties of sepia melanin samples using Scanning Electron Microscopy (SEM), Energy X-ray Diffraction (EDS), Transmission Electron Microscopy (TEM), X-ray Diffraction (XRD), Fourier Transform Infrared spectroscopy (FTIR), Raman spectroscopy, UV-VIS absorption spectroscopy as well as Photoluminescence (PL) for Grätzel solar cell application.

## 1.4. Thesis layout

**The introduction** (*chapter one*) provides a brief background on the need of solar energy in general. It introduces photovoltaic cells in which DSSC have received an increasing interest due to the simple fabrication process and relatively high conversion efficiency. Some literature surveys on sensitization of DSSC by natural dyes from flora have been given. The problem statement for this project; aims and objectives have also been provided in this chapter.

**Dye sensitized solar cells** (*chapter two*) highlights the history of the DSSC, the working principle of the cell, the materials and the criteria for the best DSSC material, the concerns around the low performance of these cells and strategies that can be employed to improve the efficiency of the DSSC. The last sub-chapter is about DSSC sensitization where the focus mainly is on natural dyes.

**Sepia melanin** (*chapter three*) highlights the meaning of melanin, the interest in sepia melanin, its general characteristics, its structure according to the literature review, functions and properties and why we are interested to use it as a broad band sensitizer for Grätzel solar cells.

**Materials and characterization techniques** (*chapter four*) is about materials used and characterization techniques. It provides brief description of the characterization techniques that were used to characterize sepia melanin, their theories as well as their respective sample preparations.

**Experimental results and discussions** (*chapter five*) covers the results obtained from the characterization of sepia melanin. It provides in particular the morphology of the sepia melanin, its chemical composition, its crystallinity as well as optical properties.

**General conclusion and future work suggestions** (*chapter six*) is the final chapter. It presents the main conclusions as well as the future work.

## 1.5. Conclusion

This chapter covered the background of the research project; the statement of the problem; the objectives of the study as well as the layout of the dissertation. In chapter two, the DSSC is discussed. The literature review on DSSC is done; the components as well as the operation of DSSC are also discussed. The sensitization of DSSC as well as types of DSSC sensitizers is discussed. The focus is on the natural dye including sepia melanin natural dye extracted from *Sepia officinalis* as a candidate for DSSC applications.

## 1.6. References


Aduloju, K.A. (2012) 'Safety assessment of cola nitida extract as sensitizer in dye sensitized solar cell', *Archives of Applied Science Research*, vol. 4(1), pp. 32-38.

Al-Bat'hi, S.A.M., Alaei, I. and Sopyan, I. (2013) 'Natural photosensitizers for dye sensitized solar cells', *International Journal of Renewable Energy Research*, vol. 3(1).

Alfa, B., Tersoo Tsepav, M., Njinga, R.L. and Abdulrauf, I. (2012) 'Fabrication and characterisation of titanium dioxide based dye', *Applied Physics Research*, vol. 4 (1).

Alhamed, M., Issa, A.S. and Doubal, A.W. (2012) 'Studying of natural dyes properties as photo- sensitizer for dye sensitizer for dye sensitized solar cells (DSSC)', *Journal of electron Devices*, vol. 16, pp. 1370-1383.

Andrade, L.M.M. (2010) *Study and characterization of Grätzel solar cells, Doctoral Thesis*, University of Porto.

Bahadur, K.I., Jyoti, N.J., Kumar, M.P. and Suman, C. (2012) 'Dye-sensitized solar cell using extract of punica Granatum L.pomegranate (bedana) as a natural sensitizer', *Research Journal of Chemical Sciences*, vol. 2(12), pp. 81-83.

Burschka, J., Pellet, N., Moon, S.-J., Humphry-Baker, R., Gao, P., Nazzeeruddin, M.K. and Grätzel, M. (2013) 'Sequential deposition as route to high performance perovskite-sensitized solar cells.', *Nature*.

Chang, H., Cho, K.-C., Chen, C.T.-L. and Jiang, L.-J. (2011) 'Preparation and characterization of anthocyanin dye and counter electrode thin film with carbon nanotubes for dye-sensitized solar cells', *Materials Transactions*, vol. 52(10), pp. 1977-1982.

Chang, H., Kao, M.-J., Tien-Li, Chen, Chen, .C.-H., Cho, K.-C. and Lai, X.-R. (2013) 'Characterization of natural dye extracted from wormwood and purple cabbage for dye-sensitized solar cells', *International Journal of Photoenergy*.

Chang, H. and Lo, Y.-J. (2010) 'Pomegranate leaves and mulberry fruit as natural sensitizersfor dye-sensitized solar cells', *Solar Energy*, vol. 84, pp. 1833-1837.

El-Agez, T.M., El Tayyan, A.A., Al-Kahlout, A., Taya, S.A. and Abdel-Latif, M.S. (2012) 'Dye-sensitized solar cells based on ZnO films and natural dyes', *International Journal of Materials and Chemistry*, vol. 2(3), pp. 105-110.

Grätzel, M. (2001a) 'Photoelectrochemical cells', *Nature*, vol. 414, pp. 338-344.

Grätzel, M. (2001b) 'Molecular photovoltaics that mimic photosynthesis', *Pure and Applied Chemistry*, vol. 73(3), p. 459–467.

Grätzel, M. (2003) 'Review dye-sensitized solar cells ', *Journal of Photochemistry and Photobiology*, vol. Photochemistry Rev. 4, p. 145.

Hagberg, D. (2009) *Synthesis of organic chromophores for dye sensitized solar cells, doctaral thesis*, Sweden: KTH Chemical Science and Engeneering Stockholm.

Halme, J. (2002) *Dye-Sensitized nanostructured and organic Photovoltaic Cells: Technical review and preliminary test, Master's thesis*, Helsinki University of Technology.

Hemamali, G.G.G.M.N. and Kumara, G.R.A. (2013) 'Dye-sensitized solid state solar with natural pigment extracted from grappes', *International Journal of Scientific and Research Publications*, vol. 3.

Hemmatzadeh, R. and Mohammadi, A. (2013) 'Improving optical absorptivity of natural dyes for fabrication of efficient dye-sensitized solar cells', *Journal of Theoretical and Applied Physics*, vol. 7, p. 57.

Hernandez-Martinez, A.R., Estevez, M., Vargas, S., Quintanilla, F. and Rodriguez, R. (2011) 'New dye-sensitized solar sells obtained from extracted bracts of bougainvillea glabra and spectabilis betalain pigments by different purification processes', *International Journal of Molecular Sciences*, vol. 12, pp. 5565-5576.

Karmakar, A.S. and Ruparelia, J.P. (2011) 'A critical review on dye sensitized solar cells', Internation Conference on Current Trends in Technology, Nuicone, 382-481.

Kaushik, M. and Kaushik, B. (2013) 'Organic solar cells: Design, synthesis and characterization', *International Journal of Engineering Sciences*, vol. 2(7), pp. 310-319.

Khan, M.A., Khan, S.M.M., Mohammed, M.A., Sultana, S., Islam, J.M.M. and Uddin, J. (2012) 'Sensitization of nanocrystalline titanium dioxide solar cells using natural dyes: Influence of acids medium on coating formulation', *American Academic & Scholarly Research Journal*, vol. 4 (5).

Kim, H.-J., Bin, Y.-T., Karthick, S.N., Hemalatha, K.V., Raj, C.J., Venkatesan, S., Park, S. and Vijayakumar, G. (2013) 'Natural dye extracted from rhododendron species flowers as a photosensitizer in dye sensitized solar cell', *International Journal of Electrochemical science*, vol. 8 , pp. 6734 - 6743.

Kim, D.J., Ju, K.-Y. and Lee, J.-K. (2012) 'The synthetic melanin nanoparticles having n Excellent Binding Capacity of Heavy Metal Ions', *Bull. Korean Chem. Soc.*, vol. 33(11), p. 3788.

Kim, I.G., Nam, H.J., Ahn, H.J., Jung and Duk-Young (2011) 'Electrochemical growth of synthetic melanin thin films by constant potential methods', *Electrochimica Acta*, vol. 56, pp. 2954-2958.

Kuang, D., Comte, P., Zakeeruddin, S.M., Hagberg, D.P., Karlsson, K.M., Sun, L., Nazeeruddin, M.K. and Gratzel, M. (2011) 'Stable dye-sensitized solar cells based on organic chromophores and ionic liquid electrolyte', *Solar Energy*, vol. 85, pp. 1189-1194.

Lai, W.H., Sub, Y.H., Teoh, L.G. and Hona, M.H. (2008) 'Commercial and natural dyes as photosensitizers for a water-based dye-sensitized solar cell loaded with gold nanoparticles', *Journal of Photochemistry and Photobiology A: Chemistry*, vol. 195, p. 307–313.

Lee, J.-W., Cho, H.-B., Nakayama, T., Sekino, T., Takana, S.-I., Minato, K., Ueno, T., Suzuki, T., Suematsu, H., Tokoi, Y. and Niihara, K. (2013) 'Dye-sensitized solar cells using purified squid ink nanoparticles coated on TiO2 nanotubes/nanoparticles', *Journal of ceramic Society of Japan*, vol. 121(1), pp. 123-127.

Li, Y., Ku, S.-H., Chen, S.-M., Ali, M.A. and AlHemaid, F.M.A. (2013) 'Photoelectrochemistry for red cabbage extract as natural dye to develop a dye-sensitized solar cells', *International Journal of electrochemical science*, vol. 8, pp. 1237-1245.

Magarelli, M. (2011) *Purification, Characterization and Photodegradation studies of modified sepia melanin (Sepia officinalis). Determination of Eumelanin content in fibers from Alpaca (Vicugna pacos), Doctoral Thesis.*, University of Camerino.

O'Regan, B. and Grätzel, M. (1991) 'A low-cost, high efficiency solar cell based on dye-sensitized colloidal TiO2 films', *Nature*, vol. 353, p. 737.

Powell, C.L. (2004) 'Economic perspectives', *An electronic Journal of the U.S. Departement of State*, vol. 9 (2).

Qin, P. (2010) *The study of organic dye for p-type dye sensitized solar cells ,Doctoral thesis*, Royal Institute of Technology.

Rodríguez, E.G. (2011) *Photoelectrochemical charactrrization of dye-sensitized solar cells based on nanostructured zinc oxide substrate*, Sevilla: University Pablo de Olavide.

Sekar, N. and Ghelot, V. (2010) 'Metal complex dyes for dye-sensitized solar cells: recent developments', *General Article, Resonance*.

Shelke, R.S., Thombre, S.B. and Patrikar, S.R. (2013) 'Comparative performance of dye-sensitized solar cells using two electrolytes', *International Journal for Research in Science & Advanced Technologies*, vol. 3, no. 2, pp. 131-136.

Smestad, P.G. and Grätzel, M. (1998) 'Demonstrating electron transfer and nanotechnology: A natural dye sensitized nanocrystalline energy converter', *Journal of Chemical Education*, vol. 75, p. 6.

Srinivasan, A. (2012) *Deposition of indium tin oxide for opto-electronics, master's thesis*, University of Frolida.

Subianto, S. (2006) *Electrochemical Synthesis of -Like Polyindolequinone, PhD thesis*, The Queensland University of Technology.

Swami, R. (2012) 'Solar cells', *International Journal of Scientific and research Publication*, vol. 2, no. 7.

Taya, S.A., El-Agez, T.M., El-Gramri, H.S. and Abdel-Latif, M.S. (2013) 'Dye-sensitized solar cells using fresh and dried natural dyes', *International Journal of Material Sciences and Applications*, vol. 2(2), pp. 37-42.

Walter, M.G., Rudineb, A.B. and Wamser, C.C. (2010) 'Porphyrins and phthalocyanines in solar photovoltaic cells', *Journal of Porphyrins and Phthalocyanines*, vol. 14, p. 759–792.

Win, T.T., Maung, Y.M. and Soe, K.K.K. (2012) 'Characterization of nano-sized ZnO electrodes with curcumin-curcumin derived natural dye extract for DSSC application', *American Journal of Materials Science and Technology*, vol. 1, pp. 28-33.

Wongcharee, K., Meeyoo, V. and Chavadej, S. (2006) 'Dye-sensitized solar cell using natural dyes extracted from rosella and blue pea flowers', *Elsevier*.

Zhou, H., Wu, L., Gao, Y. and Ma, T. (2011) 'Dye-sensitized solar cells using 20 natural dyes as sensitizers', *Journal of Photochemistry and Photobiology A:Chemistry*, vol. 219, pp. 188-194.

Zongo, S. (2012) *Nonlinear Optical properties of natural dyes based on optical resonance,master's thesis*, Cape Town: University of Western Cape.

# CHAPTER TWO: DYE-SENSITIZED SOLAR CELLS

## 2.1. Introduction

A dye-sensitized solar cell (DSSC) is a device for the conversion of visible light power into electricity, based on the sensitization of wide band gap semiconductors (Alhamed et al., 2012). DSSC contains several components: a conducting glass substrate, a mesoporous semiconductor film, a dye sensitizer, an electrolyte or mediator solution with a redox couple as well as counter electrode (Grätzel, 2003; Karlsson, 2012; Srinivasan, 2012; El-Agez et al., 2012) ions. In DSSC, the dye as a sensitizer plays a key role in absorbing sunlight and transforming solar energy into electric energy. Numerous synthetic and organic dyes have been utilized as sensitizers (Grätzel, 2003; Chiba et al., 2006; Sekar & Ghelot, 2010; Karmakar & Ruparelia, 2011).

There are so many different materials used in the literature review for DSSC components. But, since its invention in 1991 over many years ago, the components of the state-of-the art dye-sensitized solar cell did not change a lot relatively (O'Regan & Grätzel, 1991). The development has concentrated on the one hand to the change of the properties of the original components, such as the morphology and the surface properties of the $TiO_2$ electrode (Chiba et al., 2006; Lee et al., 2013), the chemical composition of the electrolyte (Shelke et al., 2013) as well as the dye sensitizer (Wongcharee et al., 2006; Hernandez-Martinez et al., 2011; Aduloju, 2012; Khan et al., 2012). On the other hand, new alternative materials and methods such as solid electrolyte and plastic substrate have been explored (Halme, 2002).

This chapter covers the introduction on DSSC; the historical background, and its operation principle; brief introduction to the materials used for the standard DSSC technology based on a liquid electrolyte and glass substrates as well as its sensitization are also discussed.

## 2.2. Historical overview of Dye-Sensitized Solar Cells (DSSC)

The historical background of DSSC began in 1839 when the French Physicist Edmond Becquel discovered the photovoltaic effect on which the DSSC operating principle is based (Hagfeldt & Grätzel, 2000; Nusbaumer, 2004). He was doing experiment on illuminated electrode metal in an electrolyte. While he was immersing the two platinum electrodes in

an illuminated solution containing a metal halide salt, he realized that there was an electric current between these two electrodes (Tung, 2010; Andrade, 2010; Wenger, 2010). In 1873, the photovoltaic effect in selenium was observed by Willoughby Smith (Green, 1982).

In 1883, the first solar cell made of a selenium/gold junction with an efficiency of about 1 % was reported by Charles Fritts (Andrade, 2010). This American inventor, Charles Fritts described this cell in detail for the first time six years later (Rosengrant, 2010). The theory behind the photovoltaic phenomenon was first described by Albert Einstein in 1904, who won the Nobel Prize in 1921 (Andrade, 2010; Rosengrant, 2010). The first “Silicon” solar cell was invented by Russell Ohl in 1940 and reported in 1941 (Green, 1982). Fourteen years later, it was discovered that the improvement of the efficiency of solar cells can be achieved by doping silicon with certain impurities up to 6% by Gerald Pearson, Calvin Fuller, and Daryl Chapin of Bell Laboratory. This discovery led to a practical application in space craft as early as in 1958 (Green, 1982; Tung, 2010).

Actually, there is an interesting convergence of photography and photoelectrochemistry because both phenomena are based on a photoinduced charge separation in a liquid-solid interface. Before being aware of such similarities and following the experiment developed by Becquerel, Vogel discovered that silver halide emulsions sensitized by a dye resulted in an extended photosensitivity to longer wavelengths in 1873 (Hagfeldt & Grätzel, 2000). Four years later, J. Moser was the first to report the dye-sensitized photovoltaic effect (Andrade, 2010; Honda, 2011). Gerischer and Tsubomura together with their co-workers in 1960, discovered dye sensitization of wide band gap semiconductors where they used ZnO as the semiconductor and different dyes such as rose bengal as photosensitizer (Karlsson, 2011).

From that time, several attempts were made to use dye-sensitized photoelectrochemical cells to convert sunlight into electricity. However, the efficiency of those devices was very low, well below 1 %, mainly due to the poor light harvesting and instability of the dyes employed. O’Regan and Grätzel described for the first time a three dimensional (bulk) heterojunction applied to the fabrication of DSSC. This new device was based on the use of semiconductor films consisting of nanometer-sized $TiO_2$ particles, together with newly developed charge-transfer dyes. These authors report an astonishing efficiency of more than 7 % (O’Regan & Grätzel, 1991). The DSSC and its inventor, Prof. Michael Grätzel, have received prestigious awards, including the Balzan Prize in 2009 and the 2010 Millennium Technology Prize, the largest technology prize in the world (Yum et al., 2011).

Several companies have accepted the challenge to bring DSSC technology “from the lab to the fab" (Dyesol, G24i, Sony, Sharp, and Toyota, among others) (Wenger, 2010). The facile assembly functional cells sensitized with berry juice can be assembled by children within fifteen minutes, the large choice of colors, the option of transparency and mechanical flexibility, and the parallels to natural photosynthesis all contribute to the widespread fascination for DSSC (Smestad & Grätzel, 1998; Grätzel, 2003; Wenger, 2010).

In 2013, the drastic improvement in the performance of DSSC has been made by Professor Michael Grätzel and co-workers at the Swiss Federal Institute of Technology (EPFL). They have developed a state solid version of DSSC called perovskite-sensitized solar cells that is fabricated by a sequential deposition leading to the high performance of the DSSC. This deposition raised their efficiency up to a record 15% without sacrificing stability (Burschka et al., 2013). The authors believe that this will open a new era of DSSC development, featuring stability and efficiencies that equal or even surpass today’s best thin-film photovoltaic devices.

## 2.3. Materials of dye-sensitized solar cells

The standard DSSC technology based on a liquid electrolyte and glass substrate are made of a transparent conducting glass electrode coated with porous nanocrystalline titanium dioxide (nc-$TiO_2$); dye molecules attached to the surface of the nc-$TiO_2$; an electrolyte containing a reduction-oxidation couple such as iodide and triiodide ions $(I^-/I_3^-)$ and a counter electrode coated by a catalyst (O'Regan & Grätzel, 1991; Karlsson, 2012). To improve the overall efficiency of the DSSC, the optimization of each component is imperative. During the last decades, investigations on all these components have been done, and a great number of research efforts have been carried out. However, there are still a lot unexplored territories in this field. The schematic diagram of the main components of a DSSC is shown on **figure 2.1**.

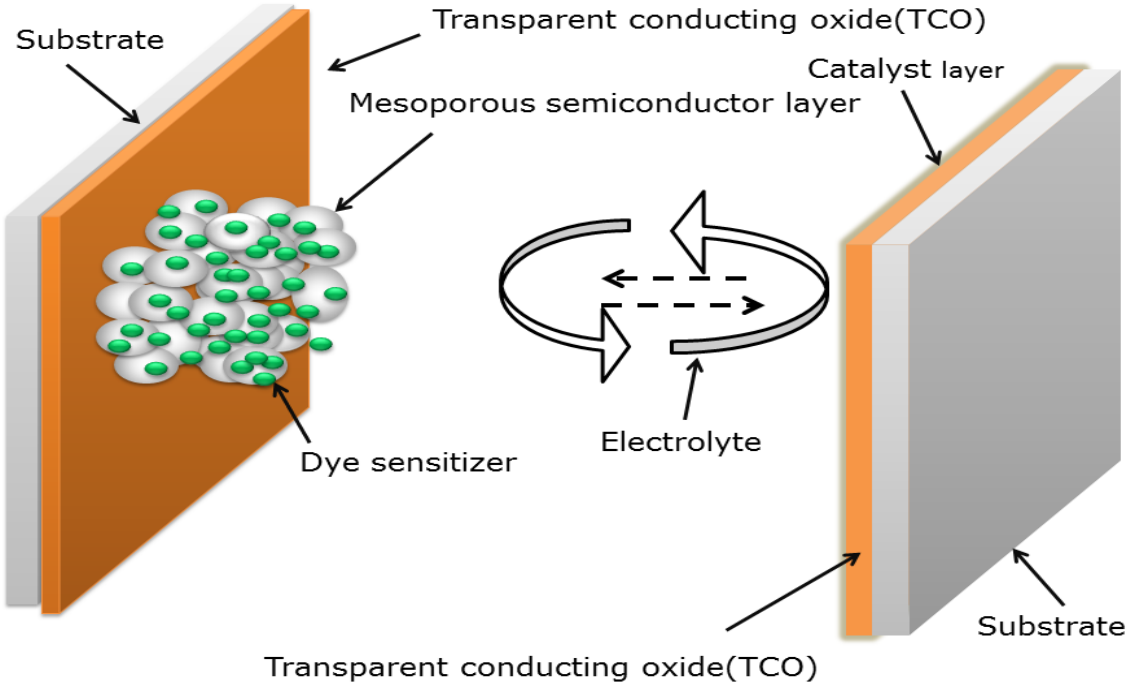


***Figure 2.1**: A schematic diagram of a dye-sensitized solar cell.*

### 2.3.1. Substrate and semiconductor

The electrodes of the standard dye-sensitized solar cell (DSSC) are prepared onto transparent conducting oxide (TCO) coated glass substrates, between which the cell is assembled. The conducting coating of the substrate works as a current collector and the substrate material itself both as a support structure to the cell and as a sealing layer between the cell and the ambient air (Grätzel, 2003). Fluorine-doped tin oxide ($SnO_2$: F or FTO) and indium tin oxide ($In_2O_3$: Sn or ITO) are the most frequently used TCO in DSSC cells (Korber et al., 2010). The choice of sheet resistance of the $SnO_2$ -coated glass plates is a compromise between conflicting beneficial properties of the TCO-coated glass: the higher the conductance the lower the transmittance and vice versa. An alternative transparent conducting oxide substrate to the glass which has been introduced and studied is TCO coated plastic foils (Kalyanasundaram & Grätzel, 1998; Halme, 2002; El-refi, 2013).

The semiconductor, typically a metal oxide, is responsible for providing the surface for dye adsorption, for collecting electrons from the excited dye and for conducting them towards

the external circuit (Grätzel, 2003). The band gap of the semiconductor should be greater than 3 eV in order to let the light pass through the semiconductor easily (Tung, 2010). In solution under irradiation, oxide semiconductor materials have good stability. Stable oxide cannot absorb visible light because they have relatively wide band gaps. To be able to absorb light, wide band gap oxide semiconductor materials (e.g. $TiO_2$, ZnO and $SnO_2$) are sensitized with photosensitizers (dyes) that are able to absorb visible light (O'Regan & Grätzel, 1991; Hara & Arakawa, 2003). Types of DSSC dye sensitizers are further discussed in sub-chapter 2.5 of this chapter.

The standard preparation procedure of the nanostructured $TiO_2$ electrode includes sintering of the deposited $TiO_2$ film at 450-500 °C. The FTO substrate has been identified as the material of choice for DSSC because it is the only TCO that the coating is stable at these temperatures. The other reason for the choice of fluorine doped tin dioxide (FTO) is the cost-effectiveness of fluorine when compared to the expensive and scarce indium in ITO (Kalyanasundaram & Grätzel, 1998). Screen-printing or doctor-blading procedure is mostly used in order to get these semiconductor layers. This technique entails the application of a paste of metal oxide nanocrystalline particles over a conducting substrate (Martineau, 2012). A crucial role in the harvesting of sunlight is played by mesoporous morphology of the semiconductor layer (Grätzel, 2001b).

Here, are some criteria for the best semiconductor for DSSC application:

- In order to promote very high light harvesting; high surface area films of nanocrystalline oxide particles, with an average size of about 20 nm is needed. This is for providing a quite significant surface area available for dye adsorption, responsible for the absorption of a high percentage of the incident sunlight. On the other hand, flat electrodes promote very low light harvesting levels due to the small absorption cross section of a monolayer of dye, which results in quite low photovoltaic efficiencies (Grätzel, 2001a; Grätzel, 2005);
- A suitable degree of porosity is also needed to promote good contact between the dye molecules adsorbed onto the semiconductor nanoparticles and the electrolyte species, ultimately ensuring the regeneration of the dye (Grätzel, 2001a);
- The porous film must form an interconnected network of nanoparticles to allow the percolation of the injected electrons. Moreover, the position of the

conduction band edge is also important and must allow charge injection from the excited state of the dye;

- The large band gap (>3 eV) of the oxide semiconductors is needed in DSSC for the transparency of the semiconductor electrode and for the absorption of large part of the solar spectrum (Tung, 2010).

A great number of common wide energy band gap semiconductors have been reviewed but anatase $TiO_2$ is the most used (O'Regan & Grätzel, 1991; Tan, 2008). In addition to $TiO_2$, other semiconductors used in porous nanocrystalline electrodes include for example: ZnO, CdSe, CdS, $WO_3$, $Fe_2O_3$, $SnO_2$, $Nb_2O_5$, and $Ta_2O_5$ (Kalyanasundaram & Grätzel, 1998; Gratzel, 2001a; Tung, 2010; Karmakar & Ruparelia, 2011; Chemistry, 2012).

Till now, $TiO_2$ is the cornerstone semiconductor for dye-sensitized nanostructured electrodes for DSSC. Due to the non-toxic, easily available and low cost characteristics, $TiO_2$ has been the mostly preferred semiconductor for the photoelectrode (Karmakar & Ruparelia, 2011; Chemistry, 2012). Titanium dioxide has two important crystalline forms which are anatase and rutile. Anatase appears as pyramid-like crystals and is stable at low temperatures, whereas needle-like rutile crystals are dominantly formed at high temperature processes (Halme, 2002).

The anatase form is preferred since it has wider band gap energy of about 3.2 eV and an absorption edge that makes it insensitive to visible light. In fact, this prevents the generation of holes by band gap excitation which would act as oxidants. In contrast, rutile has a lower band gap (≈ 3.0 eV), higher dark current and absorbs part of the near-UV region. All these characteristics make rutile less chemically stable. Furthermore, anatase crystalline form is non-toxic, thermally stable, chemically inert, readily available and cheap (Karmakar & Ruparelia, 2011).

### 2.3.2. Sensitizer dyes (photosensitizer)

The sensitizer is an essential component to absorb light in the DSSC, converting the incident light into photocurrent. Its properties have much effect on the light harvesting efficiency and the overall power conversion efficiency. The role of the sensitizer is not only light harvesting but also charge injection (Andrade, 2010). The semiconductor oxides used in DSSC are wide band gap materials, which do not absorb in the visible. The specifically engineered dye molecules placed on the semiconductor electrode are responsible for the

absorption of incident light in the DSSC. The properties of the dye molecule as attached to the semiconductor particle surface are essential. Such desirable properties can be summarized as following:

- It must bind strongly to the semiconductor surface for long term stability i.e. good adsorption to the semiconductor surface (Nazeeruddin et al., 2001);
- The dye should have a broad absorption spectrum, preferably all the way into the near-IR in order to harvest as many incident photons as possible (Nazeeruddin et al., 2001);
- Easy and straightforward synthesis for future large scale production;
- The energy levels should match the conduction band of the semiconductor and the redox potential of the hole-conductor (Redondo, 2009);
- High solubility to the solvent used in the dye impregnation is necessary;
- To minimize energy losses and to maximize the photovoltage, the exited state of the adsorbed dye molecule should be only slightly above the conduction band edge of the $TiO_2$, but yet above enough to present energetic driving force for the electron injection process. For the same reason, the ground state of the molecule should be only slightly below the redox potential of the electrolyte (Halme, 2002);
- A high extinction coefficient will enable the use of thinner semiconductor films and still keep a high degree of absorbed photons;
- Low toxicity and possibility to recycle;
- The adsorbed dye molecule should be stable enough in the working environment (at the semiconductor-electrolyte interface) to sustain about 20 years of operation at exposure to natural daylight (Nazeeruddin et al., 2001);
- Achieve a long lifetime of the injected electrons by blocking the recombination pathways i.e. the process of electron injection from the exited state to the conduction band of the semiconductor should be fast enough to outrun competing unwanted relaxation and reaction pathways (Karlsson, 2011; El-refi, 2013)

The properties of the organic sensitizers can be modified by incorporating different groups into the molecule. By choosing the right design, the sensitizer can be tuned in order to increase the long wavelength absorption, achieve a high extinction coefficient, and shift the energy levels to improve the performance of the solar cell (Karlsson, 2011).

## 2.3.3. Electrolytes

The electrolyte is a crucial part of all DSSC. It is responsible for inner charge carrier between electrodes. It regenerates the dye at the photoelectrode with the charge collected at the counter electrode (Grätzel, 2003). The electrolyte characteristics strongly affect the overall operation of the DSSC mainly due to its influence in the mass transport of charge carriers. For ideal performance and excellent efficiency, electrolyte should have high ionic conductivity so that it can transfer oxidized/reduced species to respective electrodes efficiently and should completely prevent back electrode reactions (Al-Bat'hi et al., 2013).

The redox couple in the electrolyte has the function of regenerating the dye after electron injection into the conduction band of the semiconductor, as well as to transport the positive charges (holes) towards the counter electrode. The most used liquid electrolyte in DSSC is based on the charge mediator $I^-/I_3^-$ redox couple in acetonitrile, a low-viscosity volatile solvent (Andrade, 2010). The ideal characteristics of the redox couple for the DSSC electrolyte are listed below (El-refi, 2013):

- High solubility in the solvent to ensure high concentration of charge carriers in the electrolyte;
- High diffusion coefficients in the used solvent to enable efficient mass transport;
- Absence of significant spectral characteristics in the visible region to prevent absorption of incident light in the electrolyte;
- High stability of both the reduced and oxidized forms of the couple to enable long operating life;
- Highly reversible couple to facilitate fast electron transfer kinetics;
- Chemically inert toward all other components in the DSSC (Yu, 2012).

Since the discovery of the DSSC about 23 years ago, no redox couple preceding the performance of the $I^-/I_3^-$ couple in the DSSC has been discovered (O'Regan & Grätzel, 1991). There are other electrolytes that have been used such as bromide/tri-bromide electrolytes (Walker, 2011). But the high viscosity of the common electrolytes limits their applications, ultimately reducing the efficiency of the cells. Recently, the electrolyte used in the DSSCs consists of iodine ($I^-$) triiodide ( $I_3^-$) as a redox couple in a solvent with possibly other substances added to improve the properties of the electrolyte and the performance of the operating DSSC (Alhamed et al., 2012; Chang et al., 2013).

Andrade has given a number of criteria for a suitable solvent for a high efficiency liquid electrolyte DSSC (Andrade, 2010):

- The solvent must be liquid with low volatility at the operating temperatures (-40$^{o}$C – 80$^{o}$C) to avoid freezing or expansion of the electrolyte, which would damage the cells;
- It should have low viscosity to permit the rapid diffusion of charge carriers;
- The intended redox couple should be soluble in the solvent;
- It should have a high dielectric constant to facilitate dissolution of the redox couple;
- The sensitizing dye should not be absorbed into the solvent;
- It must be resistant to decomposition over long periods of time;
- The solvent should be of low cost and low toxicity.

Some examples of solvents used in electrolyte for DSSC include: acetonitrile (Wei, 2010; Karlsson, 2011) methoxyacetonitrile (Nazeeruddin et al., 2001) methoxypropionitrile, glutaronitrile, butyronitrile, ethylene carbonate and propylene carbonate (Danger, 2012).

### 2.3.4. Counter-electrode catalysts

Counter electrodes (CE) are typically prepared by depositing a thin layer of platinum (Pt) catalyst onto the FTO conducting glass substrates. The general function of CE is to reduce the oxidized form of the redox couple in the electrolyte (Grätzel, 2003; Fauss, 2012). The CE material must be adapted to the redox system in the electrolyte.

Platinum is traditionally used as the most efficient catalyst not only because it provides high exchange current densities, but also because it is transparent. While showing excellent catalytic action, platinum has the disadvantage of being very expensive. In fact, platinum when coated electrochemically or by vapor deposition to the TCO; has been found to become unstable in the presence of the iodide electrolyte (Andrade, 2010). This is the reason why several other materials have also been used as CE in DSSC; e.g. conducting polymers, carbon black, graphite; activated carbon or single-wall carbon nanotubes and multi-walled carbon nanotube, and cobalt sulphide (Yu, 2012; Sedghi & Miankushki, 2014; Hashmi, 2014) as they are considered to be relatively cheap in comparison to platinum.

## 2.4. Principle of operation of DSSC

The heart of the operation of Grätzel cell is the absorption of the incident light by dye sensitizer adsorbed on the semiconductor electrode, the generation of excitons and injection of electrons into the conduction band of the mesoporous nanocrystallline film (O'Regan & Grätzel, 1991; Hernandez-Martinez et al., 2011). **Figure 2.2** represents the operating principle of DSSC. When light falls on the surface of the dye, the dye absorbs it and become oxidize (1). Thus, it injects electron into the conducting band of the semiconductor (2). Electrons that have been injected into the conduction band travel to the underlying TCO substrate via a diffusional random walk pathway (O'Regan & Grätzel, 1991; Grätzel, 2003, Kalyanasundaram & Grätzel, 1998;). Once collected in the TCO substrate, electrons can flow through an external circuit, creating an electrical current capable of doing useful work (3). The dye is reduced by receiving an electron from the electrolyte (4). The electrolyte is regenerated by the reduction of tri-iodide in receiving the electron from the counter electron and charge neutrality is maintained by electron migration through external circuit (5) (Sandquist, 2010; Srinivasan, 2012; Hashmi, 2014).

The operation of DSSC can be summarized by these following equations in a clear way:

$$D_{(absorbed)} + hv \rightarrow D^{*}_{(absorbed)} \quad (2.1)$$

$$D^{*}_{(absorbed)} \rightarrow D^{+}_{(absorbed)} + e^{-}_{(injected)} \quad (2.2)$$

$$D^{+}_{(absorbed)} + \frac{3}{2} I^{-} \rightarrow D_{(absorbed)} + \frac{1}{2} I_3^{-} \quad (2.3)$$

$$I_3^{-} + 2e^{-}_{(cathode)} \rightarrow 3I_3^{-} \quad (2.4)$$

The first step of the operating principle is the absorption of the photons by the dye, D and then become excited D* (**equation 2.1**). This photoexcitation is followed by the injection of electrons into the conduction band of the semiconductor (mesoporous). After the injection of the electrons, the dye is oxidized $D^{+}$ (**equation 2.2**). The dye is regenerated by the gain of electron from the electrolyte, containing a redox couple (**equation 2.3**). Iodide/triiodide couple is the preferred and effective redox couple used. Iodide regenerates the sensitizer, and itself gets regenerated by the reduction of triiodide at the counter electrode (**equation 2.4**). This way the circuit gets completed by transfer of electron via the external load (Grätzel, 2005; Park, 2010; Karlsson, 2011; Kim, 2012).

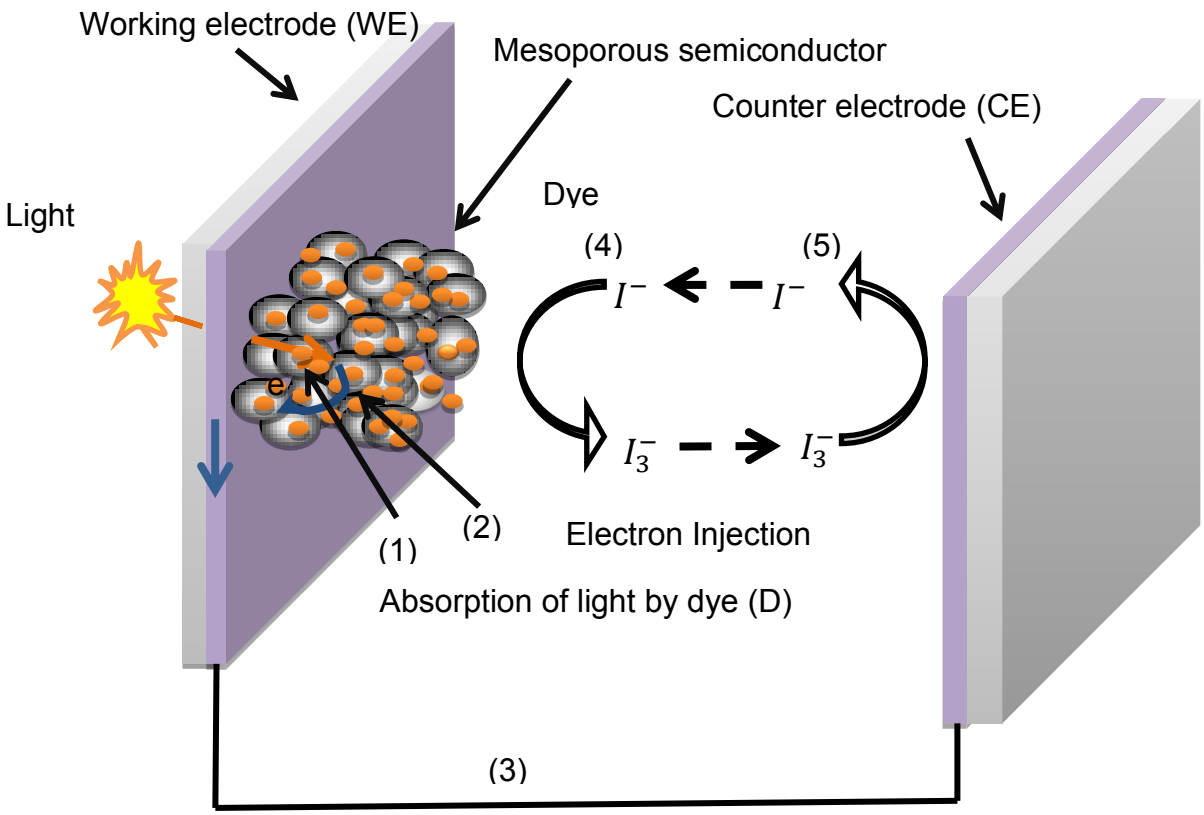


***Figure 2.2**: The operating principle of dye sensitized solar cell.*

## 2.5. Dye sensitization of DSSC

### 2.5.1. Brief description on DSSC dye sensitization

DSSC is a device for the conversion of visible light power into electricity, based on the sensitization of wide band gap semiconductors (Grätzel, 2003; Alhamed et al., 2012). The performance of the cell mainly depends on a dye used as photosensitizer. The absorption spectrum of the dye and the anchorage of the dye to the surface of $TiO_2$ are important parameters determining the efficiency of the cell. In DSSC, the dye as a sensitizer plays a key role in absorbing sunlight and transforming solar energy into electric energy (Wongcharee et al., 2006; Andrade, 2010; Alhamed et al., 2012).

Since the chosen dye plays an important role in absorbing visible light and transferring photon energy into electricity, much attention has been paid to analyze the effective sensitizer dyes (Andrade, 2010). Generally, hydrophilic groups, such as -COOH, -PO3OH, -SH, and -OH, are very important for the consistent design of dyes for DSSC. The dyes having these functional groups are the ones earmarked as good candidates for dye

research (Liu, 2012). The utilization and synthesis of numerous metal complexes and organic dyes as sensitizer have been done (Zhou et al., 2011; Al-Bat'hi et al., 2013).

Some of the most efficient sensitizers are synthetic dyes including transition metal coordination compounds such as ruthenium polypyridyl complexes because of their highly efficient metal-to-ligand charge transfer, suitable ground and excited state energy levels with respect to titanium dioxide conduction band energy (Chemistry, 2012). They also have intense and wide range absorption in whole visible range. Even if they present such attractive features, their synthesis process is costly and complicated and they are not environment friendly because they contain heavy rare metals which are undesirable from the point of view of environmental conservation aspects (Alhamed et al., 2012). Natural dye can be used as the best alternative as they have acceptable efficiency in comparison to that one of transition coordination compounds and their extraction can be done by simple procedures from flowers, leaves, fruits, animals and other natural products (Lee et al., 2013).

Natural dyes have been intensively studied; and used as DSSC dye sensitizer (Wongcharee et al., 2006; Aduloju, 2012). The main features of natural dyes are their availability, environmental friendly and low in cost. Natural dyes extracted from fruits, flowers, and leaves; show diverse colors ranging from red to purple; and are extracted through simple processes (Hernandez-Martinez et al., 2011; Alhamed et al., 2012; Zongo, 2012).

### 2.5.2. Types of dye sensitizer for DSSC

Dye sensitizers can mainly be classified into two: the inorganic dyes and organic or natural dyes. Inorganic dyes used in DSSC are mainly metal complex dyes such as complexes of Ruthenium, Osmium and Iridium. Organic dyes mainly consist of fruit dyes and natural extract dyes (Nazeeruddin et al., 2001; Sekar and Ghelot, 2010).

Since the first DSSC was made 23 years back (O'Regan & Grätzel, 1991), a lot of research has been carried out about transition-metal complexes as well as natural or organic dyes, but none has been able to match the performance of the ruthenium complexes based on the conversion yield and durability or long term stability (Karmakar & Ruparelia, 2011). Many different compounds have been investigated for semiconductor sensitization, such as porphyrins (Moon, 2011), phtalocyanines, coumarin, carboxylated derivatives of anthracene and polymeric films (Ruiz-Anchondo et al., 2010). Among the

photosensitizers investigated, transition metal complexes have been the best so far but their cost is a hindering factor in their use (Sekar & Ghelot, 2010; Karmakar & Ruparelia, 2011; Hardin et al., 2012).

#### *2.5.2.1. Metal complex sensitizers*

Metal complex sensitizers have two ligands specifically, ancillary and anchoring. Anchoring ligands are required for the complex absorption on the semiconductor surface whereas, ancillary are important for tuning of the overall properties of the complex (Nazeeruddin et al., 2001; Grätzel, 2003).

##### 2.5.2.1.1. Ruthenium and Osmium

Among all metal complexes sensitizers, the polypyridyl complexes of ruthenium dyes are the most efficient ones. They can be categorized under carboxylate polypyridyl ruthenium dyes, phosponate ruthenium dyes and polynuclear bipyridyl ruthenium (Hagberg, 2009). Much attention has been attracted by the *cis*-dithiocyanato *bis* (4,4'-dicarboxy-2,2' bipyridine) ruthenium(II) (coded as N3) that was first developed in 1991, due to a low cost compared to inorganic sensitizers and high photon-to-current conversion efficiency (O'Regan & Grätzel, 1991; Hagfeldt & Grätzel, 2000). Other efficient dyes that have been investigated are di-tetrabutylammonium cis-bis(isothiocyanato)bis(2,2'-bipyridyl-4,4'-dicarboxylato) ruthenium(II) (coded as N719), and cis-Bis(isothiocyanato)(2,2'-bipyridyl-4,4'-dicarboxylato)(4,4'-di-nonyl-2'-bipyridyl)ruthenium(II) (coded as Z907) (Hara & Arakawa, 2003; Kuang et al., 2008; Sekar & Ghelot, 2010). The **figure 2.3**, **figure 2.4,** and **figure 2.5** show the structure of N719, Z907 and N3 respectively. Ruthenium (II) and (III) complexes have been used as efficient photosensitizers because they have wide absorption bands, long-term chemical stability but suffer being costly as these are rare-earth metals, complicated synthetic routes, and low yields (Sahin et al., 2008; Karmakar & Ruparelia, 2011).

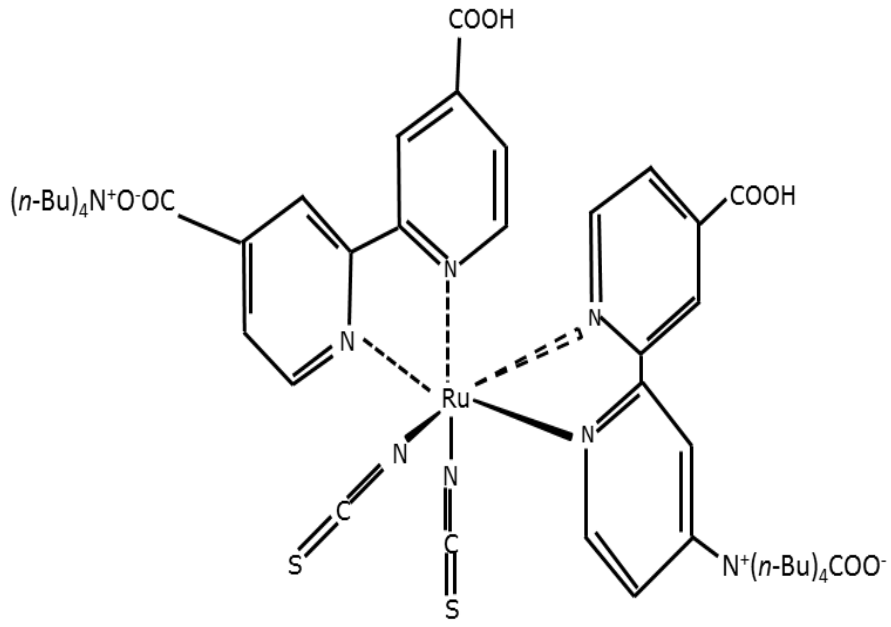


N719

***Figure 2.3**: The structure N719.*

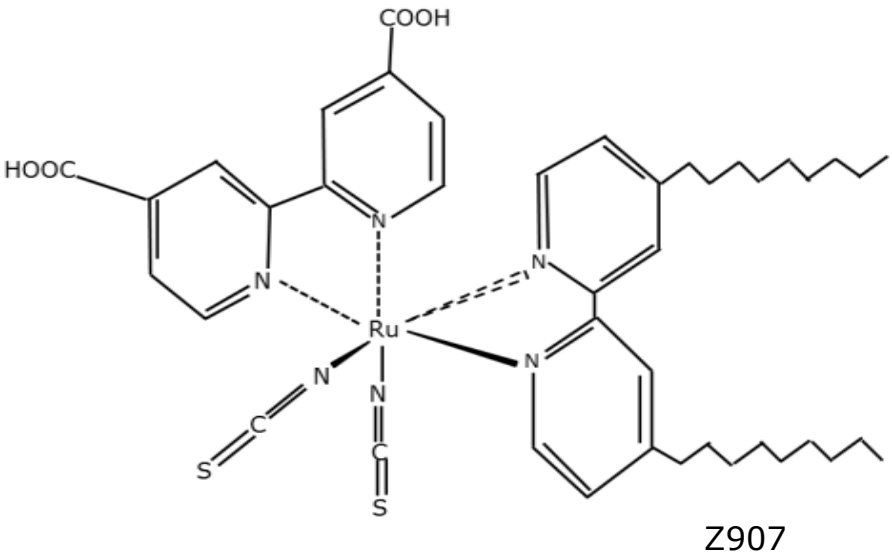


Z907

***Figure 2.4**: The structure Z907.*

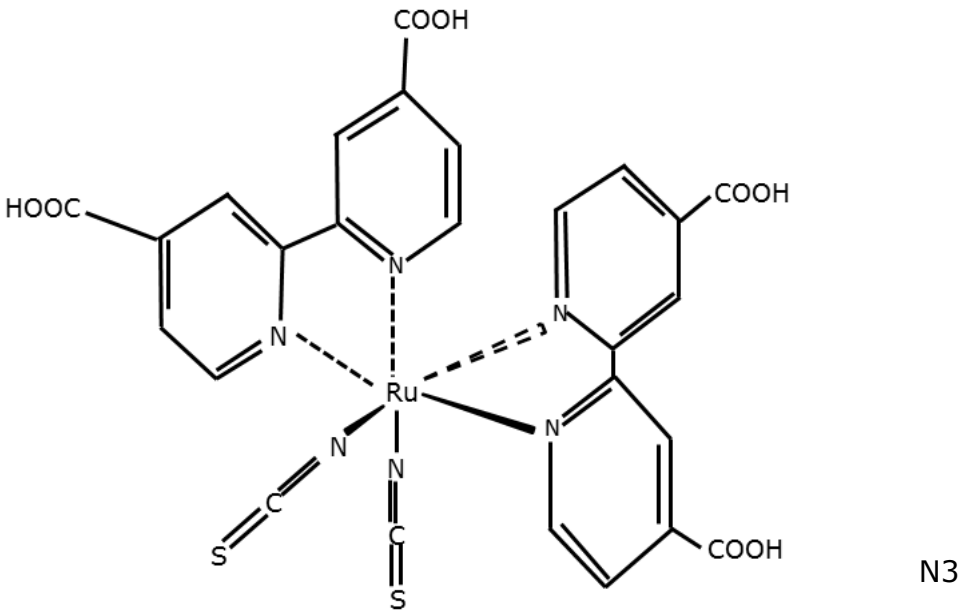


***Figure 2.5**: The structure N3.*

Osmium sensitizers were found to be 50% less efficient than Ru complexes, but they have greater photochemical stability compared to black dye (Redondo, 2009; Sekar & Ghelot, 2010). Even if Ru-based dyes have the exciting performance; Ruthenium is a heavy metal. So, disabled DSSC would present environmental risks from ruthenium toxicity; it is a rare metal and therefore any commercial application would be limited by the availability and the cost. Because of the expense and toxicity associated with metal-centered dyes, many organic dyes have been developed as alternatives (Sandquist, 2010).

2.5.2.1.2. Other metal complexes

Among other metal complexes that have been researched are copper, iron, iridium (III) and rhenium (I). While copper (I) complex has shown surprisingly higher incident photon to current efficiency (IPCE) values with solar efficiency of 1.9 to 2.3% (Redondo, 2009), iron (II) ligands have shown higher stability towards photochemical degradation with solar energy efficiency. A novel type of efficient iridium (III) sensitizers with carboxyl pyridine ligands was synthesized, yielding a maximum of 66% IPCE and 2.16% power conversion efficiency under simulated air mass 1.5sunlight. One should note that the air mass coefficient can be used to help characterize the solar spectrum after solar radiation has traveled through the atmosphere. Rhenium (I) complexes based benzathiazole derivatives

have been reported to exhibit solar energy efficiency of around 1.43-1.76% (Karmakar & Ruparelia, 2011; Sekar & Ghelot, 2010).

#### *2.5.2.2. Natural dyes*

2.5.2.2.1. Sources of natural dyes

Plants have been identified as the main sources of natural dyes. However, the extraction of natural dyes from plants sources presents challenges such as conservation. There are no specific methods for their extraction; it could depend on the goal. Other significant problem is related to the availability of the dye source as most of the plant sources are seasonal (Zongo, 2012). On the other hand, natural dyes are less stable (i.e. they degrade quickly) and then cannot be kept for a long time. Other natural dye sources include insects (e.g. cochineal beetles and lac scale insects); animal (e.g. some species of mollusk of shellfish); minerals (e.g. ferrous sulphate, ochre and clay); as well as certain microbial sources such as chlorella (e.g. red carotenoid pigments) (Karmakar & Ruparelia, 2011; Chengaiah et al., 2011; Zongo, 2012). Even if natural dyes present some challenges mentioned above through their extraction process and conservation; many diversity of sources could allow natural dyes to be found widely throughout the world.

2.5.2.2.2. Types of natural dyes by source and chemical structure

Natural dye from plant can be classified into four major groups: Betalains; flavonoids; chlorophylls; carotenoids and all of which have been used in DSSC to varying degrees (Hagberg, 2009; Azeredo, 2009; Sandquist, 2010; Zongo, 2012). Each group is going to be further discussed.

- ***Betalains***

Betalain dyes have recently gained more interest in the food industry. The betalain pigments derived from betalamic acid are divided in two subgroups: the red betacyanins and yellow betaxanthins (Azeredo, 2009; Sandquist, 2010). Bougainvillea extracts is one source of betalain used as DSSC sensitizer. The obtained solar energy conversion efficiency was of 0.48 % (Hernandez-Martinez et al., 2011). The most important compound of betalains is referred to the betacyanin of red color found in roots, flowers, fruits and other plant tissues. Betalains are water soluble and are also nitrogen-containing compounds derived from the amino acid tyrosine and demonstrate strong light absorption (Azeredo, 2009). Hemmatzadeh and Mohammadi have fabricated an efficient and cheap

DSSC from *Pastinaca sativa* and *Beta vulgaris* which are source of dyes having the –COOH to bind to the $TiO_2$ (Hemmatzadeh & Mohammadi, 2013).

- ***Flavonoids***

Flavonoids constitute an important group of natural dyes used in the food industry, because of the varieties of colors that they exhibit. These compounds are responsible for the attractive color that many fruits and vegetables exhibit, from a white/cream color; to red, purple, blue and yellow (Zongo, 2012). The most common flavonoid component is *anthocyanin*, which is responsible for the attractive orange-red and violet color that appears in many flowers and fruits (Li et al., 2013). Carbonyl and hydroxyl groups present in the anthocyanin molecule can be bound to the surface of a porous $TiO_2$ film. This makes electron transfer from the anthocyanin molecule to the conduction band of $TiO_2$ (Alhamed et al., 2012; Li et al., 2013). The anthocyanin dye from red cabbage and grapes have been used as sensitizer in DSSC (Kumara & Hemamali, 2013; Li et al., 2013). Anthocyanin from black rice extraction was used as the DSSC dye sensitizer (Noor et al., 2011). The one from mulberry fruits achieved the photoelectric efficiency of 0.672% (Chang et al., 2011). One should note that several colored fruits and leaves containing anthocyanins are not suitable for DSSC sensitization (e.g. strawberries) as for a dye to chelate to $TiO_2$; it must have several –COOH or –OH groups (Smestad and Grätzel, 1998).

- ***Chlorophylls***

Chlorophylls acting as an active photosensitizer in the photosynthesis of green plant are an attractive compound to be used as a DSSC photosensitizer in visible range as its maximum peak of absorption was found to be at 670nm (Noor et al., 2011). Noor et al. used only chlorophylls (from *pandan* extract) and found the efficiency of 0.24; and this efficiency photo-conversion increased to 0.42 while mixed with the anthocyanin (from *black rice* extraction) dye. There was also found more absorption peaks when chlorophylls dye was mixed with anthocyanin dyes. This showed that there were high efficiency for photo-conversion and enhancement of the stability of the chlorophylls from the effect of mixing it with other dyes (Noor et al., 2011; Alhamed et al., 2012; Zongo, 2012).

- ***Carotenoids***

Carotenoids are organic pigments naturally occurring in the chromoplasts of plants and some other photosynthetic organisms such as algae, and in some types of fungi and bacteria, where they have diverse and important functions and actions (Ruiz-Anchondo et

al., 2010). Carotenoids are responsible for the yellow-orange and red color of many flowers, fruits, vegetables, roots and autumn leaves (Sandquist, 2010). The results obtained by calculations of the molecular structures and properties of five natural carotenoids (crocetin, bixin, norbixin, transbixin, and retinoic acid) have been reported to have attractive features for DSSC application as dye sensitizer. Among these features include the presence of carboxylic acid groups in their structure; which enables their anchoring on the surface of the semiconductor film electrode, and the injection of electrons into the conduction band of the semiconductor (Ruiz-Anchondo et al., 2010; Li et al., 2013).

The dye of interest in this study is sepia melanin from cuttlefish called *Sepia officinalis;* which is further discussed in the chapter three*.* Melanins are the major pigments which are present in the surface of vertebrates. These pigments are responsible for coloration in animals and plant (Subianto, 2006; Magarelli, 2011). Because melanin has interesting chemical complexity, different studies have identified some of its physical and chemical properties. However, there is still a lot work to do on melanins since their structures are not well known (Magarelli, 2011).

The important feature that makes them to be attractive for Grätzel cell application is this: Melanins have the capacity to absorb a wide range of electromagnetic radiation ranging from visible light (hence its color is dark) and UV radiation up to the Some peaks are undetectable as EDX may not be a reliable method to quantify elements in low weight % x-ray region (Magarelli, 2011). On the other hand, melanin is reported to have the ability to bind different metallic ions (Kim et al., 2012). Melanin can also conduct electricity and is thus considered a semiconductor material (Subianto, 2006). The hydroxyl and carboxylic functional groups of melanin from *Sepia officinallis* present the possibility that a purified extract of the squid ink pigment may induce strong interaction with the hydroxyl group of $TiO_2$ surface (Lee et al., 2013).

## 2.6. Conclusion

The chapter has discussed DSSC in details. It covered the brief introduction and the literature review on DSSC; the description of its components as well as the operating principles. The sensitization of DSSC has been discussed and the different types of DSSC dye sensitizers. Sepia melanin is discussed further in the following chapter three. This chapter covers the meaning; applications, general characteristics, and structure of sepia

melanin. Some reasons for the interest on melanin currently are discussed. Chapter three also covers the melanins biological functions, properties as well as the possibility to apply sepia melanin from *Sepia officinalis* as a $TiO_2$ photosensitizer for Grätzel solar cell application.

## 2.7. References


Aduloju, K.A. (2012) 'Safety assessment of cola nitida extract as sensitizer in dye sensitized solar cells', *Archives of Applied Science Research*, vol. 4 (1), pp. 32-38.

Al-Bat'hi, S.A.M., Alaei, I. and Sopyan, I. (2013) 'Natural photosensitizers for dye sensitized solar cells', *International Journal of Renewable Energy Research*, vol. 3(1).

Alfa, B., Tsepav, M.T., Njinga, R.L. and Abdulrauf, I. (2012) 'Fabrication and characterisation of titanium dioxide based dye', *Applied Physics Research*, vol. 4 (1).

Alhamed, M., Issa, A.S. and Doubal, A.W. (2012) 'Studying of natural dyes properties as photo- sensitizer for dye sensitizer for dye sensitized solar cells (DSSC)', *Journal of electron Devices*, vol. 16, pp. 1370-1383.

Andrade, L.M.M. (2010) *Study and characterization of Grätzel solar cells, Doctoral thesis*, University of Porto.

Azeredo, H.M.C. (2009) 'Betalains: properties, sources, applications, and stability', *International Journal of Food Science and Technology*, pp. 2365-2376.

Bahadur, K.I., Jyoti, N.J., Kumar, M.P. and Suman, C. (2012) 'Dye-sensitized solar cell using extract of punica granatum L.pomegranate (bedana) as a natural sensitizer', *Research Journal of Chemical Sciences*, vol. 2(12), pp. 81-83.

Burschka, J., Pellet, N., Moon, S.-J., Humphry-Baker, R., Gao, P., Nazeeruddin, M.K. and Grätzel, M. (2013) 'Sequential deposition as a route to high-performance perovskite-sensitised solar cells', *Nature*, vol. 499, p. 318.

Chang, H. and Lo, Y.-J. (2010) 'Pomegranate leaves and mulberry fruit as natural sensitizersfor dye-sensitized solar cells', *Solar Energy*, vol. 84, pp. 1833-1837.

Chang, H., Cho, K.-C., Chen, T.-L., Chu, K.-H. and Jiang, L.-J. (2011) 'Preparation and characterization of anthocyanin dye and counter electrode thin film with carbon nanotubes for dye-sensitized solar cells', *Materials Transactions*, vol. 52 (10), pp. 1977-1982.

Chang, H., Kao, M.-J., Tien-Li, Chen, Chen, .C.-H., Cho, K.-C. and Lai, X.-R. (2013) 'Characterization of natural dye extracted from wormwood and purple cabbage for dye-sensitized solar cells', *International Journal of Photoenergy*.

Chemistry, Z.X. (2012) *Characterization of the dye-sensitized solar cell*, Massachusetts: Worcester Polytechnic Institute.

Chengaiah, B., Mallikarjuna Rao, K., Kumar, K.M., Alagusundaram, M. and Chetty, C.M. (2011) 'Medical importance of natural dye : A review  medicinal importance of natural dye a review', *International Journal of PharmTech Research*, vol. 2(1), pp. 144-154.

Chiba, Y., Islam, A., Watanabe, Y., Komiya, R., Koide, N. and Han, L. (2006) 'Dye-sensitized solar cells with conversion efficiency of 11.1%', *Japanese Journal of Applied Physics*, vol. 45, pp. 638-640.

Danger, B.R. (2012) *Photochemical investigation of porphyrins for use in dye-sensitized solar cells*, Saskatoon: University of Saskatchewan.

El-Agez, T.M., Tayyan, A.A.E., Al-Kahlout, A., Taya, S.A. and Abdel-Latif, M.S. (2012) 'Dye-sensitized solar cells based on ZnO films and natural dyes', *International Journal of Materials and Chemistry*, vol. 2(3), pp. 105-110.

El-refi, K.S. (2013) *Dye-sensitized solar cells using $TiO_2$ as a semiconducting layer*, Gaza: Islamic University of Gaza.

Fauss, B. (2012) *Optimizing the DSSC fabrication process using lean six sigma*, Arizona : Arizona State University.

Grätzel, M. ( 2001b) 'Molecular photovoltaics that mimic photosynthesis', *Pure and Applied Chemistry*, vol. 73 (1), pp. 459-467.

Grätzel, M. (2001a) 'Photoelectrochemical cells', *Nature*, vol. 414, pp. 338-344.

Grätzel, M. (2003) 'Review Dye-Sensitized Sol Cells"', *Journal of Photochemistry and Photobiology*, vol. Photochemistry Rev. 4, p. 145.

Grätzel, M. (2005) 'Solar energy conversion by dye-sensitized photovoltaic cells', *Inorganic Chemistry*, vol. 6841-6851, p. 44.

Green, M.A. (1982) *Solar cells: Operating principles, technology and system applications*, Australia: University of South Wales.

Hagberg, D. (2009) *Synthesis of Organic Chromophores for Dye Sensitized Solar cells, Doctaral thesis*, Sweden: KTH Chemical Science and Engeneering Stockholm.

Hagberg, D. (2009) *Synthesis of organic chromophores for dye-sensitized solar cells, Doctoral thesis*, SE Stockholm: KTH Chemicals Sciences and Engineering.

Hagfeldt, A. and Grätzel, M. (2000) 'Molecular photovoltaics', *Account of Chemical Research*, vol. 33(5), pp. 269-277.

Hagfeldt, A., Cappel, U. and Boschloo, G. (2012) *Mesoporous dye-sensitized solar cells*, Uppsala: Elsevier.

Halme, J. (2002) *Dye-sensitized nanostructured and organic photovoltaic cells: Technical review and preliminary test, Master's thesis*, Department of Engineering Physics.

Hara, K. and Arakawa, H. (2003) *Dye-sensitized solar cells*, Tsukuba: National Institute of Advanced Industrial Science and Technology (AIST).

Hardin, B.E., Snaith, H.J. and McGehee, M.D. (2012) 'The renaissance of dye-sensitized solar cells', *Review articles | focus Nature photonics*.

Hashmi, S.G. (2014) *Towards metal free counter electrodes for dye-sensitized solar cells*, Finland: Aalto University.

Hemmatzadeh, R. and Mohammadi, A. (2013) 'Improving optical absorptivity of natural dyes for fabrication of efficient dye-sensitized solar cells', *Journal of Theoretical and Applied Physics*, vol. 7, p. 57.

Hernandez-Martinez, A.R., Estevez, M., Vargas, S., Quintanilla, F. and Rodriguez, R. (2011) 'New dye-Sensitized solar cells obtained from extracted bracts of bougainvillea glabra and spectabilis betalain pigments by different purification processes', *International Journal of Molecular Sciences*, vol. 12, pp. 5565-5576.

Ho Chang, Y.-J.L. (2010) 'Pomegranate leaves and mulberry fruit as natural sensitizersfor dye-sensitized solar cells', *Solar Energy* , vol. 84, pp. 1833-1837.

Honda, S. (2011) *Dye modification of donor/acceptor interfaces in polymer solar cells, Doctoral thesis*, Kyoto: Kyoto University.

Kalyanasundaram, K. and Grätzel, M. (1998) 'Applications of functionalized transition metal complexes in photonics and optoelectronic devices', *Coordination Chemistry reviews*, vol. 77, pp. 347-414.

Karlsson, K.M. (2011) *Design, synthesis and properties of organic sensitizers for dye-sensitized solar cells, Doctoral thesis*, Royal Institute of Technology.

Karlsson, M. (2012) *Material development for solid-state dye-sensitized solar cells*, Acta Universititatis Upsaliensis.

Karmakar, A.S. and Ruparelia, J.P. (2011) 'A critical review on dye-sensitized solar cells', pp. 382-481.

Khan, M.A., Khan, S.M.M., Mohammed, M.A., Sultana, S., Islam, J.M.M. and Uddin, J. (2012) 'Sensitization of nanocrystalline titanium dioxide solar cells using natural dyes: Influence of acids medium on coating formulation', *American Academic & Scholarly Research Journal*, vol. 4 (5).

Kim, B. (2012) *Molecular engineered sensitizers containing heterocyclic spacers in a D-π-A system and their use in DSSCs*, Raleigh: North Carolina State University.

Kim, D.J., Ju, K.-Y. and Lee, J.-K. (2012) 'The synthetic melanin nanoparticles having an excellent binding capacity of heavy metal ions', *Bull. Korean Chem. Soc.*, vol. 33 (11), p. 3788.

Korber, A.K.C., Wachau, S.F., Gassenbauer, Y., Harvey, S.P., Proffit, D.E. and Mason, T.O. (2010,) 'Transparent conducting oxides for photovoltaics: Manipulation of fermi level, work function and energy band alignment', *Materials*, vol. 3, pp. 4892-4914.

Kuang, D., Comte, P., Zakeeruddin, S.M., Hagberg, D.P., Karlsson, K.M., Sun, L., Nazeeruddin, M.K. and Grätzel, M. (2011) 'Stable dye-sensitized solar cells based on organic chromophores and ionic liquid electrolyte', *Solar Energy*, vol. 85, pp. 1189-1194.

Kuang, D., Klein, C., Snaith, H.J., Humphry-Baker, R. and Zakeeruddin, G.M. (2008) 'A new ion-coordinating ruthenium sensitizer for mesoscopic dye-sensitized solar cells', *Inorganica Chimica Acta*, vol. 361, p. 699–706.

Kumara, G.R.A. and Hemamali, G.G.G.M.N. (2013) 'Dye -sensitized solid state solar with natural pigment extracted from grappes', *International Journal of Scientific and Research Publications*, vol. 3(11).

Lai, W.H., Su, Y.H., Teoh, L.G. and Hona, M.H. (2008) 'Commercial and natural dyes as photosensitizers for a water-based dye-sensitized solar cell loaded with gold nanoparticles', *Journal of Photochemistry and Photobiology A: Chemistry*, vol. 195, p. 307–313.

Lee, J.-W., Cho, H.-B., Nakayama, T., Tohoru, S., T., S.-I., Minato, K., Ueno, T., Suzuki, T., Suematsu, H., Tokoi, Y. and Niiharal, K. (2013) 'Dye-sensitized solar cells using purified squid ink nanoparticles coated on TiO2 nanotubes/nanoparticles', *Journal of Ceramic Society of Japan*, vol. 121(1), pp. 123-127.

Li, Y., Ku, S.-H., Chen, S.-M., Ali, M.A. and AlHemaid, F.M.A. (2013) 'Photoelectrochemistry for red cabbage extract as natural dye to develop a dye-sensitized solar cells', *International Journal of electrochemical science*, vol. 8, pp. 1237-1245.

Liu, Y. (2012) *Synthesis and characterization of electron-responsive materials*, Kochi: Kochi University of Technology.

Magarelli, M. (2011) *Purification, characterization and photodegradation studies of modified sepia melanin (Sepia officinalis).Determination of Eumelanin content in fibers fromAlpaca (Vicugna pacos).Doctoral thesis*, University of Camerino.

Martineau, D. (2012) *Dye solar cells for real: The assembly guide for making your own solar cells*, Aubonne: Solaronix.

Moon, S.-J. (2011) *Solid-state sensitized heterojunction solar cells: effect of sensitizing systems on performance and stability*, école polytechnique Fédérale de Lausanne.

Nazeeruddin, M.K., Pechy, P., Renouard, T., Zakeeruddin, S.M., Humphry-Baker, R., Comte, P., Liska, P., Cevey, L., Costa, E., Shklover, V., Spiccia, L., Deacon, G.B., Bignozzi, C.A. and Grätzel, M. (2001) 'Engeneering of efficient panchromatic sensitizers for nanocrystalline tio2-based solar cells', *American Chemical Society*, vol. 123, pp. 1613-1624.

Noor, M.M., Buraidah, M.H., Yusuf, S.N.F., Careem, M.A., Majid, S.R. and Arof, A.K. (2011) 'Performance of dye-sensitized solar cells with (PVDF-HFP)-KI-EC-PC electrolyte and different dye materials', *International Journal of Photoenergy*.

Nusbaumer, H. (2004) *Alternative redox systems for the dye-sensitized solar cell*, Lausanne: Ecole Polytechnique Federale de Lausanne.

O'Regan, B. and Grätzel, M. (1991) 'A low-cost, high efficiency solar cell based on dye-sensitized colloidal $TiO_2$ films', *Nature*, vol. 353, pp. 737-740.

Park, N.-G. (2010) 'Methods to improve light harvesting efficiency in dye-sensitized', *Journal of Electrochemical Science and Technology*, vol. 1, pp. 69-74.

Redondo, A.H. (2009) *Copper(I) polypyridine complexes: the sensitizers of the future for dye-sensitized solar cells (DSSCs)*, Base: Universität Basel.

Rodríguez, E.G. (2011) *Photoelectrochemical characterization of dye solar cells based on nanostructured zinc oxide substrate*, Sevilla: University Pablo de Olavide.

Rosengrant, D. (ed.) (2010) *Solar power module, backgrounder: Solar cells: sunlight to electricity*, Kennesaw: Kennesaw State University.

Ruiz-Anchondo, T., Flores-Holguín, N. and Glossman-Mitnik, D. (2010) 'Natural carotenoids as nanomaterial precursors for molecular photovoltaics: A computational DFT study', *Molecules*, vol. 15, pp. 4490-4510.

Sahin, C., Tozlu, C., Ocakoglu, K., Zafe, C., Varlikli, C. and Icli, S. (2008) 'Synthesis of an amphiphilic ruthenium complex with swallow-tail bipyridyl ligand and its application in nc-DSC', *Inorganica Chimica Acta*, vol. 361, p. 671–676.

Sandquist, C.S. (2010) *Impoved efficiency of betalain-based dye-sensitized solar cell and a method of measuring Raman spectroscopy of betalain through quenching of fluorescence with $TiO_2$ colloidal nanoparticles, Masters thesis*, Washington State: Washington State University.

Sedghi, A. And Miankushki, H.n. (2014) 'Effect of multi walled carbon nanotubes as counter electrode on dye sensitized solar cells', *International Journal of electrochemical science*, vol. 9, pp. 2029 - 2037.

Sekar, N. And Ghelot, V. (2010) 'Metal complex dyes for dye-sensitized solar cells: Recent developments', *General Article, Resonance*.

Shelke, R.S., Thombre, S.B. and Patrikar, S.R. (2013) 'Comparative performance of dye Sensitized solar cells Using two electrolytes', *International Journal for Research in Science & Advanced Technologies*, vol. 3(2), pp. 131-136.

Smestad, P.G. and Grätzel, M. (1998) 'Demonstrating electron transfer and nanotechnology: A natural dye sensitized nanocrystalline energy converter', *Journal of Chemical Education*, vol. 75, p. 6.

Srinivasan, A. (2012) *Deposition of indium tin oxide for opto-electronics, Master's thesis*, Frolida: University of Frolida.

Subianto, S. (2006) *Electrochemical Synthesis of -Like Polyindolequinone, PhD thesis*, The Queensland University of Technology.

Tan, K.W. (2008) *Commercialisation potential of dye-sensitized mesoscopic solar cells, Masters thesis*, Nanyang Technological University.

Taya, S.A., El-Agez, T.M., El-Gramri, H.S. and Abdel-Latif, M.S. (2013) 'Dye-sensitized solar cells using fresh and dried natural dyes', *International Journal of Material Sciences and Applications*, vol. 2(2), pp. 37-42.

Tung, Y.C. (2010) *Effect of morphologies and electronic properties of metal oxide nanostructure layer on dye-sensitized solar cells, Doctoral thesis*, University of Hong Kong.

Walker, D. (2011) *Corrole Sensitized Solar Cells. Doctoral thesis*, Pasadena, California: California Institute of Technology.

Wei, D. (2010) 'Review dye-sensitized solar cells', *International Journal of Molecular Sciences*, vol. 11, pp. 1103-1113.

Wenger, S. (2010) *Strategies to optimizing dye-sensitized solar cells: organic sensitizers , tandem device structures, and numerical device modeling, Doctaral thesis*, La faculté sciences de base laboratoire de photonique et interfaces programme doctal en chimie et génie chimique, Ecole Polytechnique Fédérale de Lausanne.

Win, T.T., Maung, Y.M. and Soe, K.K.K. (2012) 'Characterization of nano-sized ZnO electrodes with curcumin derived natural dye extract for DSSC application', *American Journal of Materials Science and Technology*, vol. 1, pp. 28-33.

Wongcharee, K., Meeyo, V. and Chavadej, S. (2006) 'Dye-sensitized solar cell using natural dyes extracted from rosella and blue flowers', *Elsevier*.

Yu, Z. (2012) *Liquid redox electrolytes for dye-sensitized solar cells , Doctoral Thesis*, Stockholm.

Yum, J.-H., Baranoff, E., Wenger, S., Nazeeruddin, M.K. and Gratzel, M. (2011) 'Panchromatic engineering for dye-sensitized solar cells', *Energy &Environmental Science*, vol. 4, p. 842.

Zhou, H., Wu, L., Gao, Y. and Ma, T. (2011) 'Dye-sensitized solar cells using 20 natural dyes as sensitizers', *Journal of Photochemistry and Photobiology A:Chemistry*, vol. 219, pp. 188-194.

Zongo, S. (2012) *Nonlinear optical properties of natural dyes based on optical resonance, Master's Thesis*, Cape Town: University of Western Cape.

# CHAPTER THREE: SEPIA MELANIN

This chapter is a literature survey about sepia melanin which is the dye of interest in this project. Sepia melanin is the melanin isolated from ink sac of the cuttlefish *Sepia officinalis* and it has been proposed as a standard for natural melanin (Centeno and Shamir, 2008; Peruru et al., 2012). In addition to the definition, some properties, applications of melanin in general; the general characteristics; the structure; the interest as well as the application of sepia melanin as a broad band sensitizer for DSSC were discussed.

## 3.1. What is melanin?

Melanins are biopolymers widely distributed in many parts of living organisms. They constitute a major group of biological polymers responsible for much of diversity of coloration in animal world. Melanins are usually classified in eumelanins, which are dark pigments containing nitrogen, and pheomelanins, which are yellow to reddish-brown and also contain sulfur (Centeno and Shamir, 2008; Derby, 2014; Huang et al., 2004). Eumelanin and pheomelanin are both found in the skin, hair and eyes of many animal species, including humans, where they act as photoprotectants (absorbing harmful ultraviolet and visible radiation). Dark-skinned people have more melanin in their skin than light-skinned people have (Katritzzky et al., 2002; Magarelli et al., 2010). Eumelanin is the more common form, and is the type studied in this thesis.

For other essential biopolymers such as proteins, nucleic acids as well as carbohydrates, they are well characterized. Their monomeric units and connectivity are well known and the methodologies for determination of the sequences of their connection are well-established. In contrary, structures of melanin are still unknown because till now; no available methods allowing to accurately determine their structures (Subianto, 2006; Alarfaj et al., 2012; Sajjan et al., 2013). There are many factors hindering accurate characterization of melanin and some are the following: Melanins are insoluble in a broad range of solvents and pH. Their purification is difficult which leads to the heterogeneity in their structural features. In addition, the methods to accurately determine the ratio of the various units present in melanin are not yet found. The molecular structure and organization of melanin are complicated and not completely known (Subianto, 2006; Peles, 2011). To completely characterize the polymer, one must be able:

- To determine the molecular weight as well as the monomer(s) sequences. When more than one type of monomers are present, it is necessary to determine their sequence and their special representation;
- To specify the location of all point: determine the location of all polyfunctional monomers;
- To specify the bonding between each pair of monomers (Blois, 1964).

Different studies have been done on conducting polymers for long time because of its interesting chemical complexity (Derby, 2014). This led to the identification of some of its chemical and physical properties. Despite the extensive studies done in the field of conducting polymers, there is this biopolymer (melanin) which technically fulfils the requirement of being a conducting polymer (Subianto, 2006), but has not received any significant attention with regards to its use as an electronic material.

Melanin is a semiconductor thus it can conduct electricity. Melanin is known to have the capacity to absorb in wide range of electromagnetic radiation (from visible light to UV radiations). Melanin is a photo-protective agent for animals. It was also reported that melanin has the capacity to bind different metallic ions. This important property of presenting free radicals makes melanin to be a stable free radical (Kim et al., 2012). Melanins have shown an antiviral activity. It is widely accepted that melanin in human skin plays a crucial part in protecting the nuclei of epidermal cells from damage by solar radiation (Magarelli, 2011). The melanin in eye may also serve a photo-protective role (Kim et al., 2012). Most people know melanin only as a sunscreen, but it also plays a part in thermoregulation system where absorbed solar radiation is converted into heat**.** All these properties of melanin listed above make melanin an attractive material to use in different applications as mentioned below.

## 3.2. Application of melanin

Melanins also have applications in agriculture, medicine, cosmetic and pharmaceutical industries (Tarangini and Mishra, 2013). Many commercial products contain melanin as active ingredients; including creams that act as filters for single-response protection against UV radiation (Alarfaj et al., 2012). Melanins are used in cosmetics to fade defects of the skin diseases called ‘vitiligo’ which is caused by a loss of melanin in the skin, due to destruction of melanin-forming cells known as melanocytes (Magarelli, 2011; Sajjan et al., 2013). Melanins are used in medical field as a contrast in x-ray studies of the digestive

system. It has been shown that melanin can be used as a tool of contrast by being ingested by patients. The production of sunglasses with a high ability to block UV radiations has been done by adding melanin to plastics. Melanin are also used to prevent damage to objects in museums or libraries because when coated to the internal surface of fluorescent lamp, they eliminate entirely the escape of UV light which usually occurs at a low level in these lamps (Magarelli, 2011). The melanin is also consumed in enjoying food from squid in its ink (Derby, 2014). Due to the presence of melanin polymer in sepia ink, sepia ink possesses antimicrobial activity (Peruru et al., 2012). Sepia (the name used for the ink from *Sepia officinalis*) was extensively used from Greco-Roman times through the 19th century as an ink and pigment used in writing, drawing and painting; because of its color and permanence. Sepia ink is also applied for inkjet printers as a non-poisonous black ink (Lee et al., 2013; Derby, 2014). Melanin coating is model of coating for both biological investigations and smart surface science (Bernsmann et al., 2010).

It is expected that there will be many new future applications and products that are based on melanins and this will lead to the increase in demand for melanin. There are many researches being carried out on melanin. Fortunately, melanin is abundant because it can be extracted from animal tissues and plants at low cost (Derby, 2014). One of the challenges for this method is that the melanin obtained generally has low purity and there is variation in composition in each batch. However, this melanin can also be synthesized by chemical methods which guarantee its purity.

## 3.3. Sepia melanin: general characteristics

Sepia melanin is the melanin derived from the ink sack of various species of cephalopoda, more commonly from the cuttlefish *Sepia officinalis* (Centeno and Shamir, 2008). This melanin is insoluble in organic solvents, acids, aqueous solutions, and only partially dissolves in alkaline solutions. Sepia ink from *Sepia officinalis* contains $CaCO_3$, $MgCO_3$, NaCl and $Na_2SO_4$, enzymes and other substances (Magarelli, 2011; Peruru et al., 2012). Purified sepia melanin is a black powder and so hygroscopic that should be refrigerated at -20 ° C to avoid decomposition. Sepia melanin is also sensitive to oxygen, pressure and pulses of radiation which produce a fragmentation of melanosomes similar to what happens in the skin (Magarelli et al., 2010). *Sepia officinalis* from which the commercial sepia melanin used in this project was extracted is shown in **figure 3.1**.

***Sepia officinalis***

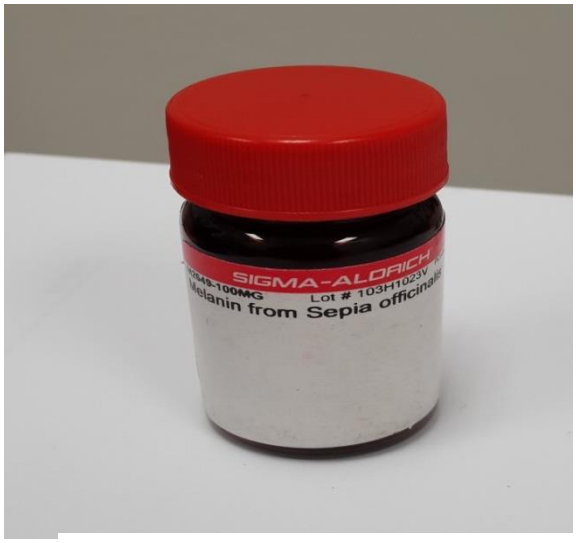


**Sepia melanin from *Sepia officinalis***

***Figure 3.1****: Sepia officinalis and the commercial sepia melanin.*

Inking acts as an anti-predator defense for *Sepia officinalis*. It is a defense coupled to jetting and changes in body coloration, such as in the black-ink-jet maneuver. When the *Sepia officinalis* is frightened and in terror, it produces this blackness and muddiness in the water, as it were a shield held in front of the body (Derby, 2014). Magarelli reported that the melanin in sepia has the character of heavy metal absorbing substances, since the results showed that the heaviest element Fe was absorbed in greater proportion than other metal ions in the structure of sepia melanin (Magarelli, 2011). From this important result, Magarelli suggested that from sepia melanin, it could be possible to open new applications in the industry including solar cells. Because of their high purity and relatively simple procedure; sepia melanin from the ink sacs of *Sepia officinalis* are used as standard for natural melanin (Ju et al., 2012).

## 3.4. Structure of sepia melanin

Sepia melanin is made of eumelanin (refer to the types of melanins explained in **3.1** subchapter) which is the most common form and the type studied in this thesis. Eumelanin is a mixture of polymers that are highly cross-linked and irregular, composed of DHI and DHICA, DHI- and DHICA-derived units. It has been proposed that sepia, a eumelanin, is a copolymer of approximately 20% of 5, 6- dihydroxyindole (DHI)-derived units, and 75% of 5, 6- dihydroxyindole-2-carboxylic acid (DHICA)-derived units. Pyrrole-2, 3-dicarboxylic acids (PDCA) and pyrrole-2, 3, 5-tricarboxylic acids (PTCA) occur in the eumelanin

polymer as a result of the oxidation of the DHI and DHICA units (**figure 3.2**) (Katritzzky et al., 2002; Glassa et al., 2012; Derby, 2014).

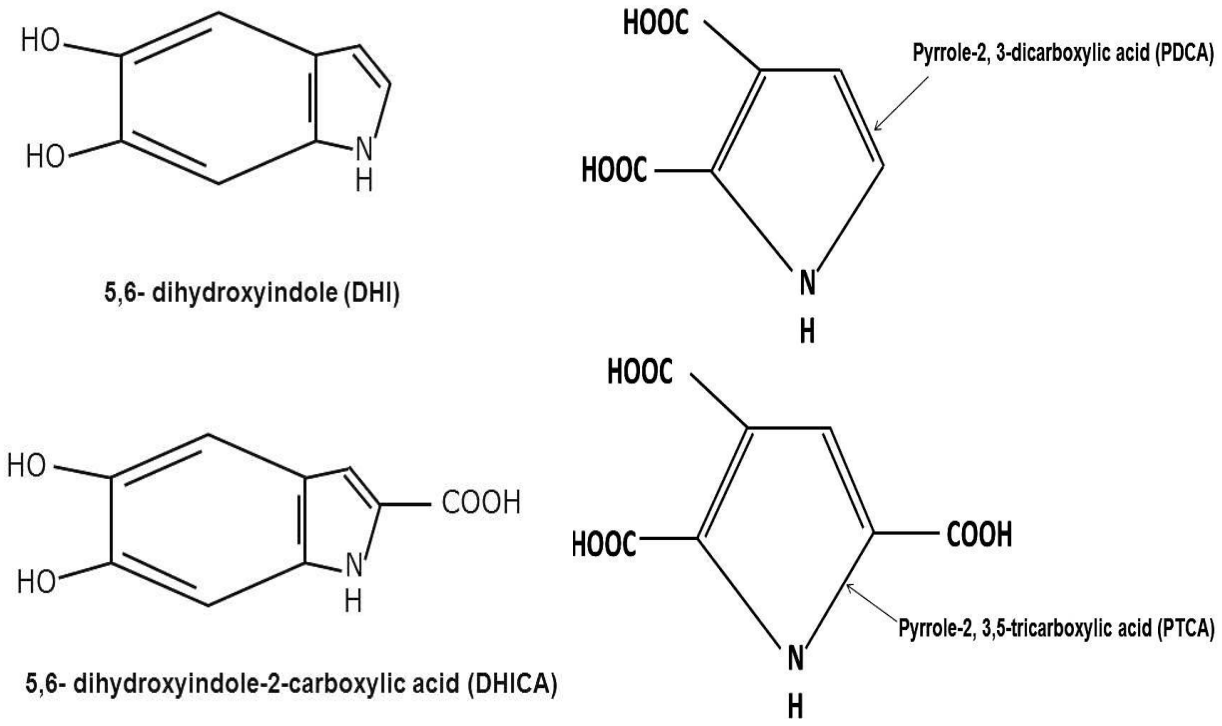


***Figure 3.2**: DHI, DHICA, Pyrrole-2, 3-dicarboxylic acid, and Pyrrole-2, 3, 5- tricarboxylic acid blocks of sepia eumelanin.*

## 3.5. The interest in sepia melanin

Melanin is of interest as a model system of understanding disorder in biological systems. The biological functionality of melanin depends on disorder which is considered as its essential part. This property distinguishes melanin from other much more intensively studied biomolecule systems such as nucleic acid, proteins and carbohydrates (Reisz, 2006).

Even if melanin has a role of photoprotection, it has also been implicated in the chain of event that leads to the malignant melanoma skin cancer. Melanoma is a cancer that begins in the melanocyte and because most of these cells still make melanin, melanoma tumors are often brown or black (Bothma, 2008). The link between melanin and melanoma

cancer is very poorly understood now even if it has shown that highly pigmented skin is more protected from carcinogenesis than low pigmented skin.

Sepia melanin isolated from the ink sacs of *Sepia officinalis*, is commonly used as standard in many researches on melanin characteristics such as spectroscopy, photoreactivity, and morphology of this class of black pigments. This is because of its high purity as more than 98% of melanosomes concentration in tissues is eumelanin. Moreover, sepia melanin is relatively cheap since it is readily available and easily extracted; as it can be isolated simply by centrifugation and purified by washing with distilled water (D'Amico, 2008; Magarelli, 2011).

## 3.6. Biological functions and properties of melanin

A great number of investigations on the role of melanin have been done, but till now it is still not well understood. Melanins have been reported to have a diverse number of functions in the biosystem, including photosensitization, metal ion chelation, photoprotection to absorb a broad range of electromagnetic radiation, antibiotic, thermoregulation (Ju et al., 2012). Melanins are found all over the body from the skin and blood to the nervous system but the role of melanin in all these system is unclear. However, some studies come out with some of its biological functions among them the main one was photoprotection (Subianto, 2006; Tarangini and Mishra, 2013). Melanin has important role in the skin's barrier function by preventing damage by UV radiation. It absorbs UV radiation, thus protecting the cell's nuclei from DNA (Deoxyribonucleic acid) damage (Gawkrodger, 2002; Perna et al., 2013).

Melanin plays important roles in insect ecology including defence against parasites, mate signalling and protection against UV radiation as well as thermoregulation. The role of melanin in thermoregulation has received particular attention (Alarfaj et al., 2012). Many species use behaviour, such as solar basking or avoidance, to achieve the temperatures that are optimal for activity. Melanisation of wings or body increases solar absorption and allows dark-coloured insects to raise their body temperature to the thermal optimal for the activity more effectively than can light-coloured insects under cool condition (Ellers and Boggs, 2004; Karl et al., 2009). Most people know melanin only as a sunscreen but it plays also the role in thermoregulation system. Melanin has potential as an anticancer agent, an antimicrobial properties against a diversity of organisms. Melanin has been reported to have an anti-retroviral activity, a potential target for anti-melanoma therapy; anti-

inflammatory activity as well as anti-oxidant activity (Alarfaj et al., 2012; Fahmy and Soliman, 2013; Derby, 2014).

The level of skin pigmentation significantly affects the incidence of skin cancer, and several of the properties of melanin are thought to be highly significant in providing this protective effect (Derby, 2014). The most well-known characteristic of cutaneous melanin is its ability to absorb much of the visible and UV light spectrum. Melanin also acts as a physical shield to minimise the penetration of UV into the subcutaneous layers. There is little information on other non-photoprotective roles for melanin in the skin. The complex role of melanin as both skin photoprotector and photosensitizer has been the basic of numerous studies. Melanin as skin protector has been attributed to the various functions such as UV filter, light scattered, photon energy dissipater, free radical trap, antioxidant as well as metal chalator (Wondrak et al., 2006; Chen et al., 2013). The other biological function of melanin is the capacity of binding towards various metal ions including heavy metals.

## 3.7. Sepia melanins as broad band sensitizers for DSSC

Melanin is known to have the capacity to absorb in wide range of electromagnetic radiation (from visible light to UV radiations) (Subianto, 2006). Several researches have been carried out to determine the origin of this wide range absorption of melanin and the following three alternative models have been proposed:

- Melanin is an amorphous semiconductor, which naturally results in a broadband absorption spectrum (Longuet-Higgins, 1960; Reisz, 2006);
- The broadband absorbance is due to a scattering phenomenon (Peles, 2011);
- Melanin consists of many chemically distinct species and the broadband spectrum is formed by the superposition of the peaked spectra of these species. This is the so called “chemical disorder model” (McGinness et al., 1974; Reisz, 2006).

An amorphous semiconductor model explains naturally black color of melanin and this prove the broadband absorbance of eumelanin. This model was suggested first in 1960 by Longuet-Higgins (Longuet-Higgins, 1960). The broadband absorption spectrum according to this model is because of the amorphous semiconductor band structure of melanin. In this case, eumelanin is considered as a large indole heteropolymer having a delocalized system. This model was supported by the publication of McGinness et al. (1974) which reported for the first time amorphous semiconductor switching behavior in eumelanin films

(McGinness et al., 1974). Reisz reported that this behavior was only previously observed in inorganic materials (Reisz, 2006).

Melanin which comprises the main component of the *Sepia officinalis* ink pigment, was regarded to motivate the strong interaction with the $TiO_2$ surface and photosensitization. Lee et al. reported that there is the possibility that a purified extract of the squid ink pigment may induce strong interactions with the hydroxyl groups of a $TiO_2$ surface because of the hydroxyl and carboxylic functional groups of eumelanin which are the main component of sepia ink (Lee et al., 2013).

The melanin is a natural photoprotective agent and it is known to have a broadband absorbance in UV-Vis region of solar radiation. Using simple electrochemical means from aqueous solution, melanin can be synthesized. It conducts electricity as it is an amorphous semiconductor. In addition, melanins have free sites which would be free for the binding to the surface (Subianto, 2006). All these features make it an attractive alternative to ruthenium polypyridyl complexes containing a heavy metal, which is undesirable from point of view of the environmental aspects and for which the synthesis process is complicated and costly (O'Regan and Grätzel, 1991; Alhamed et al., 2012).

## 3.8. Conclusion

This chapter was a literature survey about sepia melanin which is the dye of interest in this project. The definition and properties of sepia melanin has been given as well as that one of melanin in general. Unlike other biopolymers having well known structures, the structure of melanin is not well known (Sajjan et al., 2013; Derby, 2014). Melanins are applied in agriculture, medicine, cosmetic and pharmaceutical industries. Because of their high purity and relatively simple procedure; sepia melanin from the ink sacs of *Sepia officinalis* are used as standard for natural melanin.

This chapter provided the structure of eumelanin as the main components of sepia melanin (more than 98% of melanosomes concentration in tissues is eumelanin). There is interest of using sepia melanin as it is relatively cheap, readily available and easily extracted. Many biological functions of melanin have been discussed.

Some attractive features of sepia melanin for DSSC application have been provided. Sepia melanin was reported to have motivated the strong interaction with the $TiO_2$ surface and photosensitization because of the hydroxyl and carboxylic functional groups of eumelanin

which is the main component of sepia melanin (Lee et al., 2013). Sepia melanin is known to have a broadband absorbance in UV-Vis region of solar radiation. Using simple electrochemical means from aqueous solution, melanin can be synthetized. It conducts electricity as it is an amorphous semiconductor. In addition, melanins have several -OH,-COOH function groups which would be free for the binding to the surface.

All these features make it an attractive alternative to ruthenium polypyridyl complexes containing a heavy metal, which is undesirable from point of view of the environmental aspects and for which the synthesis process is complicated and costly.

In the following chapter, the materials used and characterization techniques are discussed. Brief description of analysis techniques used to investigate the morphology, chemical composition, crystalline structure and optical properties of sepia melanin has been provided as well as their respective sample preparation technique used in this project are provided.

## 3.9. References


Alarfaj, N.A., Abdalla, M.A.E. and Al-Hamza, A.M. (2012) 'A Sensitive electrogenerated chemiluminescence assay for determination of melanin in natural and biological samples', *International Journal of Electrochemical Science*, vol. 7, pp. 7888 - 7901.

Alhamed, M., Issa, A.S., Douba and Wael, A. (2012) 'Studying of natural dyes properties as photo-sensitizer for dye Sensitized solar cells (DSSC)', *Journal of electron Devices*, vol. 16, pp. 1370-1383.

Bernsmann, F., Ersen, O., Voegel, J.-C., Jan, E., Kotov, N.A. and Ball, V. (2010) 'Melanin-containing films: Growth from dopamine solutions versus layer-by-layer deposition', *ChemPhysChem*, vol. 11, p. 3299 – 3305.

Blois, M.S. (1964) ' Electron spin resonance studies on melanin', *Biophysical Journal*, vol. 4, p. 487.

Bothma, J.P. (2008) *Exploring the structure-propertyrelationships in eumelanin, Masters thesis*, Brisbane: Queensland University.

Centeno, S.A. and Shamir, J. (2008) 'Surface enhanced Raman scattering (SERS) and FTIR characterization of the sepia melanin pigment used in works of art', *Journal of Molecular Structure*, vol. 873, p. 149–159.

Chen, C.-T., Ball, V., Gracio, J.J.d.A., Singh, M.K., Toniazzo, V., Ruch, D. and Buehler, M.J. (2013) 'Self-assembly of tetramers of 5,6-dihydroxyindole explains the primary physical properties of Eumelanin: Experiment, simulation and design', *American Chemical Society*, vol. 7(2), p. 1524–1532.

D'Amico, F. (2008) *Control of structural conformation and electronic properties of organic semiconductors thin films, Doctoral thesis*, Macerata: Camerino University.

Derby, C.D. (2014) 'Cephalopod ink: Production, chemistry, functions and applications', *Marine Drugs*, vol. 12, pp. 2700-2730.

Derby, C.D. (2014) ' Cephalopod ink:Production, Chemistry, Functions and applications', *Mar. Drugs*, vol. 12, pp. 2700-2730.

Ellers, J. and Boggs, C. (2004) 'Funtional ecological implications of intraspecific differences in wing melanisation in Colias butterflies', *Biological Journal of the Linnean Society*, vol. 82, pp. 79-87.

Fahmy, R., S. and Soliman, A.M. (2013) 'In vitro antioxidant, analgesic and cytotoxic activities of Sepia officinalis ink and Coelatura aegyptiaca extracts', *African Journal of Pharmacy and Pharmacology*, vol. 7(22), pp. 1512-1522.

Gawkrodger, J.D. (2002) *Dermotology, An illustrated Colour Tex*, 3rd edition, Sheffield: Churchill Livingstone.

Giacomantonio, C. (2005) *Charge Transport in Melanin, a Disordered Bio-Organi Conductor*, Brisbane: The Department of Physics, Faculty of Engineering and Physical Sciences, University of Queensland.

Glassa, K., Ito, S., Wilby, P.R.p., Sota, T., Nakamura, A., Bowerse, C.R., Vinther, J., Dutta, S., Summons, R., Briggs, D.E.G., Wakamatsu, K. and Simona, J.D. (2012) 'Direct chemical evidence for eumelanin pigment from the Jurassic period', *PNAS Early Edition*, pp. 1-6.

Huang, Z., Lui, H., Chen, X.K., Alajlan, A., McLean, D.I. and Zeng, H. (2004) 'Raman spectroscopy of in vivo cutaneous melanin', *Journal of Biomedical Optics*, vol. 9(6), p. 1198–1205.

Ju, K.-Y., Lee, Y., Lee, S., Park, S.B. and Lee, J.-K. (2012) 'Bioinspired polymerization of dopamine to generate melanin-like nanoparticles having an excellent free-radical-scavenging property', *Biomacromolecules*, vol. 12, pp. 625-632.

Karl, I., Geister, T.L. and Fischer, K. (2009) 'Intraspecific variation in wing and pupal melanization in copper butterflies (Lepidoptera: Lycaenidae)', *Biological Journal of the Linnean Society*, vol. 98, pp. 301-312.

Katritzzky, A.R., Akhmedov, N.G., Denisenko, S.N. and Denisko, O.V. (2002) '1H NMR spectroscopic characterization of solutions of sepia melanin, sepia melanin free acid and human hair melanin', *Pigment Cells Res*, vol. 15(2), pp. 93-97.

Kim, D.J., Ju, K.-Y. and Lee, J.-K. (2012) 'The synthetic melanin nanoparticles having an excellent binding capacity', *Bull. Korean Chem. Soc*, vol. 33(11), pp. 3788-3792.

Lee, J.-W., Cho, H.-B., Nakayama, T., Sekino, T., Takana, S.-I., Minato, K., Ueno, T., Suzuki, T., Suematu, H., Yoshinori, T. and Niihara, K. (2013) 'Dye-sensitized solar cells using purified squid ink nanoparticles coated on TiO2 nanotubes/nanoparticles', *Journal of ceramic Society of Japan*, vol. 121(1), pp. 123-127.

Longuet-Higgins, H.C. ( 1960) 'On the origin of the free radical property of melanins', *Archivesof Biochemistry and Biophysics* , vol. 86, p. 231.

Magarelli, M. (2011) *Purification, characterization and photodegradation studies of modified sepia melanin Sepia (Sepia officinalis).Determination of Eumelanin content in fibers from Alpaca (Vicugna pacos), Doctoral Thesis.*, Macerata: University of Camerino.

Magarelli, M., Passamonti, P. and Renieri, C. (2010) 'Purification, characterization and analysis of sepia melanin from commercial Sepia ink (Sepia officinalis)', *Rev CES Med Vet Zootec*, vol. 5(2), pp. 18-28.

McGinness, J.E., Corry, P. and Proctor, P. (1974) 'Amorphous semiconductor switching in melanins', *Science*, vol. 183, p. 853.

O'Regan, B. and Gratzel, M. (1991) 'A low-cost, high efficiency solar cell based on dye-sensitized colloidal TiO2 films', *Nature*, vol. 353, p. 737.

Peles, D.N. (2011) *Application of photoemission electron microscopy to melanin and melanosom*, Carolina: Duke University.

Perna, G., Lasalvia, M., Gallo, C., Quartucci, G. and Capozzi, V. (2013) 'Vibrational characterization of synthetic eumelanin by means of raman and surface enhanced raman scattering', *The Open Surface Science Journal*, vol. 5, pp. 1-8.

Peruru, D., S, R., Ahmed VH, N., Sandeep, Priya, S., Raju, S., Nazan, S. and Begum, S. (2012) 'Isolation of eumelanin from Sepia officinalis and investigation of its antimicrobial activity by ointment formulation', *International Journal of Pharmacy*, vol. 2(2), pp. 67-72.

Reisz, J. (2006) *The spectroscopic properties of Melanin, Doctoral Thesis*, Brisbane: University of Queensland.

Sajjan, S.S..A.O., Kulkarni, G.B., Nayak, A.S., Mashetty, S.B., Karegoudar and B., T. (2013) 'Properties and functions of melanin pigment from Klebsiella sp. GSK', *Korean Journal of Microbiology and Biotechnology*, vol. 41(1), p. 60–69.

Subianto, S. (2006) *Electrochemical synthesis of –like polyindolequinone, Doctaral thesis*, Brisbane: Inorganic material research Program, the Queensland University of Technology.

Tarangini, K. and Mishra, S. (2013) 'Production, characterization and analysis of melanin from isolated marine Pseudomonas sp. using vegetable waste', *Research Journal of Engineering Sciences*, vol. 2(5), pp. 40-46.

Wondrak, G.T., Jacobson, K., M., Jacobson and L., E. (2006) 'Endogenous UVA-photosensitizers: mediators of skin photodamage and novel targets for skin photoprotection', *Photochemical& Photobiological Sciences*, vol. 5, p. 215–237

# CHAPTER FOUR: MATERIAL AND CHARACTERIZATION TECHNIQUES

This chapter gives a brief description of the techniques that have been used during this project as well as their respective sample preparations. It is divided into two parts. The first part is related to the materials used and the second part is about techniques and sample preparations.

## 4.1. Materials

Sepia melanin powder (standard) from *Sepia officinalis* was obtained from Sigma-Aldrich (Chemie GmbH Kappelweg 1 D-91625 Schnelldorf, Germany) (**figure 4.1)**. This purified sepia melanin is a black powder, hygroscopic that has been kept refrigerated at - 20° C to avoid any photo-chemical of photo-physical alterations. Methanol HPLC grade, acetone (99%) were used to clean substrates for X-ray diffraction (XRD) analysis sample preparation. For Transmission Electron Microscopy (TEM), it was used to make sepia melanin suspension.

The Fourier Transform Infrared (FTIR) analysis was done on the pellet sample made from KBr (99.99%) from Fluka (Germany) was mixed with sepia melanin. Sodium hydroxide (ACS reagent, ≥97.0%, pellets from Sigma-Aldrich) was used to make the solution of 0.1 mole of sodium hydroxide. The solvent that was used in UV-Vis spectrometry and PL characterization was obtained using this solution drop by drop in deionized water in order to raise its pH up to 10.9354 and this pH was measured. Slides, microscope plain, size 25 mm × 75 mm have been used as substrates for XRD characterization; to prepare the thin films, the concentrated solution was drop-coated on them.

***Figure 4.1**: The commercial sepia melanin (on the left) and its solution as well as the solvent used to make that solution (on the right). The solvent was used to prepare sepia melanin samples for UV-Vis spectrometry and PL characterization. This solvent was obtained using this solution drop by drop in deionized water in order to raise its pH up to 10.9354.*

## 4.2. Characterization techniques

The characterization of sepia melanin for solar cells application requires accurate and well-understood techniques. This chapter presents brief description of various characterisation techniques utilized in this study as well as their respective sample preparations.

Melanins are difficult to characterize because of their intractable chemical properties and the heterogeneity in their structural features. Melanin pigments, in fact, are composed of many different types of monomeric units that are connected through strong carbon-carbon bonds (Magarelli, 2011). Its high insolubility and undefined chemical entities are two obstacles in its complete characterization. An accurate definition of melanin biopolymer does not exist as its structure is not well known till now (Meng and Kaxiras, 2008; Kumar et al., 2013; Arun et al., 2014).

This project aims to investigate the morphology, chemical composition, crystalline structure as well as optical properties of sepia melanin samples. The morphological characterization and particle size distribution for sepia melanin has been done by scanning

electron microscopy (SEM) on surface structure and transmission electron microscopy (TEM) to confirm the morphology obtained from SEM. The chemical composition and crystallinity was determined by Energy X-rays Dispersive (EDS) spectroscopy and XRD respectively. Raman spectroscopy, Fourier transform infrared spectroscopy (FTIR), UV-VIS spectroscopy as well as photoluminescence spectrometer (PL) have been used for optical characterization. Raman and FTIR were used in determining the group functions which are present in sepia melanin, and these function groups serve as the binding cites to $TiO_2$ for DSSC application. The UV-Vis characterisation shows the capacity of sepia to absorb electromagnetic waves as one of the very important criteria for a good dye sensitizer. The best dye sensitizer should absorb photons as much as possible; so that the excited dye molecules will inject many electrons in the conducting band of $TiO_2$ to produce much electricity. **Table 4.1** summarizes all characterization techniques that have been be used in this project.

***Table 4.1****: Analytic techniques required for the study of sepia melanin.*

| Characterization techniques | The expected outcome |
|---|---|
| **Scanning Electron Microscopy (SEM)** | Surface morphology |
| **Energy Dispersive X-Ray Diffraction (EDS)** | Elemental composition |
| **Electron Microscopy(TEM)** | Grain size and morphology |
| **X-ray Diffraction (XRD)** | Crystallinity, grain size and orientation |
| **Fourier Transform Infrared (FTIR)** | The analysis of the structure |
| **Raman spectrometry** | Chemical structure |
| **Ultraviolet-Visible Spectroscopy (UV-Vis)** | Electronic structure, optical properties and chemical structure |
| **Photoluminescence(PL)** | Electronic structure |

## 4.2.1. Scanning Electron Microscopy (SEM) and Energy Dispersive Spectroscopy (EDS)

### *4.2.1.1. Sample preparation*

The sepia melanin powder was coated with gold-palladium (Au: Pd; 6O: 40) layer using a coating sputter coater (Quorum Q 150 TES) to increase the conductivity of the sample. SEM and EDS were performed on the sample using Carl Zeiss Auriga Field Emission Scanning Electron Microscope (FEG SEM) imaging at 5 keV. EDS spectra was collected with an OXFORD instruments X-MAX solid state silicon drift detector at 20 keV.

### *4.2.1.2. Description of technique*

SEM is a type of electron microscopy that images a surface of a sample by scanning it with a beam of electrons in a raster scan pattern. The electrons interact with the atoms that make up the sample, and produce signals that contain information about the sample's surface topography, composition, and other properties such as electrical conductivities (Egerton, 2005).

**Figure 4.2** is a picture of the setup of SEM used during this work, while **figure 4.3** gives the schematic of the principle of the technique.


***Figure 4.2****: Scanning Electron Microscopy (Carl Zeiss Auriga FE-SEM) that has been used in this project.*

The main components of SEM include:

- Source of electron
- Column down which electrons travel with electromagnetic lenses
- Electron detector
- Sample chamber
- Computer and display to view the images

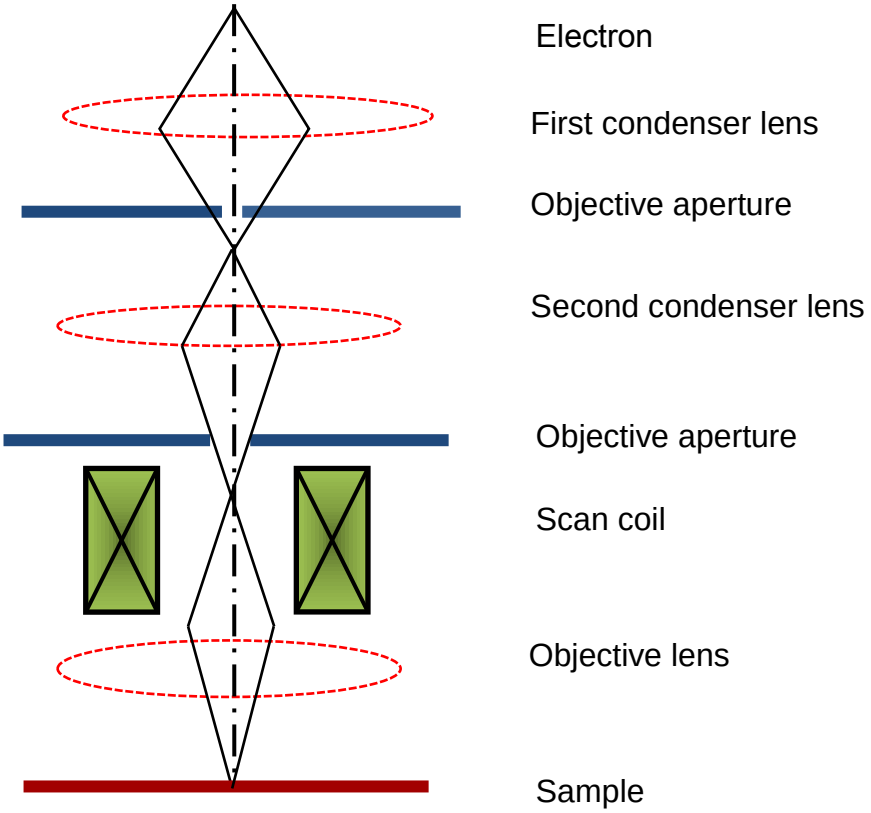


***Figure 4.3**: A schematic diagram of scanning electron microscopy.*

### *4.2.1.3. Theory*

SEM has been widely used in investigating the morphology of various polymers. SEM image shows compositional contrast that result from different atomic number elements and their distribution (Fagerland, 2014). The basic operation of a SEM is the production of electron by heating of a cathode. Among the most commonly used metals to produce electrons, tungsten is the best because of its relatively low work functions and high melting points. The sample is mounted on a stage contained in the chamber area. As electrons travel in vacuum only, the column and the chamber are evacuated by a combination of pumps. The level of the vacuum depends on the design of the microscope (Egerton, 2005; Cummings, 2012; Fagerland, 2014).

The produced electrons at the top are accelerated downwards and passed through a combination of lenses and apertures to produce a fine beam of electrons which hits the surface of the sample. Scan coils which are situated above the objective lens controls the position of the electron beam on the sample. These coils allow the beam to be scanned over the surface of the sample. The electron beam scans; and allows the collection of information about a defined area on the sample as the name of the microscope suggests (Egerton, 2005; Cummings, 2012; Fagerland, 2014).

While SEM micrographs display compositional contrast that results from different atomic number elements and their distribution, EDS allows the identification of what those particular elements are and their relative proportions (atomic % for example). EDS analysis usually involves the generation of an X-ray spectrum from the entire scan area of the SEM (Egerton, 2005). From EDS we get the corresponding X-ray spectra that were generated from the entire scan area by SEM. The Y-axis shows the counts (number of X-rays received and processed by the detector) and the X-axis shows the energy level of those counts (Egerton, 2005; Fagerland, 2014).

## 4.2.2. Transmission Electron Microscopy (TEM)

### *4.2.2.1. Sample preparation*

Sample for TEM analysis were prepared by depositing a small drop of dilute dispersion of sepia melanin ultrasonicated in acetone TEM grids. The TEM grids were coated with a thin amorphous carbon support (~20nm); as it has a relatively low electron density, it provides a uniform substrate for imaging samples. The sample was left 10 minute for approximatively under the lamp light to dry. The ultra-sonication procedure of the solution of sepia melanin powder in acetone created colloidal dispersions without affecting the native chemical structure or composition of the material. No post-processing was conducted on the images presented by TEM. It should also be noted that the acetone ultra-sonication process did not appear to alter the structural or chemical properties of either the synthetic or natural melanins. The dispersions so-produced settled upon standing for several minutes before being dropped onto lays amorphous carbon support.

### *4.2.2.2. Description of technique*

TEM is a powerful tool for directly imaging nanomaterials. It is used in order to obtain quantitative measures of particle; morphology, and/or grain size as well as size

distribution. The formation of images obtained from TEM is due to the transmission of a focused beam of electrons through a sample as the light microscope produces the images (Egerton, 2005; NanoComposix, 2012; Fagerland, 2014).

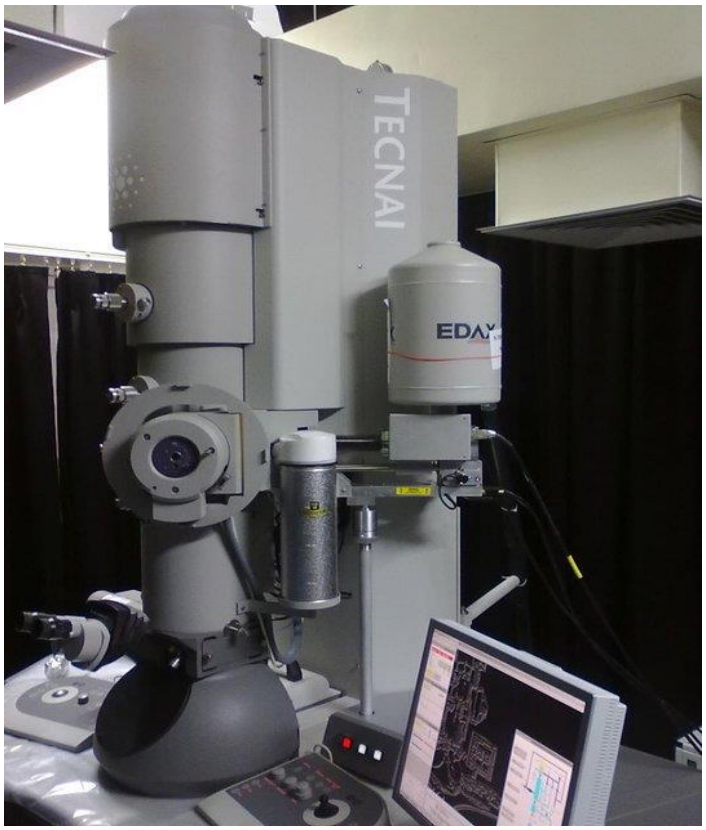


***Figure 4.4:*** *Transmission electron microscope (TEM) used in the experiment.*

HRTEM was used to investigate the internal morphology, and the particle distribution of the sepia melanin nanoparticles. For size and morphology characterization; the measurement of individual non-agglomerated spherical particles is straightforward. An accurate size statistics can be more complicated to obtain when nanoparticles have irregular shape or when they are bound together. In this case, image analyzer softwares such as image-J come in. This software helps to determine the cross-sectional area of the particles and convert the area to an equivalent spherical diameter (Ferreirak and Rasband, 2010; Baecker, 2010; NanoComposix, 2012).

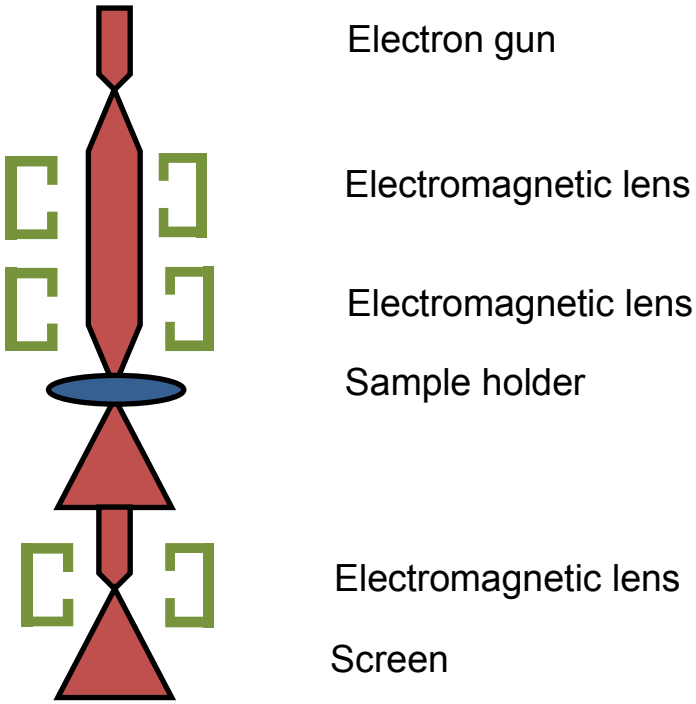


***Figure 4.5**: The schematic representation of transmission electron microscope.*

TEM technique is the most powerful one to investigate at the nanometer scale the structural properties of nanocrystals. It works on the same principle as a light microscope (optical microscope); the only difference is that TEM uses electrons instead of photons. TEM use electrons as 'light source' and as they have much lower wavelength, it is possible to obtain resolutions that are a thousand times better than with a light microscope.

#### *4.2.2.3. Theory*

The working principle of TEM is illustrated (**figure 4.5**) as follows:

1. An electron beam is produced by thermionic emission from a tungsten filament on application of current, and a potential difference generated extracts the electrons. Electrons can also be produced using a field emission gun with a tungsten tip when subjected to intense electric field;
2. This electron beam propagates in vacuum to illuminate the sample to be analyzed. The TEM uses electromagnetic lenses to focus the electrons into a very thin beam;
3. The electron beam then interacts while travelling through the sample. Depending on the density of the material present, some of the electrons are scattered and disappear from the beam;

4. At the bottom of the microscope the unscattered electrons hit fluorescent screen, which gives rise to a 'shadow image' of the sample with its different parts displayed in varied darkness according to their density;
5. The image is then captured with a CCD camera for analysis. It is possible to observe the image area exposed under the electron beam (image mode).

## 4.2.3. X-Ray Diffraction

### *4.2.3.1. Samples preparation*

For XRD analysis, the samples used were thin films of sepia melanin. The preparation procedure of thin films will be described in the following subsections. After preparing the solution to be coated, it was applied to the substrates. For effective coating, the substrate should be well cleaned and the solution to coat should be highly concentrated. The substrate cleaning as well as the coating process is explained below.

- **Preparation of the substrates**

The first step is to cut substrates into 2x2 cm. The cleaning process was done into two steps so that the substrates were ready for drop coating.

First of all, after washing the substrates with deionized water and rinsed them in acetone, they were kept 15 minutes in ultrasonic bath. After this step they were washed and then rinsed in methanol in ultrasonic bath for 15 minutes. Finally the substrates were washed and rinsed with deionized water in the ultrasonic bath. After the entire ultrasonic bath, the substrates were dried in air for half an hour to be ready for drop coating.

- **Drop coating process**

The last step for sample preparation was to drop coat the sepia solution on the cleaned substrates. This process was done and the samples were left for 24 hours to be dried by air. Thus, these samples were ready for XRD measurements.

### *4.2.3.2. Description of the technique*

Atoms are the basic constituent of material. The foundation to build our understanding of properties, synthesis, and structure of the material, is to know better how atoms are arranged into crystals and microstructure. XRD is an experimental technique that allows to identify the crystalline structure of crystalline and polycrystalline materials. The periodic

nature of crystal lattices creates specific rules for the amount of x-rays leaving a sample when bombarded with monochromatic x-rays (Petkov, 2008; Fultz and Howe, 2013). XRD basis is described by the Bragg's equation. Bragg discovered that diffraction could be pictured as a reflection of the incident beam from the lattice planes (**figure 4.6**) (Fultz and Howe, 2013).

***4.2.3.3. Theory***

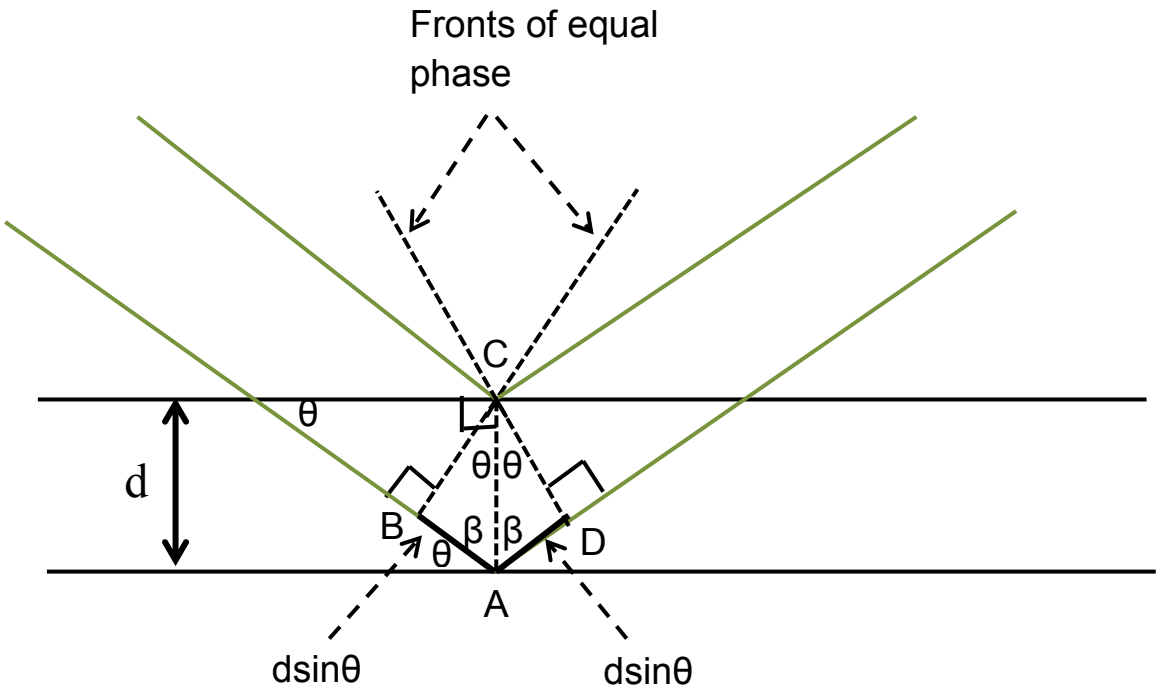


***Figure 4.6****: The geometry for interference of a wave scattered from two planes separated by a spacing d. The dashed lines are parallel to the crests or troughs of the incident and diffracted wave fronts. The important path length difference for the two rays is the sum of the two dark segments.*

**Bragg's law** is used as the simplest way to explain diffraction phenomenon when a monochromatic radiation interacts with a crystalline structure. It gives the condition for constructive interference for x-rays incident on a set of lattice planes. Constructive interference occurs when the intensities of the waves add to each other while the opposite is destructive interference where the intensities cancel each other. It provides a simple relationship between scattering angle and lattice parameter (Petkov, 2008; Lellig, 2011; Fultz and Howe, 2013).

**Bragg's equation** can be derived mathematically as follows: From the triangle ACB, one can prove that the angle $\beta = \frac{\pi}{2} - \theta$, and from triangles ABC and ADB, one can see that,

$$BA = AD = AC\ Cos\beta, \quad (4.1)$$

$$AC = d \quad (4.2)$$

$$BA + AD = 2AD \quad \text{(Path difference)} \quad (4.3)$$

Using equation 4.1 and 4.2 into equation 4.3, we get

$$d\ Cos\beta + d\ Cos\beta = 2AD$$

$$2dCos\left(\frac{\pi}{2} - \theta\right) = 2dsin\theta = 2AD \quad (4.4)$$

The constructive wave interference corresponding to the strong diffraction occurs when from the combination of reflected rays are in phase. This means that their path difference is a whole multiple of the wavelength (Fultz and Howe, 2013).

Therefore; in this case equation 4.4 can be written as,

$$2dsin\Theta = n\lambda \quad (4.5)$$

d: lattice interplanar spacing of the crystal

θ: x-ray incidence angle (Bragg angle)

λ: wavelength of the characteristic x-rays, and

n: an integer constant.

The angle θ is also known as the Bragg's angle. Since the angle of reflection of a plane surface is equal to the angle of incidence, the Bragg angle also defines the scattering angle, which is the angle between the incident radiation and the scattered radiation and equals $2\theta$. The relation **4.5** is known as **Bragg's equation**. It gives the angle *θ*, at which a set of planes of spacing d cooperatively reflects x-radiation of wavelength λ in the $n^{th}$ order.

A typical XRD spectrum shows several peaks at fixed θ angles. By the peaks position, it is possible to identify also the kind of crystals present on the sample (Petkov et al., 2007; Petkov, 2008). From x-ray diffraction pattern of a material; we can get much more information. The sharp and clear diffraction peaks are obtained from the crystals having precise periodicities over long distances. The broadened, distorted, and weakened diffraction peaks are obtained from crystals having defects; as their periodicity in their atomic arrangements are less precise. Even if amorphous materials diffraction patterns

lack sharp diffraction peaks, XRD is used to characterise them (Petkov et al., 2007; Fultz and Howe, 2013; Casadevall et al., 2012).

In analysing the experimental XRD pattern, there are appropriate software packages which are available to identify peaks and then search from the International Centre for Diffraction Data (ICDD) database to find candidate materials. In the case of the sample containing a mixture of unknown crystalline phases; computerized searches for pattern matches are particularly valuable. The task of indexing a diffraction pattern is helped with information about chemical compositions and candidate crystal structures. The phase of the material to be analysed by XRD can be identified with handbooks of phase diagrams, and their diffraction patterns found in the ICDD database (Fultz and Howe, 2013). The atomic pair distribution function (PDF) technique which is a specialized approach, has been developed to analyse diffuse (i.e. non-Bragg type) XRD patterns and obtain important structural information for bulk non-crystalline materials such as near atomic neighbor separations and coordination numbers (Petkov et al., 2007).

Even if a computerized match of full patterns has been found often to be helpful, there can be confusion to assign a diffraction peak to a specific diffraction pattern when the sample contains multiple phases where there is an overlapping of peaks from different patterns. It is easy to distinguish individual diffraction patterns, but sometimes the crystalline diffraction pattern is not indexed (Fultz and Howe, 2013).

## 4.2.4. Fourier Transform Infrared Spectrometry

### *4.2.4.1. Sample preparation*

In preparing samples for FTIR investigation; the amount of sepia melanin (standard) was about 4 mg. This amount was mixed with about 1400 mg of KBr. In order to ensure that the produced pellets enable accurate spectra, the mixture was blended using a mortar and pestle. The obtained powder was compressed into pellets by using hydraulic press (Beckman 00-25 Glenrothes five Scotland). This pellet was ready for FTIR analysis.

### *4.2.4.2. Description of technique*

The characterization of the material by using FTIR spectroscopy consists in making a spectrum of radiation energy absorbed by material molecules and interpretation of the obtained spectrum. FTIR spectroscopy technique is usually one of the most preferred techniques used to give a correct assignment of the observed spectral characteristic of

functional groups corresponding to different absorption bands which are responsible of the absorption (Centeno and Shamir, 2008). FTIR is the characterization technique which is both rapid, non-destructive and requires small sized samples. In the material to be analysed, chemical bonds vibrate at a characteristic frequency representative of their structure, bond angle and length (Swann and Patwardhan, 2011). Their individual molecules have the ability to interact with incident radiation by absorbing the radiation at specific wavelengths. To individual absorption peaks, individual chemical bonds can be identified and assigned in order to identify qualitatively or quantitatively individual compounds in complex systems (Sundar, 2012).


***Figure 4.7****: Fourier Transform Infrared Spectroscopy (The Thermo Scientific Nicolet iS10) used in this project.*

FTIR spectrometer is important for the interpretation of the structure, binding capacity, affinity and sites of metal ions in melanin. These are important factors for better understanding the metals melanin complexity and its consequences (Magarelli, 2011). FTIR spectroscopy is measurement of the wavelength and intensity of the absorption of mid-infrared light by a sample. Mid-infrared light (4000 - 200 $cm^{-1}$) is energetic enough to excite molecular vibrations to higher energy states (Swann and Patwardhan, 2011).

The wavelength of many IR absorption bands is characteristic of specific types of chemical bonds, and IR spectroscopy finds its greatest utility for qualitative analysis of organic and

organometallic molecules. IR spectroscopy is used to identify particular compound or a newly synthesized molecule (D'Amico, 2008).

#### *4.2.4.3. Theory*

For FTIR spectroscopy, IR radiation is passed through a sample. A part of the radiation is absorbed by the sample and the other part is transmitted. The FTIR spectrum represents the absorption and transmission of the molecular in creating a spectral fingerprint of the sample. To overcome the slow scanning speeds of older dispersion infrared instrument, the method that measures all of the infrared frequencies simultaneously, rather than individually is used (Heerden, 2009).

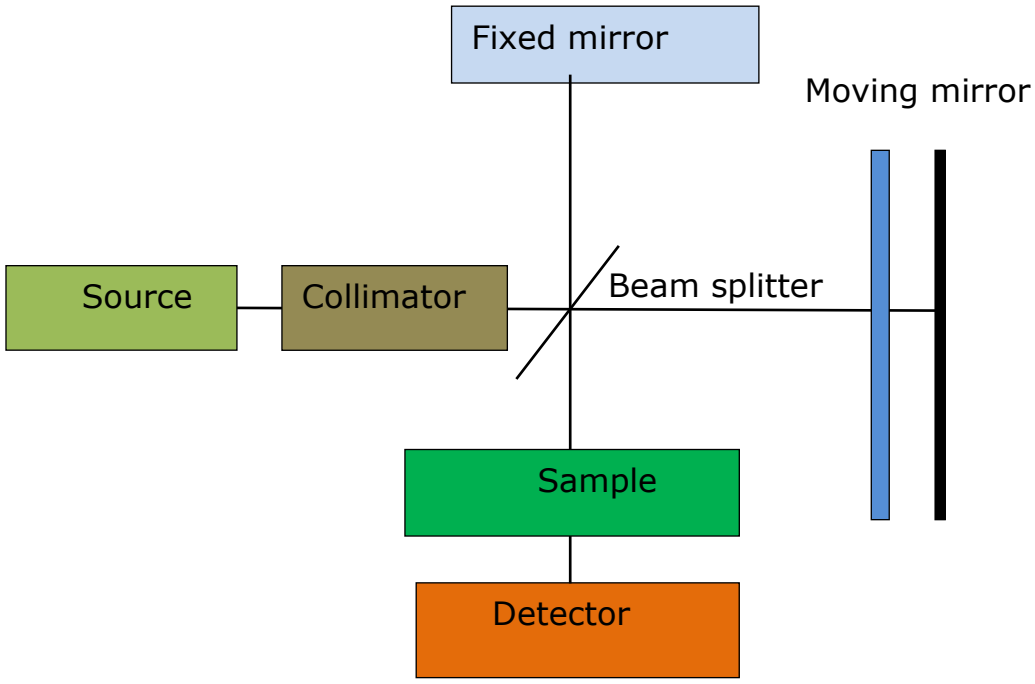


***Figure 4.8:*** *Block diagram of an FTIR spectrometer.*

A common FTIR spectrometer consists of a source, interferometer, sample compartment, detector, amplifier, A/D convertor, and a computer. The source generates radiation which passes the sample through the interferometer and reaches the detector. Then the signal is amplified and converted to digital signal by the amplifier and analog-to-digital converter, respectively. Eventually, the signal is transferred to a computer in which Fourier transform is carried out. FTIR spectrometer operates on principle called *Fourier transform*. The mathematical expression of Fourier transform $F(\omega)$ is given by:

$$F(\omega) = \frac{1}{2}\int_{-\infty}^{+\infty} f(r)e^{i\omega r}\,dr \qquad (4.6)$$

And the reverse Fourier transform $f(r)$ is given by

$$f(r) = \frac{1}{2\pi}\int_{-\infty}^{+\infty} F(\omega)e^{-i\omega r}\, d\omega \qquad (4.7)$$

where $\omega$ is angular frequency, $r$ is the optical path difference, $F(\omega)$ is the spectrum, and $f(r)$ is called the interferogram.

The interferogram is determined experimentally in FTIR spectroscopy, and the corresponding spectrum (frequency against intensity plot), is computed using Fourier transform. This transformation is carried out automatically and the spectrum is displayed.

The core of FTIR spectrometers is the Michelson interferometer that is used to split one beam of light into two so that the paths of the two beams are different. The Michelson interferometer recombines the two beams and conducts them into the detector. In the detector, the difference of the intensity of these two beams is measured as a function of the difference of the paths.

The basic integral equation used in the Fourier transform spectroscopy can be derived from the definition of Fourier integral theorem and the principle of superposition of waves mathematically as follows:

Let the amplitude of the wave (traveling in the *z* direction) incident on the beam splitter be given as

$$E(z,\nu) = Eo(\upsilon)e^{(i\omega t - 2\pi\upsilon z)}d\upsilon \qquad (4.8)$$

Where $Eo(\upsilon)$is the maximum amplitude of the beam at $z = 0$. The amplitude of the beam is divided at the beam splitter and two beams are produced. Let $z_1$ and $z_2$ be the distances traveled by the beams when they recombine. Each beam undergoes one reflection from the beam splitter and one transmission through the beam splitter. If $s$ and $t$ are the reflection and transmission coefficients, respectively, of the beam splitter, then the amplitude of the recombined wave $Er$ is given by

$$Er[z_1, z_2, \upsilon] = stEo(\upsilon)[e^{(i\omega t - 2\pi\upsilon z_1)} + e^{(i\omega t - 2\pi\upsilon z_2)}]d\upsilon \qquad (4.9)$$

By definition, the intensity after recombination of the beams for the fixed $d\upsilon$ spectral range is given as

$$I(z_1, z_2, \nu)d\nu = Er((z_1, z_2, \nu)Er^*(z_1, z_2, \nu)d\nu \qquad (4.10)$$

This equation leads to

$$2E_0^2(\upsilon)|st|^2[1+\cos(2\pi(z_1-z_2)\upsilon]d\nu \quad (4.11)$$

The total intensity at any path difference $x = z_1 - z_2$ for the whole spectral range is obtained by the integration of

$$Ir(x) = 2|st|^2 \int_0^\infty E_0^2(\upsilon)d\upsilon + 2|st|^2 \int_0^\infty E_0^2(\upsilon)\cos(2\pi x\upsilon]d\nu \quad (4.12)$$

Fourier transform converts intensity into spectrum as

$$E_0^2(\upsilon) = (1/\pi|st|^2 \int_0^\infty [I_r(x) - \tfrac{1}{2}I_r(0)]cos2\pi\upsilon x dx \quad (4.13)$$

In equation 4.13, $I_r(0)$ represents the flux associated with waves at zero arm displacement where the waves for all frequencies interact coherently. Thus, $I_r(0)$ is the flux associated with coherent interference and $I_r(x)$ is the flux associated at path difference $x$. $[I_r(x) - \frac{1}{2}I_r(0)]$ is called the *interferogram,* i.e., the oscillations of the signal about the value $\frac{1}{2}I_r(0)$.

## 4.2.5. Raman spectroscopy

### *4.2.5.1. Description of the technique*

Raman spectroscopy is the study of the chemical structure and physical form of a molecule, identification of substances from characteristic spectral patterns and quantitative determination of the amount of a substance in a sample.

In this project Raman spectroscopy has been used as a complementary technique to FTIR to analyse the chemical structure of sepia melanin. For this technique, a monochromatic radiation is used to irradiate the sample and then scattered from the molecule with one vibrational unit of energy different from the incident beam. The information on the vibrational modes in the measured sample is provided by the energy shift of Raman scattered light towards low (Stokes) as well as high (Anti-Stoke) frequencies (Sundar, 2012). This unit of energy, which is characteristic of the scattering molecule is detected and measured. From the obtained spectrum, one can identify the vibrations of a molecule (Huang et al., 2004; Centeno and Shamir, 2008).

For Raman spectroscopy analysis, there is observation of associated with incident radiation and another pair of new wavenumbers. The origin of the modified frequencies

found in Raman scattering is explained in terms of energy transfer between the scattering system and the incident radiation. During the interaction between system and radiations, the system undergoes the transition from a lower energy level to an upper energy level. This transition is due to the gain of energy from incident radiation. Raman shifts are typically reported in wavenumber, which have units of inverse length, as this value is directly related to energy (Sundar, 2012; Murphy, 2013).

#### *4.2.5.2. Theory*

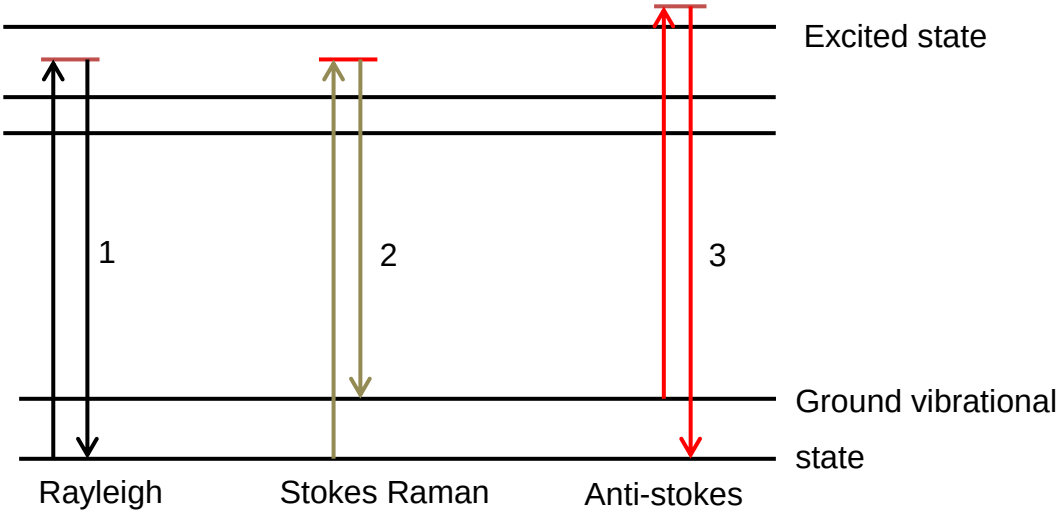


***Figure 4.9**: Diagram of the Rayleigh and Raman scattering processes When the light wave with a given wavenumber interacts with the molecules, the most of its part is transmitted without change in wavenumber and this phenomenon is called Rayleigh scattering (1) while the scattered radiation is released (Raman scattering) with different wave number (2 and 3).*

We can use classical electrodynamics to understand the cause of both Raman and Rayleigh scattering. The following derivation is from Murphy ( 2013).

The electric field of an incident laser beam is given by

$$E(t) = E_0 \cos 2\pi\upsilon_0 t \qquad (4.14)$$

where $\upsilon_0$ is the laser frequency. When the laser light illuminates a sample of interest, this electric field polarizes the material. The induced dipole moment is given by

$$p = \alpha E(t) = \alpha\, E_0 \cos 2\pi\upsilon_0 t \qquad (4.15)$$

where $\alpha$ is the atomic or molecular polarizability of the sample. Because the electric field is oscillatory, the polarization of the material will also vary, although not necessarily at the same frequency. The displacement of atoms in the material due to this varying polarization

will excite the normal modes of oscillation of the sample structure. The atomic displacements (specifically those of the nuclei) in the sample are given by

$$q = q_0 \cos 2\pi \upsilon_m t \tag{4.16}$$

where $q$ is the displacement, and $\upsilon_m$ is the frequency of a normal mode of oscillation. Because the induced dipole moment, which depends on displacement of charges, is related to the polarizability equation 4.15, the polarizability is related to the nuclear displacement (4.16). For small-amplitude vibrations, we can make the approximation

$$\alpha = \alpha_0 + \left(\frac{\partial \alpha}{\partial q}\right)_0 q \tag{4.17}$$

where $\alpha_0$ the unperturbed polarizability and the derivative is evaluated at equilibrium (no nuclear displacement, the relaxed state

By substituting equation 4.17 into equation 4.15, we obtain

$$p = \alpha_0 E_0 \cos 2\pi \upsilon_0 \ t + \left(\frac{\partial \alpha}{\partial q}\right)_0 q E_0 \cos 2\pi \upsilon_0 \ t \tag{4.18}$$

And then by substituting equation 4.16 into equation 4.18, we obtain

$$p = \alpha_0 E_0 \cos 2\pi \upsilon_0 \ t + \left(\frac{\partial \alpha}{\partial q}\right)_0 q_0 E_0 \cos 2\pi \upsilon_0 \ t \cos 2\pi \upsilon_m t \tag{4.19}$$

Finally, by using a trigonometric identity, we arrive at a useful result

$$p = \alpha_0 E_0 \cos 2\pi \upsilon_0 \ t + \frac{1}{2}\left(\frac{\partial \alpha}{\partial q}\right)_0 q_0 E_0 \left[\cos\{2\pi \ (\upsilon_0 + \upsilon_m) \ t \ \} + \cos\{2\pi (\upsilon_0 + \upsilon_m) \ t\}\right] \tag{4.20}$$

The first term in this expression gives rise to Rayleigh scattering; the dipole radiation re-emitted from the induced dipole has the same frequency as the incident radiation $(\upsilon_0)$. The second term gives rise to Raman scattering; radiation of two distinct shifted frequencies is reradiated from the induced oscillating dipole. The re-emitted radiation in this case has frequencies that are shifted down (Stokes scattering) and up (anti-Stokes scattering) by a normal mode frequency.

An important feature of equation 4.20 is the partial derivative attached to the Raman scattering term. This factor indicates that for Raman scattering to occur, the polarizability of the material must change with small vibrational displacement from equilibrium. In effect, for a vibrational mode to be Raman active, the associated displacement must change the polarizability of the material around the bond.

## 4.2.6. UV-Vis absorption spectroscopy

### *4.2.6.1. Sample preparation*

Sepia melanins are sparingly insoluble in water at neutral pH or in the organic solvent commonly used in UV-Vis spectroscopy; thus the solvent used here was ultrapure water at pH 10.93 adjusted by adding the amount of 0.1M NaOH drop by drop. To make sepia melanin solution, 10mg of sepia melanin were weighed and dissolved into 100 ml of water at pH 10.93.

### *4.2.6.2. Description of technique*

UV-visible spectroscopy refers to the measurement of the wavelength and intensity of absorption of electromagnetic waves by a sample (Magarelli, 2011; Cummings, 2012). Useful ultra-violet (UV) and visible (Vis) absorption spectra are produced by the absorption of electromagnetic radiation with wavelengths in the 200-400 nm (UV) and 400 to 800 nm (Vis) regions of the electromagnetic radiation. The UV region having highest energies and the shortest wavelengths (100-200 nm), is difficult to make measurements in and is relatively uninformative. The UV-Vis spectra have broad features that are of limited use for sample identification but are very useful for quantitative measurements.

Ultraviolet and visible light are energetic enough to promote outer electrons to higher energy levels. Since the UV-Vis range reaches over the range of human visual acuity of approximately 400 - 750 nm, UV-Vis spectroscopy is useful to characterize the absorption, transmission, and reflectivity of a variety of technologically important materials, such as pigments, coatings, windows, and filters. For recording at least a portion of UV-Vis spectrum in order to characterize the optical or electronic properties of the material, UV-Vis spectrometry is applied.

### *4.2.6.3. Theory*

When light impinges on an organic compound such as polymers having a high degree of conjugations, they absorb radiations in UV-Vis region of electromagnetic wave spectrum. The photons having energy less than the band gap are transmitted whereas those of equal or greater than the band gap are absorbed. Molecules within the polymer undergo electronic transitions from the ground state to the excited state (Heerden, 2009). The absorption of a photon is responsible for this transaction as it make an electron to jump

from the band at lower energy to the one above with higher energy. The transaction is only possible if there is an electron in the ground state in the lower band.

The ratio of the radiation intensity transmitted by the film of thickness $x$ ($I_x$) to that transmitted by a known reference ($I_0$) is known as the transmittance ($T$) of the film and is given by:

$$T = \frac{I_x}{I_0} \tag{4.21}$$

The transmittance is often measured in percent ($\%T$), because many instruments are calibrated with its very convenient scale of 0 to 100. In this case the more useful quantity is the amount of radiation absorbed which consists of absorbance ($A$). This quantity is given by:

$$A = ln\frac{I_O}{I_x} = ln\frac{1}{T} \tag{4.22}$$

The equation 4.22 can also be written as:

$$A = ln1 - lnT = -lnT$$

Or $$A = -lnT \tag{4.23}$$

The possible energy absorptions vary depending upon the nature of the bonds within a molecule. For organic molecules, one can find electrons in strong $\sigma$ bonds, in weak π bond or non-bonding, n. While absorption of energy, all of these types of electrons can jump to excited anti-bonding states which is free.

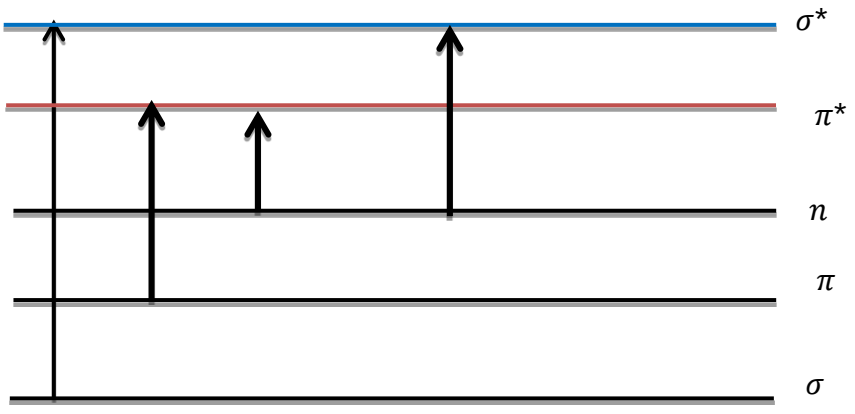


***Figure 4.10**: Various possible electronic transitions in a molecule.*

The diagram in **figure 4.10** presents the situation where the anti-bonding states are noted with an asterisk as $\sigma$* and $\pi$*.

Most $\sigma \rightarrow \sigma^*$ absorption transition for individual bonds occur below 200 nm in the vacuum/ultraviolet region. The $\pi \rightarrow \pi^*$ and $n \rightarrow \pi^*$ absorptions occur in the near ultraviolet/visible region. Various wavelengths of radiation are absorbed by different molecules that are present in the solution. Therefore, there are various light absorbing and these groups are known as chromophores (Magarelli, 2011).

### 4.2.7. Photoluminescence spectrometry

The process of photoluminescence (PL) consists of a process by which a substance absorbs photons and re-radiates it through various mechanisms. This technique is widely used to investigate the energy levels of materials in providing fundamental information on the electronic properties and impurity levels of these materials. To record PL spectra, the sample of material under investigation is excited by a laser, with energy higher than the optical band gap (Eg) of the material. This lead to the generation of electron-hole pairs (excitons) that recombine by one of several mechanisms (Riesz, 2007; Cummings, 2012).

For PL measurements; the same procedures used for sample preparation for UV-Vis has been used but with variation of concentration. Photoluminescence emission spectra for the sepia melanin were recorded using Nanolog$^{TM}$ spectrofluometer. A band passes of side entrance, exit as well as first intermediate slits were 5 nm. The increment of 1.00 nm and an integration of 0.1 s were used. Spectra were automatically corrected to account for differences in pump beam power at different excitation wavelengths using a reference beam. Background scans were performed under identical instrumental conditions with the deionized water. Spectra were collected using quartz 1 cm square cuvette.

## 4.3. Conclusion

This chapter has given a brief description of the techniques that have been used during this project. For each technique; a brief description, theory as well as the corresponding sample preparation were discussed. The techniques discussed are classified according to their expected characterization on sepia melanin.

Morphological characterization has been done by SEM and TEM. These characterization techniques provided different micrographs showing the morphological structure of sepia melanin. In order to determine size distribution from the micrographs; image-J software was used, and histograms from the obtained data was plotted.

The crystalline structure characterization and elemental composition of sepia melanin have been performed by XRD and EDS respectively. The XRD provided the X-ray pattern diffraction giving information of the crystallinity whereas EDS provided information on the elements composition of sepia melanin.

Optical spectroscopy using FTIR, Raman, UV-VIS and PL spectroscopy have been useful for sepia melanin analysis. The important functional groups which are the binding cites of $TiO_2$ can be determined from FTIR and Raman spectra. UV-Vis spectra provide the information about the intensity of absorbance of sepia melanin. This is one of the criteria for the choice or rejection as of sepia melanin as DSSC dye sensitizer.

The following chapter reports the results obtained from all these characterization techniques, and the discussion on each result is provided. The results and discussion are done in the following order: the first results and their respective discussions are for morphological characterization (TEM and SEM). The following are the discussion of the results for the chemical elemental characterization (EDS) and XRD for crystallinity characterization. Finally, the results from FTIR, Raman, UV-VIS as well as PL for optical characterization are discussed. From all obtained results and discussion, the conclusion is provided.

## 4.4. References


Arun, G., Angeetha, M., Eyini, M. and Gunasekaran, P. (2014) 'Effect of copper sulphate and resorcinol on the extracellular production of melanin and laccase by Schizophyllum commune Fr. and Pleurotus cystidiosus var. Formosensis', *Indian Journal of Advances in Plant Research*, vol. 1(5), pp. 55-61.

Baecker, V. (2010) 'Workshop: Image processing and analysis with ImageJ and MRI Cell Image Analyzer', in *Image processing and analysis with ImageJ and MRI Cell Image Analyzer*, Montpellier RIO Imaging.

Casadevall, A., Nakouzi, A., Crippa, P.R. and Eisner, M. (2012) 'Fungal melanins differ in planar stacking distances', *PLoS ONE*, vol. 7(2).

Centeno, S.A. and Shamir, J. (2008) 'Surface enhanced Raman scattering (SERS) and FTIRcharacterization of the sepia melanin pigment used in works of art', *Journal of Molecular Structure*, vol. 873, p. 149–159.

Cummings, F.R. (2012) *TiO2 nanotube based dye- sensitized solar cells, PhD thesis*, Cape Town: Uniiversiitty of the Western Cape.

D'Amico, F. (2008) *Control of structural conformation and electronic properties of organicsemiconductors thin films, PhD Thesis* , Department of Physics, Camerino University.

Egerton, R.F. (2005) 'An Introduction to TEM, SEM, and AEM', in *Physical Principles*, Alberta: University of Alberta.

Fagerland, S.K. (2014) *Investigation of focused ion Beam/scanning electron microscope parameters for slice and view and Energy dispersive X-ray spectroscopy of embedded brain tissue, Masters thesis*, Norwegian University of Science and Technology.

Ferreirak, T. and Rasband, W. (2010) *ImageJ user guide*, ImageJ/Fiji 1.46.

Fultz, B. and Howe, J. (2013) 'Transmission Electron Microscopy and Diffractometry of Materials', in *Graduate Texts in Physics*, Springer-Verlag Berlin Heidelberg.

Heerden, B.A.V. (2009) *Charge transfer efficiency and optical properties of P3HT/PCBM spin coated thin films, Masters thesis*, University of the Western Cape.

Huang, Z., Lui, H., Chen, X.K., Alajlan, A., McLean, D.I. and Zeng, H. (2004) 'Raman spectroscopy of in vivo cutaneous melanin', *Journal of Biomedical Optics* , vol. 9(6), p. 1198–1205.

Kumar, C.G., Sahu, N., Reddy, G.N., Prasad, R.B.N., Nagesh, N. and A., K. (2013) 'Production of melanin pigment from Pseudomonas stutzeri isolated from red seaweed Hypnea musciformis', *Letters in Applied Microbiology*, Available: ISSN 0266-8254.

Lellig, P. (2011) *Application of a hybrid blocking layer in dye-sensitized solar cells, Doctoral thesis*, Mainz: Johannes Gutenberg-Universität.

Magarelli, M. (2011) *Purification, Characterization and Photodegradation studies of modified sepia melanin (Sepia officinalis). Determination of Eumelanin content in fibers from Alpaca (Vicugna pacos), Doctoral Thesis.*, University of Camerino.

Meng, S. and Kaxiras, E. (2008) 'Theoretical models of eumelanin protomolecules and their optical properties', *Biophysical Journal* , vol. 94, p. 2095–2105.

Murphy, B. (2013) *Investigations into anomalous spectroscopic effects in GE124 and recomandations for alternative materials, Bacheror thesis*, California: Pomona College, Claremont.

NanoComposix (2012) 'Transmission Electron Microscopy Analysis of nanoparticles', *NanoComposix*, vol. 1(1).

Petkov, V. ( 2008) 'Nanostructure by high energy X-ray diffraction', *Materialstoday*, vol. 11(1).

Petkov, V., Ohta, T., Hou, Y. and Ren, Y. (2007) 'Atomic-scale structure of nanocrystals by high-eEnergy X-ray diffraction and atomic pair distribution function analysis: study of FexPd100-x (x ) 0, 26, 28, 48) nanoparticles', *Journal of Physics and Chemicastry*, vol. 111(2) , pp. 714-720.

Riesz, J. (2007) *The spectroscopic properties of melanin, Doctoral thesis*, The University of Queensland.

Sundar, P.N.R. (2012) *Films minces à base de Si nanostructuré pour des cellules photovoltaïques de 3ème génération, These de doctorat*, Université de Caen Basse-Normandie.

Swann, G.E.A. and Patwardhan, S.V. (2011) 'Application of Fourier Transform Infrared Spectroscopy (FTIR) for assessing biogenic silica sample purity in geochemical analyses and palaeoenvironmental research ', *Climate of the Past*, vol. 7, p. 65–74.

# CHAPTER FIVE: RESULTS AND DISCUSSIONS

## 5.1. Morphological characterization and chemical composition

### 5.1.1. Scanning Electron Microscopy (SEM) and Energy Dispersive Spectroscopy (EDS)

#### *5.1.1.1. Scanning Electron Microscopy*

SEM and EDS were performed on the same sample using Carl Zeiss Auriga Field Emission Scanning Electron Microscope (FEG SEM) imaging at 5 keV. EDS spectra was collected with an OXFORD instruments X-MAX solid state silicon drift detector at 20 keV.

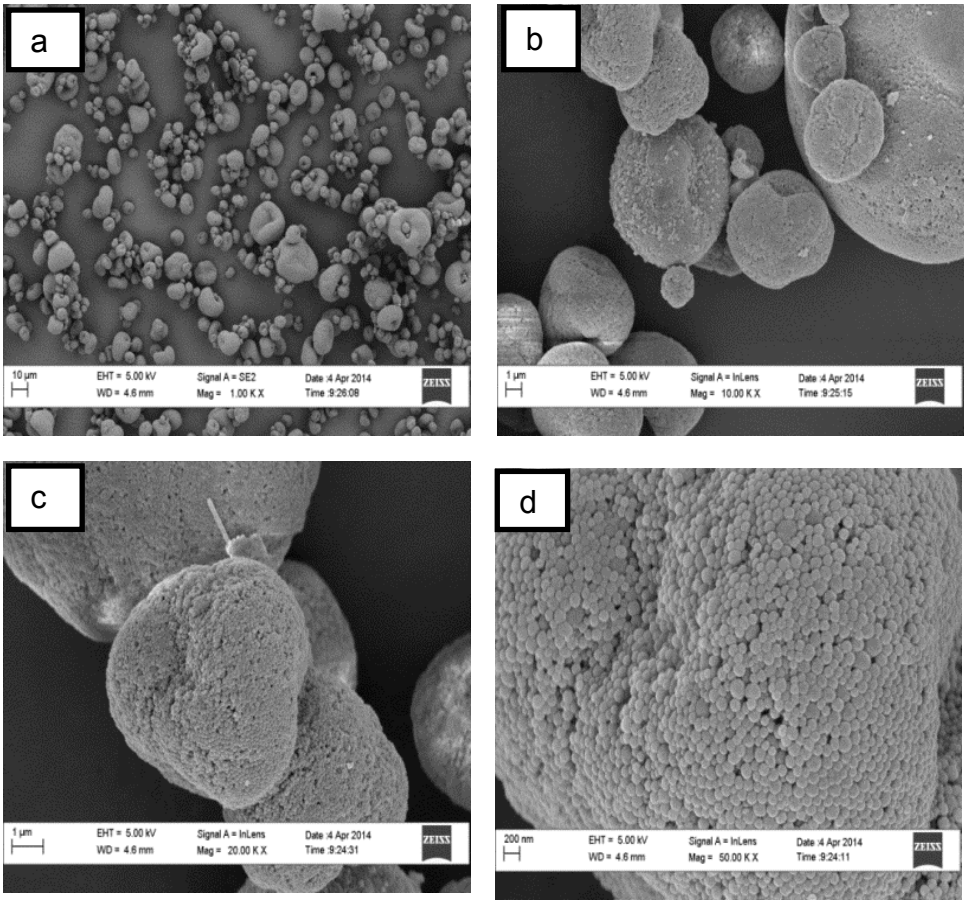


***Figure 5.1****: SEM micrographs of sepia melanin granules at 1.00K X (a), 10.00K X (b), 20.00 K X (c) and 50.00 K X (d) magnifications.*

The sepia melanin powder was coated with gold-palladium (Au: Pd; 6O:40) layer using a coating sputter coater (Quorum Q 150 TES) within 10 minutes to increase the conductivity

of the sample. The low resolution SEM micrographs of the sepia melanin sample are shown on **figure 5.1**.

Sepia melanin is formed by many aggregates agglomerated together. These aggregates are formed also by small spherical granules with different size distributions and this start to become clear at the higher resolution. At a scale of 10 µm and1.00 K X magnification, sepia melanin appeared to be formed by aggregates with different sizes that are grouped together (**figure 5.1a**). In increasing the magnification 10 times and reducing the scale to 1 µm, the aggregates seem to be formed by small granules (**figure 5.1b**). When the magnification is increased further up to 20.00 K X at the same scale, the small granules forming the aggregates start to be a little beat clear **(figure 5.1c)**. Due to the increasing of magnification further up to 50 K X, and change the scale from micro-meters to nanometers order (from 1 µm to 200 nm), granules start appearing to be spherical (**figure 5.1d**). The histogram of diameter distribution for sepia melanin aggregates measured from **figure 5.1a** is shown on **figure 5.2.**

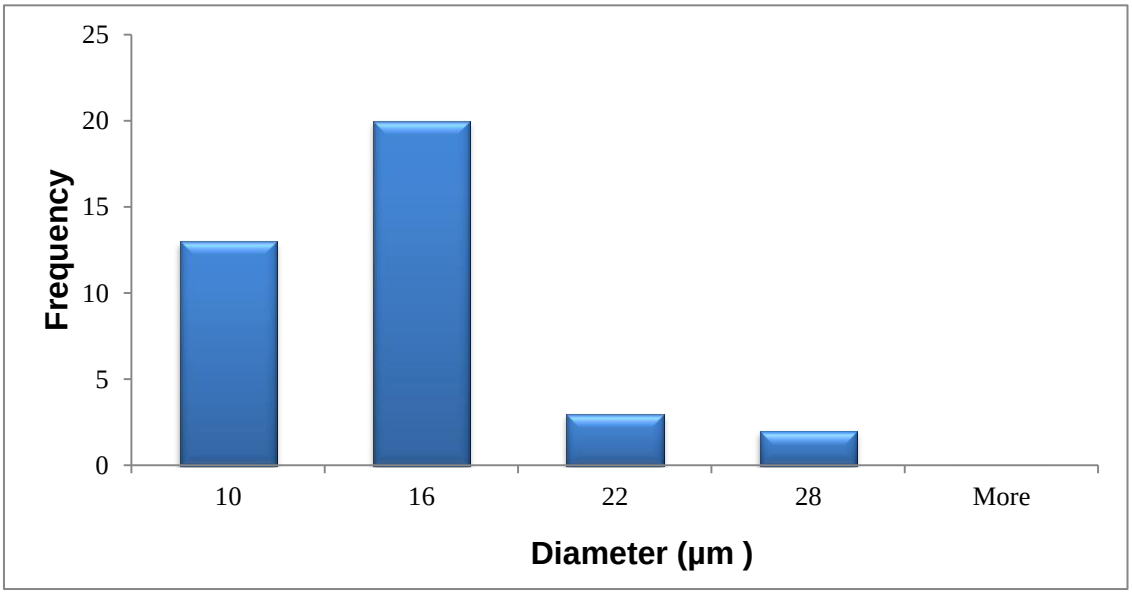


***Figure 5.2**: Diameter distributions of sepia melanin aggregates (**figure 5.1a**).*

The measured aggregate diameters were in between 6 - 30 µm, and the calculated average diameter is about 12 µm. After finding the diameter distribution of sepia melanin aggregates, the diameters of their small granules were measured. The measurement was done on two 100 nm scaled SEM micrographs at different magnification (100 K X and 200 K X) as shown in **figures 5.3** and **5.5**, respectively. Both result revealed that the granule diameters are in the range of 100 nm and 200 nm.

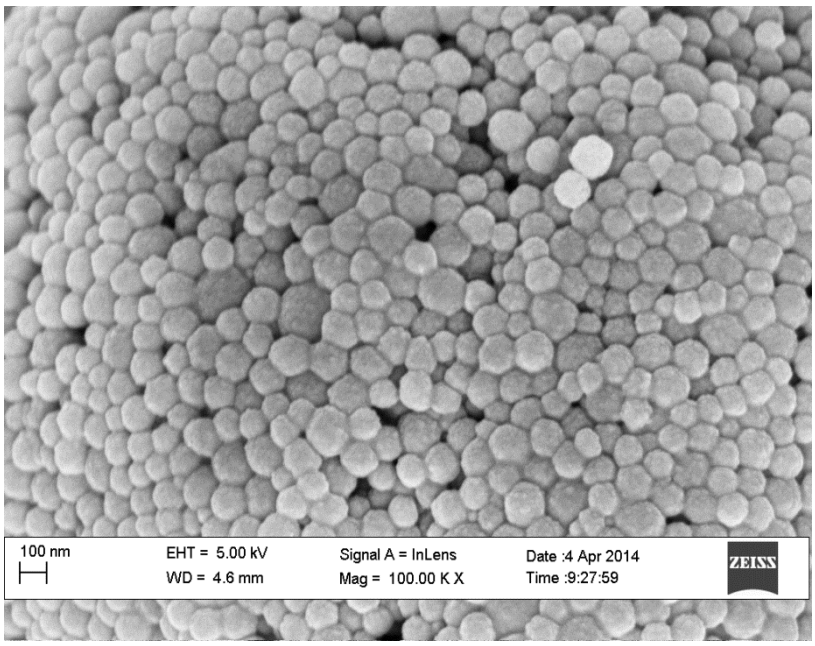


***Figure 5.3**: SEM micrographs of sepia melanin granules at 100.00 K X magnification.*

The diameter distribution measured from SEM micrograph (**figure 5.3**) is represented on the histogram (**figure 5.4**). Particle diameter was in the range of 100 and 200 nm, and the calculated average diameter is 137 nm. Kim et al. reported the average diameter of melanin nanoparticles to be 135 nm (Kim et al., 2012).

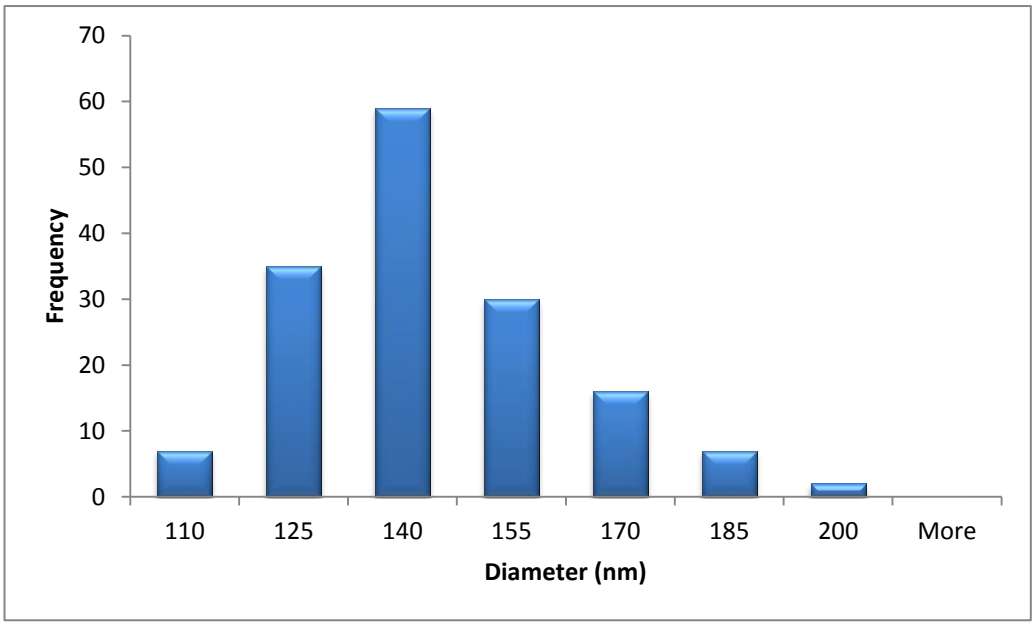


***Figure 5.4**: The histogram of diameter distribution of granules of sepia melanin aggregates from SEM micrograph (**figure 5.3**).*

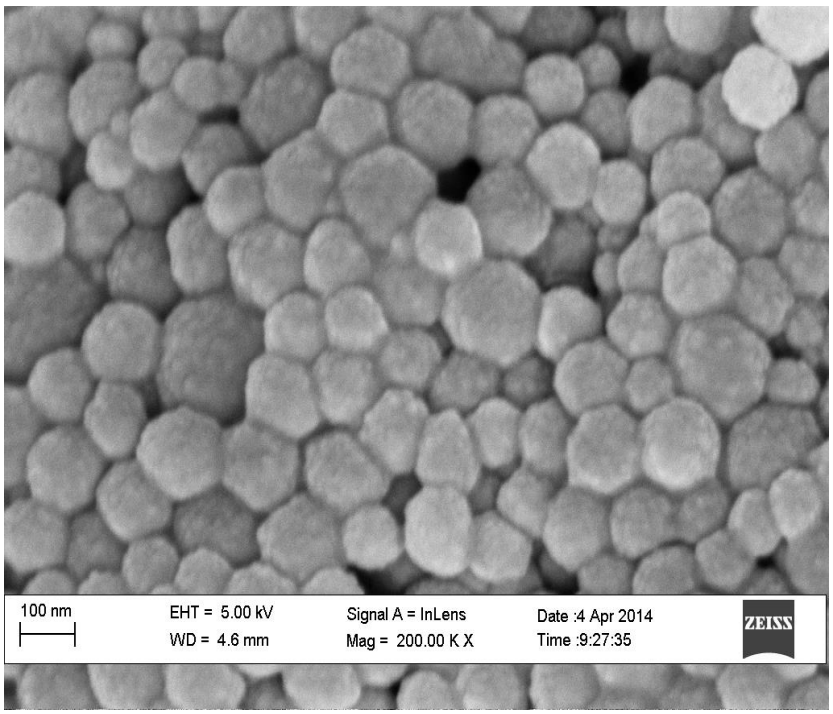


***Figure 5.5****: SEM micrographs of sepia melanin granules at 200.00 K X magnification.*

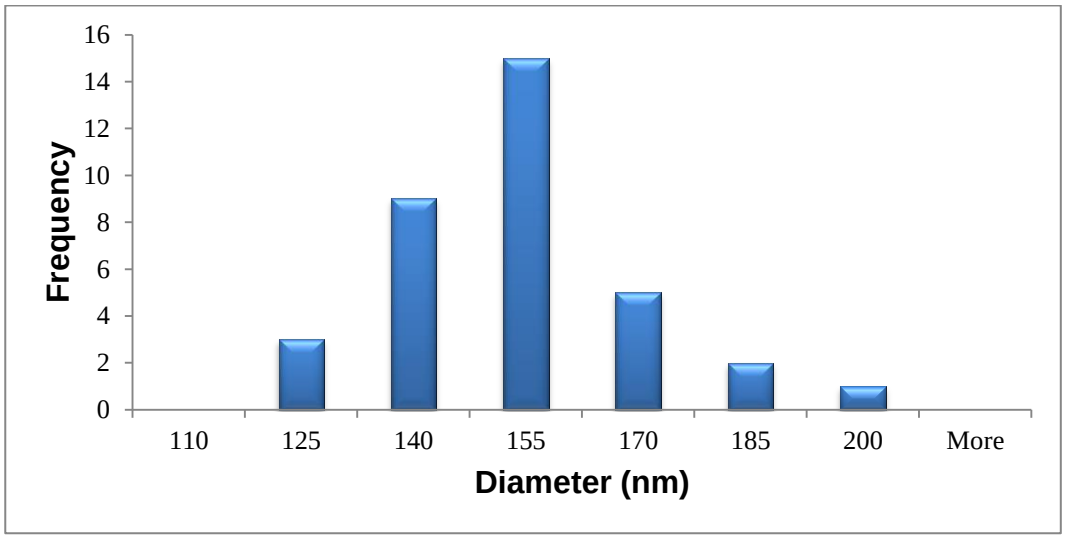


***Figure 5.6****: The histogram of diameter distribution of granules of sepia melanin aggregates from SEM micrograph (**figure 5.5**).*

The above histogram (**figure 5.6**) shows the diameter distribution of sepia melanin granules measured from SEM micrograph (**figure 5.5**). It was found that sepia melanin is made of aggregate of spherical particles having about 100 - 200 nm in diameter as shown by the histogram (**figure 5.6**). The calculated average diameter was 145 nm. These results are comparable to the results obtained from the SEM micrograph at 100 K X magnification and the same scale (**figure 5.3**).

The obtained diameter distributions for sepia melanin from SEM micrographs were in good agreement with the ones reported in literature. It was reported that the size diameter of spherical particles forming natural melanin varies in the range of 100 - 200 nm (Riesz, 2007; Lee et al., 2013; Natalio et al., 2011).

#### *5.1.1.2. Energy Dispersive X-ray spectroscopy*

The EDS qualitative analysis consists of the identification of the lines in the x-ray spectrum using tables of energies or wavelengths and the EDS quantitative analysis (determination of the concentrations of the elements present) by measuring line intensities for each element in the sample and for the same elements in calibration standards of known composition (Kortright & Thompson, 2001).

The measurement was done on five different spots from SEM micrographs (at 100 K X magnification for all of them) to make sure that the chemical composition is the same for different positions of the sample.

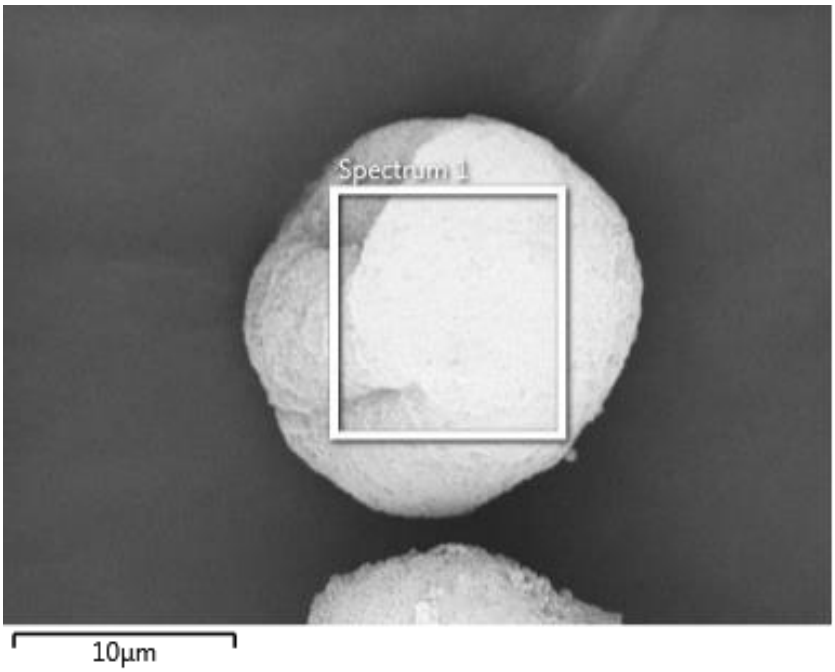


***Figure 5.7****: SEM micrographs of sepia melanin granules at 100.00 K X magnification and 10 µm scaled.*

All presented EDS spectra in this dissertation were plotted from raw data collected from EDS. The first EDS spectrum collected from SEM micrograph (**figure 5.7**) of sepia melanin is shown on **figure 5.8**. This spectrum was collected on SEM micrograph scaled at 10 µm while the remaining spectra were collected from 1 µm SEM micrographs scaled.

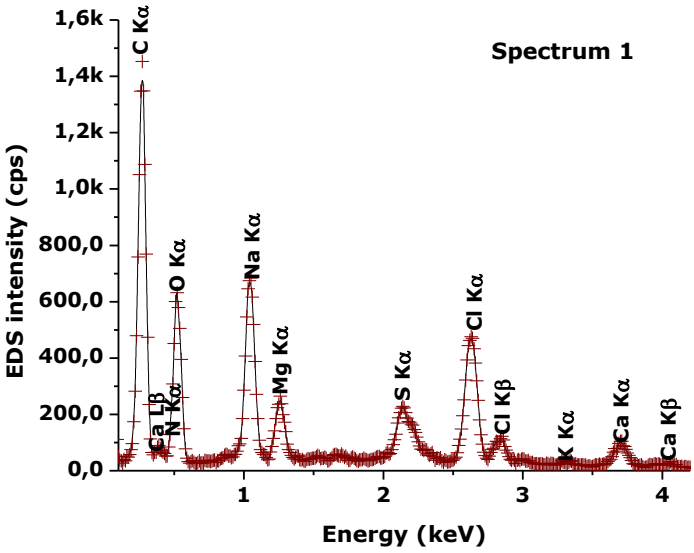


***Figure 5.8**: EDS spectrum measure from SEM micrograph on first spot (**figure 5.7**).*

On this EDS spectrum, one can distinguish the peaks of C, O, Na, Mg, Cl, S, Ca, K as well as N even if the two last elements are low in intensity. This spectrum is the only one showing the existence of K element in sepia melanin among all the five spectra as the measurement was done on a big portion of the sample. The potassium was not present in all other four spectra (**figure 5.10, figure 5.12, figure 5.14** and **figure 5.16**), while nitrogen was not only present on two of them (**figure 5.10** and **figure 5.16**).

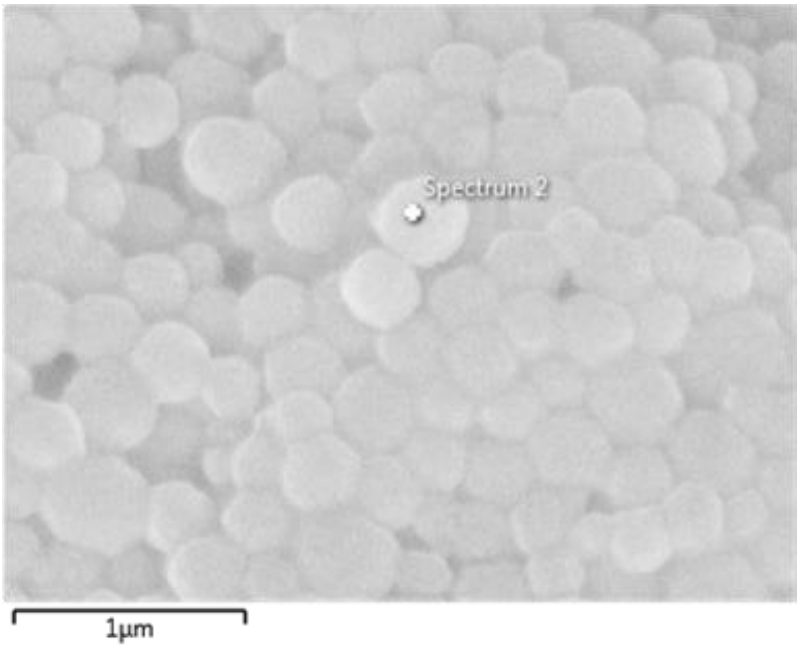


***Figure 5.9**: SEM micrographs of sepia melanin granules at 100.00 K X magnification.*

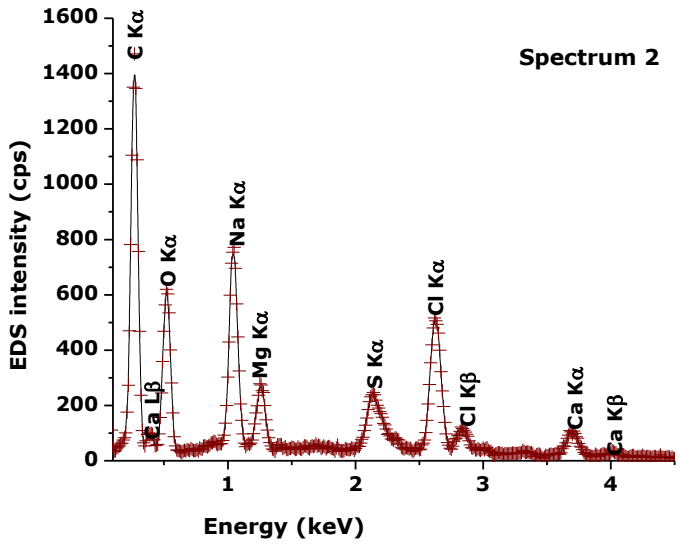


***Figure 5.10**: EDS spectrum measured from SEM micrograph on second spot (**figure 5.9**).*

**Figure 5.10** is the EDS spectrum collected from the second spot (**figure 5.9**). On this spot, the detected elements were only C, O, Na, Mg, Cl, S, and Ca. The concentrations as well as the maximum intensities of emitted x-ray lines were different from those obtained at the first spot.

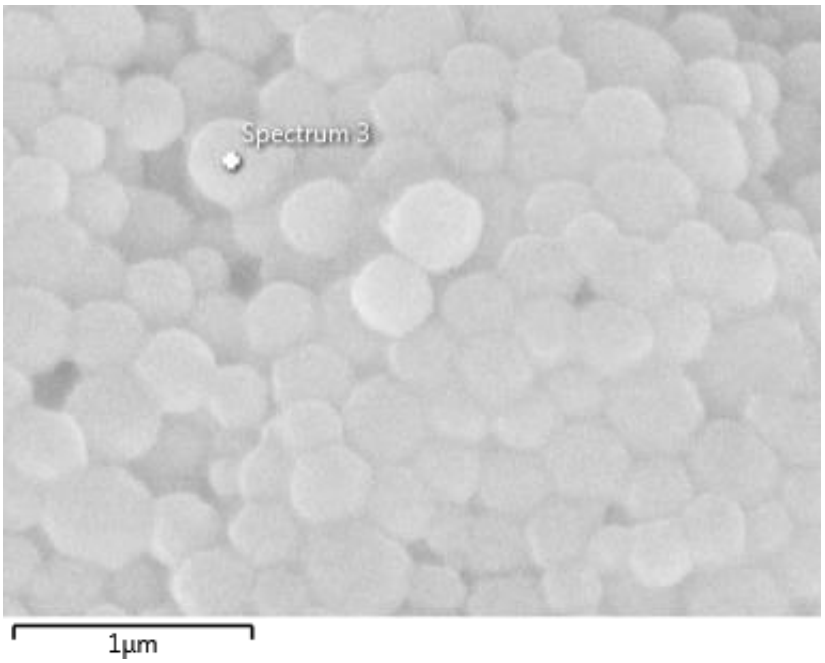


***Figure 5.11**: SEM micrographs of sepia melanin granules at 100.00 K X magnification.*

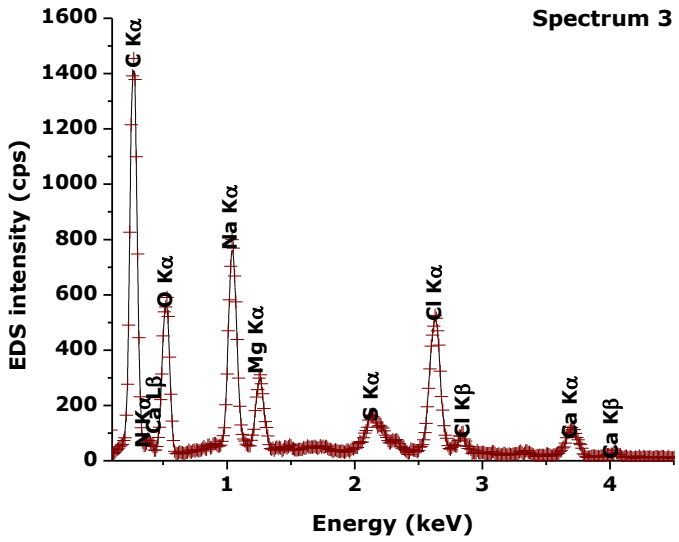


***Figure 5.12**: EDS spectrum measured from SEM micrograph on third spot (**figure 5.11**).*

**Figure 5.12** is EDS spectrum collected from the third spot (**figure 5.11**). On this spot, the detected elements were only C, O, Na, N, Mg, Cl, S, and Ca. The concentrations as well as the maximum intensities of emitted x-ray lines were different from those obtained on other spots.

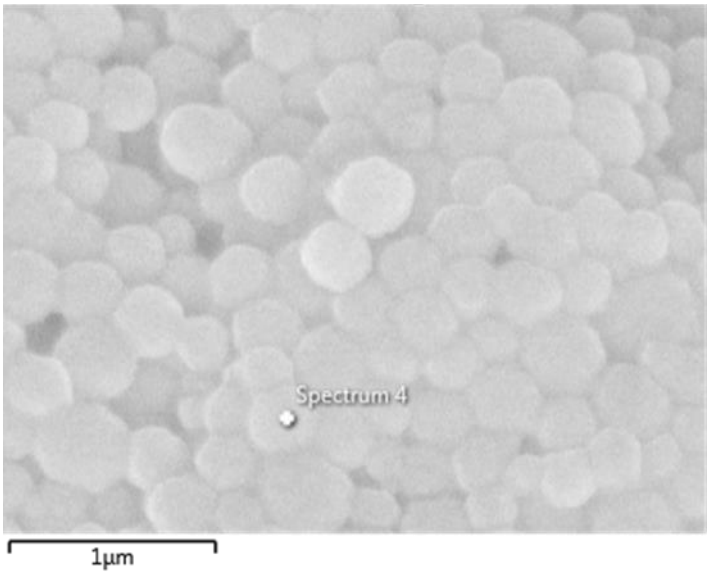


***Figure 5.13**: SEM micrographs of sepia melanin granules at 100.00 K X magnification.*

The EDS spectrum (**figure 5.14**) collected from the fourth spot (**figure 5.13**). On this spot, the detected elements were only C, N, O, Na, Mg, Cl, S, and Ca. The concentrations as well as the maximum intensities of emitted x-ray lines were different from those obtained on other spots.

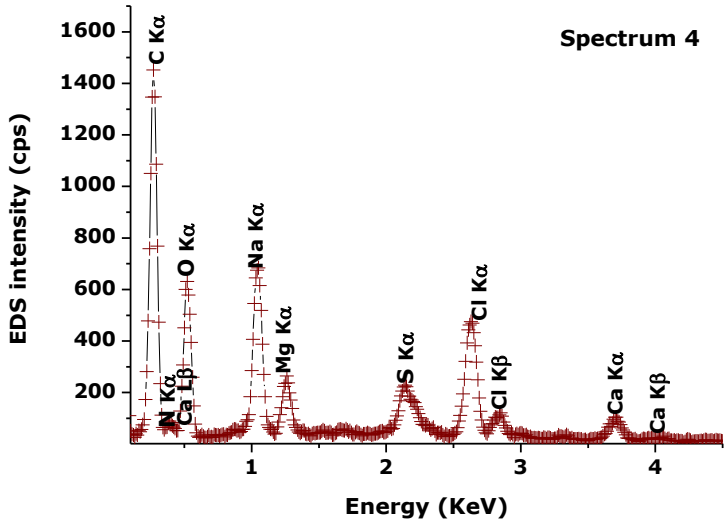


***Figure 5.14**: EDS spectrum measured from SEM micrograph on fourth spot (**figure 5.13**).*

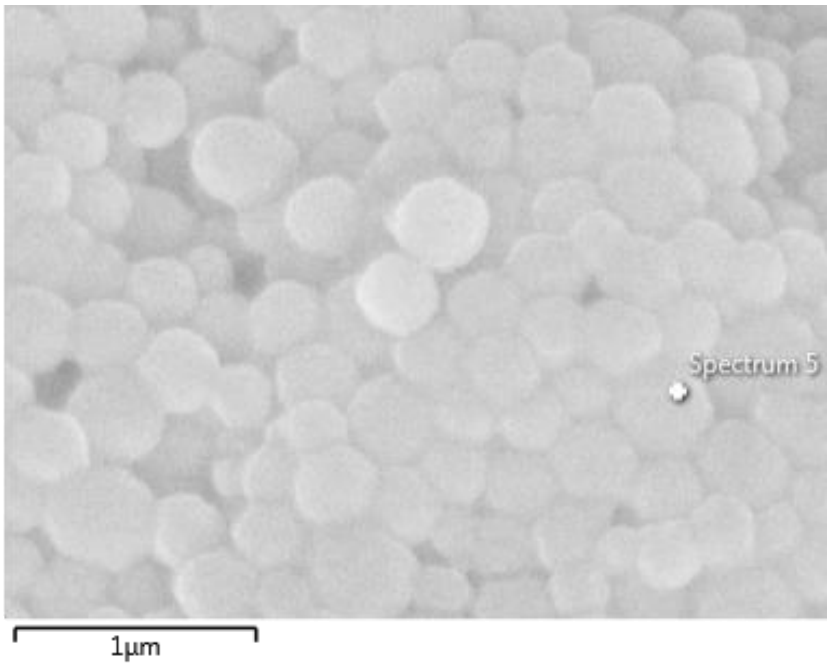


***Figure 5.15**: SEM micrographs of sepia melanin granules at 100.00 K X magnification.*

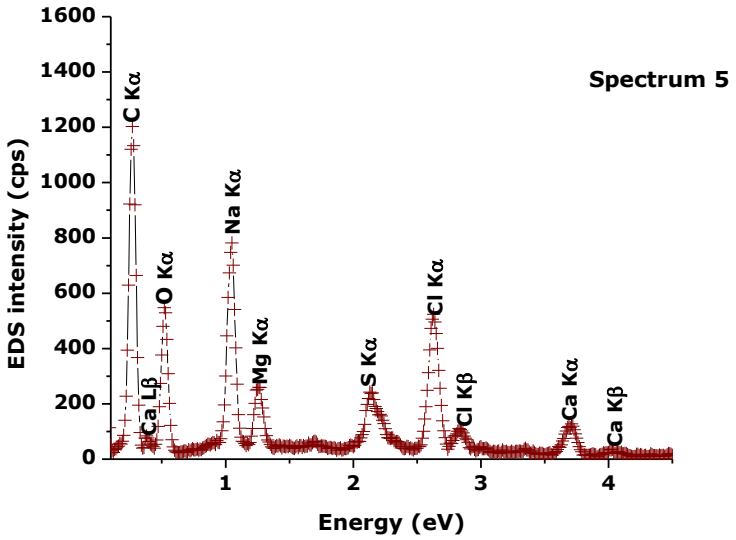


***Figure 5.16**: EDS spectrum measured from SEM micrograph on fifth spot (**figure 5.15**).*

**Figure 5.16** is the EDS spectrum collected from the fifth spot (**figure 5.15**). On this spot, the detected elements were only C, O, Na, Mg, Cl, S, and Ca. The concentrations as well as the maximum intensities of emitted x-ray lines were different from those obtained on other spots.

The table below (**table 5.1**) represent the summary of all elements detected from the five spectra, and their corresponding photon energies of x-ray emission lines in electron volt. For each specrum, the element and their collected maximum intensities for K-, and L-shell emission lines are presented. The results shows that the intensity of emitted x-ray lines from all five spot were not the same and this justified the difference in concentrations for all detected elements. Briefly, the detected elements are not distributed uniformly in the samples. The difference in concentration is shown on **table 5.2**.

***Table 5.1**: The summary of all elements detected from the five spectra, their corresponding photon energies of x-ray emission lines in electron volts.*

| Element | E | $I_{S1}$ | $I_{S2}$ | $I_{S3}$ | $I_{S4}$ | $I_{S5}$ |
|---|---|---|---|---|---|---|
| **C Kα** | 0.277 | 1453.0 | 1471.0 | 1455.0 | 1256.0 | 1203.0 |
| **N Kα** | 0.392 | 90.0 | - | 79.0 | 71.0 | - |
| **O Kα** | 0.520 | 632.0 | 620.0 | 590.0 | 530.0 | 548 |
| **Na Kα** | 1.041 | 684.0 | 772.0 | 800.0 | 725.0 | 782.0 |
| **Mg Kα** | 1.254 | 265.0 | 279.0 | 800.0 | 274.0 | 260.0 |
| **S Kα** | 2.307 | 229.0 | 247.0 | 166.0 | 153.0 | 240.0 |
| **Cl Kα** | 2.622 | 476.0 | 516.0 | 526.0 | 476.0 | 524.0 |
| **Cl Kβ** | 2.816 | 122.0 | 122.0 | 103.0 | 103.0 | 111.0 |
| **K Kα** | 3.314 | 36.0 | - | - | - | - |
| **Ca Kα** | 3.692 | 105.0 | 105.0 | 120.0 | 123.0 | 111.0 |
| **Ca Kβ** | 4.012 | 24.0 | 37.0 | 24.0 | 31.0 | 36.0 |
| **Ca Lβ** | 0.341 | 65.0 | 65.0 | 79.0 | 53.0 | 84.0 |

On **table 5.1**, E stands for the photon energy from x-ray data booklet while $I_S$ stands for the maximum intensities of the emitted x-ray lines peaks).The table shows how the intensities of emitted x-ray lines differ from on spot to another.

***Table 5.2**: The atomic concentrations of different elements found in commercial sepia melanin and their respective atomic numbers (%).*

| Elements | C | N | O | Na | Mg | Cl | K | Ca |
|---|---|---|---|---|---|---|---|---|
| **Spectrum1** | 55.49 | 7.14 | 24.33 | 6.19 | 1.67 | 4.02 | 0.14 | 1.01 |
| **Spectrum 2** | 60.21 | - | 24.7 | 7.24 | 2.03 | 4.63 | - | 1.27 |
| **Spectrum 3** | 55.23 | 7.06 | 23.34 | 6.81 | 2.08 | 4.21 | - | 1.19 |
| **Spectrum 4** | 52.98 | 8.97 | 23.19 | 7.04 | 2.03 | 4.41 | - | 1.37 |
| **Spectrum 5** | 59.46 | - | 23.73 | 7.93 | 2.13 | 5.1 | - | 1.65 |
| **Mean values** | 56.674 | 4.634 | 23.858 | 7.042 | 1.988 | 4.474 | 0.028 | 1.298 |

After calculating the average values of concentrations for each element, it was found that C and O were the most abundant in sepia melanin with concentration average concentrations of about 57% and 24% respectively. This analysis revealed that the major compositions of sepia melanin are C, O, Na, Cl, while the minor are Mg, Ca, K, S and N. Some peaks are undetectable as EDX may not be a reliable method to quantify elements in low weight %. This result serves as an additional support which reflects the purity of this sepia melanin there is no additional elemental peak.

### 5.1.2. Transmission Electron Microscopy (TEM)

For further investigation on the morphology of sepia melanin in order to confirm the results obtained by SEM, the Fei Tecnai $G^2$20, HRTEM having Field Gun Resolution TEM operating at 200 kV with an information limit of 0.12 nm was used.

For both SEM and TEM characterizations, the size particle distribution was measured using particle size analysis software called image-J. The image-J software can calculate the area and pixel value statistics of user-defined selection and intensity threshold objects. It can also measure the spacing between the lines as well as the length from TEM and SEM micrographs. Watt et al. as well as Bothma found that the diameters of sepia melanin granules which are roughly spherical were 100 nm upwards (Bothma, 2008; Watt et al., 2009). The diameter of the aggregated spherical granules constituting sepia melanin was reported to be about 150 nm (Moses et al., 2006).

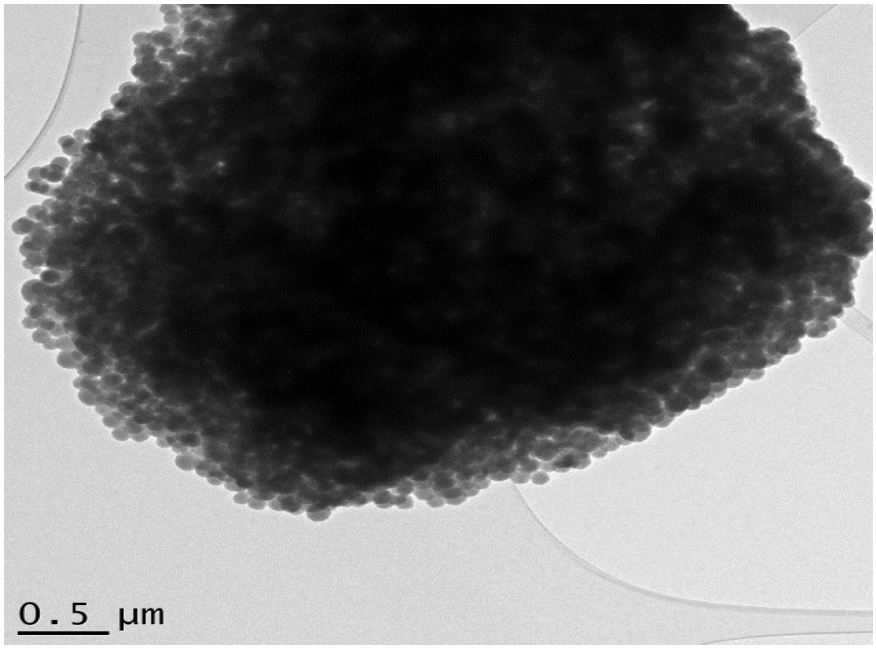


***Figure 5.17****: TEM micrograph of agglomerated sepia melanin nanoparticles scaled 0.5 µm.*

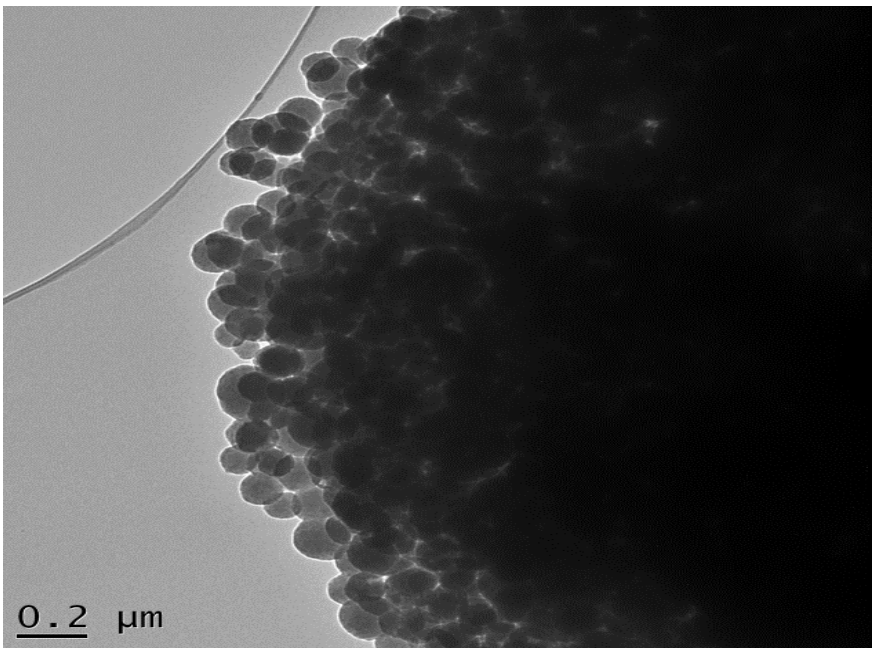


***Figure 5.18**: Typical TEM micrographs of agglomerated sepia melanin nanoparticles scaled 0.2 µm.*

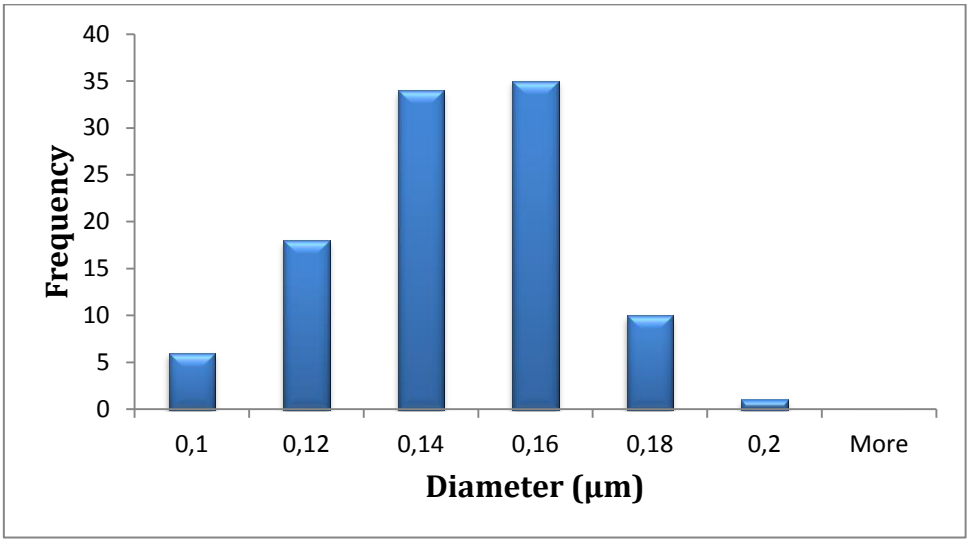


***Figure 5.19**: The distribution of granule diameters measured from TEM micrograph (**figure 5.18**).*

TEM micrograph shows that the granules of sepia melanin are spherical (**figure 5.17** and **figure 5.18**). The granule size was measured from TEM micrograph to determine if the diameter distribution is in agreement with that one obtained from SEM micrograph. The histogram (**figure 5.19**) presents the diameter distribution of small granules of sepia melanin. In decreasing the scale from 100 nm (**figure 20a**) to 50 nm (**figure 20b**) and increasing magnification, the structure of granule start to be a little bit clear.

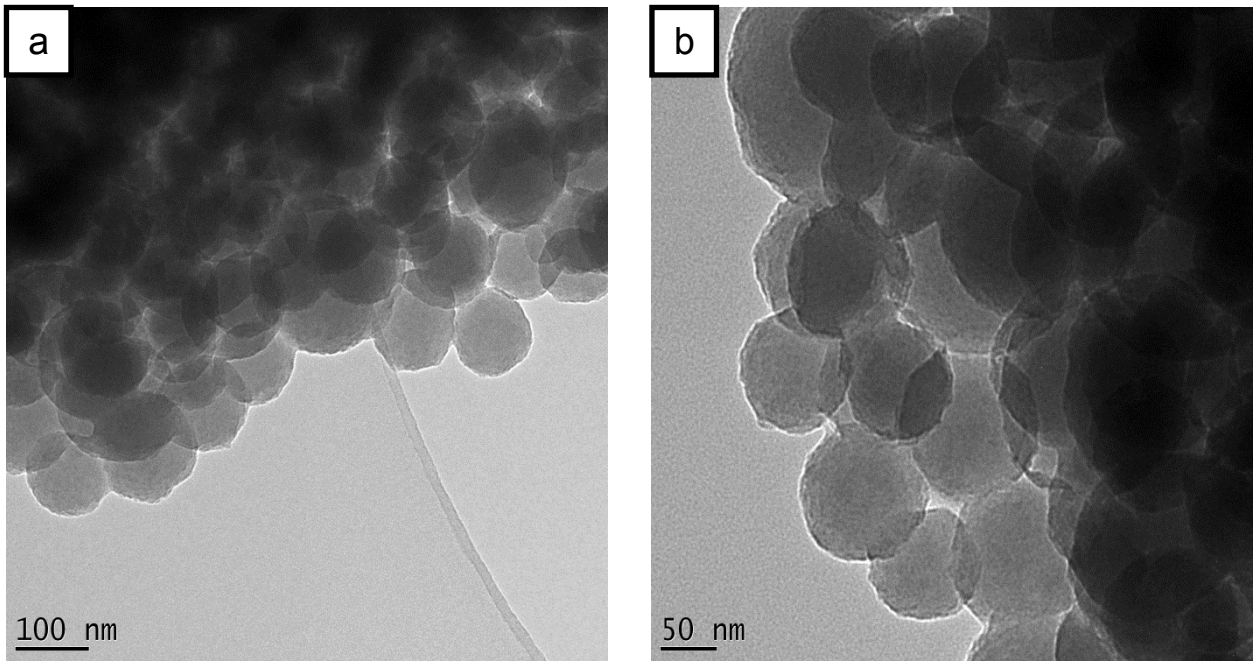


***Figure 5.20**: TEM micrographs of agglomerated sepia melanin nanoparticles scaled 100 nm (a), and 50 nm (b).*

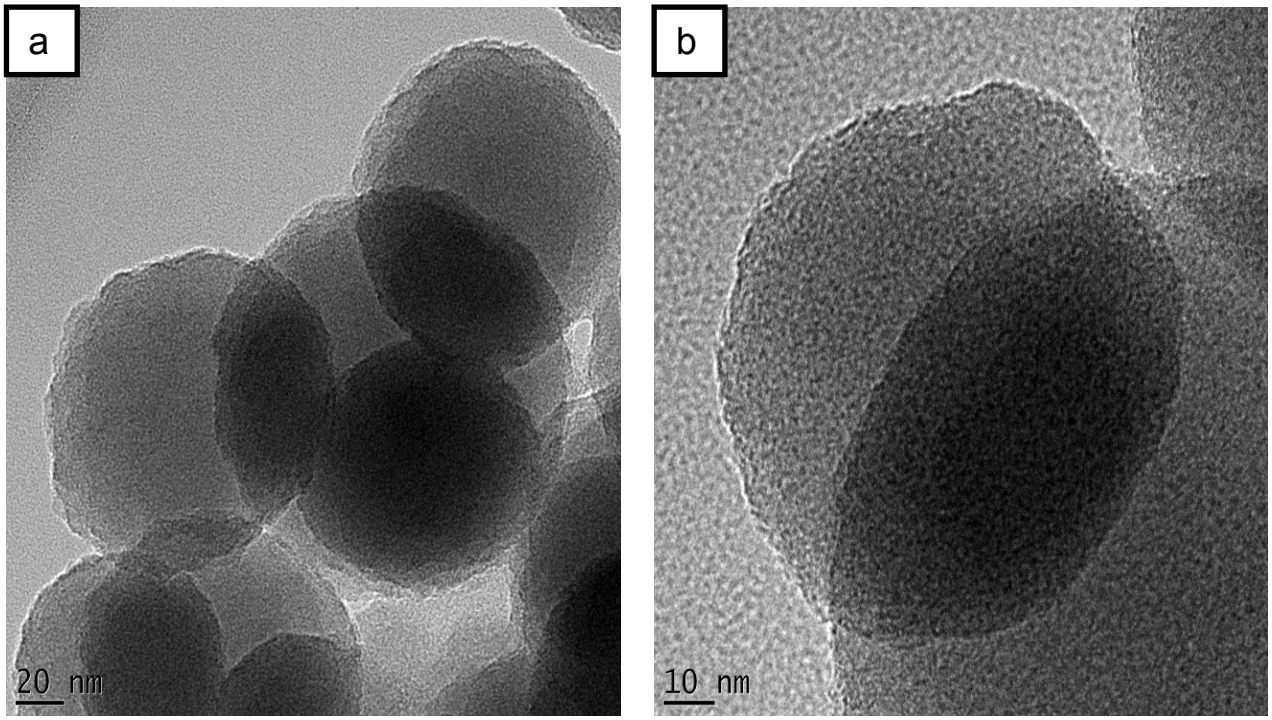


***Figure 5.21**: TEM micrographs of agglomerated sepia melanin nanoparticles scaled 20 nm (a), and 10 nm (b).*

In decreasing further the scale from 20 nm (**figure 21a**) to 10 nm (**figure 21b**); the polymers chains forming sepia melanin start to be observed. At high magnification and 2

nm scale (**figure 22**), the chains are well observed so that the distance between polymer chain can be easily measured using Image-J software.

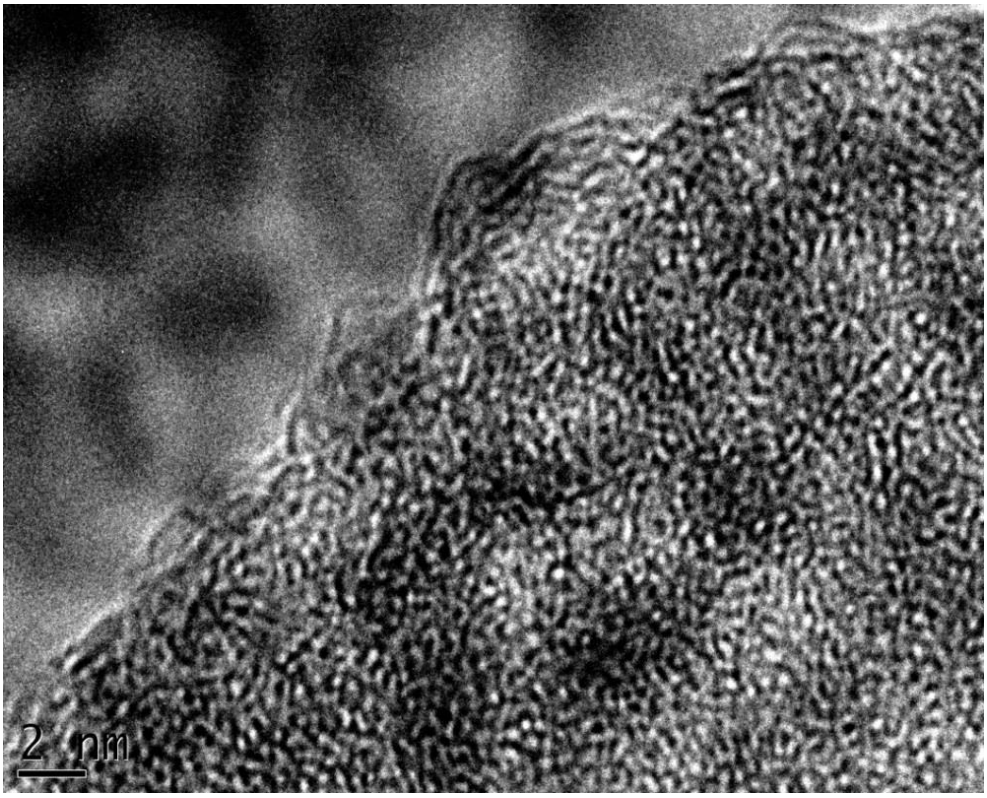


***Figure 5.22**: TEM micrograph of sepia melanin nanoparticles scaled 2 nm*

The **figure 5.22** shows the TEM micrograph at high resolution. From TEM micrograph, it was possible to measure the distance between polymers layers of sepia melanin.

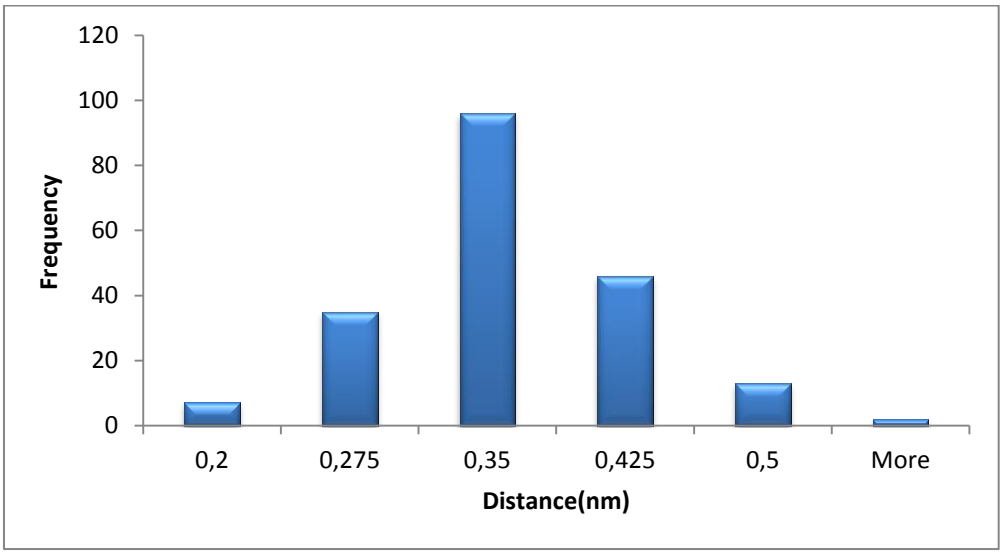


***Figure 5.23**: The distribution of distance distances between chains of polymers measured from TEM micrograph (**figure 5.22**).*

The **figure 5.23** shows the distribution of distances between chains of polymers. The average interlayer distance measured from the TEM micrograph (**figure 5.22**) using image-J software is 0.323 nm = 3.23 Å. This confirms the supramolecular organization predicted from the corresponding TEM micrograph (**figure 5.21**). The obtained value is in good agreement with that one obtained by Chen et al by simulations (Chen at al., 2013).

SEM and Transmission Electron Microscopy (TEM) observations show that the sepia melanin powder consists of spherical nano-scaled particles with a nearly double size distribution.

# 5.2. Structure characterization

## 5.2.1. X-Ray Diffraction (XRD)

**Figure 5.24** represents XRD spectra of a highly concentrated sepia melanin solution drop coated into 2x2 cm cleaned glass substrates. The sepia melanin was scanned using a BRUKER AXS D8 Advance x-ray diffractometer with Cu-$K_\alpha$, radiation with wavelength, λ ($K_{\alpha 1}$) = 1.5406 Å. The x-ray tube was powered with a current of 40 mA and a voltage of 40 kV. The step size and the step time were 0.027 $^{o}$ and 176 s respectively. The scanning rate was 2 $^{o}$/min x-ray beam at 25 $^{o}$ C.

A typical XRD spectrum shows peaks at fixed 2Θ angles. By the peaks position, it is possible to identify the kind of crystals present on the sample. This is done by doing qualitative phase analysis (search match) using software like for example the PANAlytical X'pert Highscore plus software employing the ICDD PDF database for comparison in order to identify the crystal phase. The observation of the results from sepia melanin sample was the lack of structure in the diffraction pattern corresponding to any significant crystallinity in this sepia melanin. The spectrum was dominated by a broad non-Bragg diffraction pattern.

The produced sharp peaks in diffraction spectrum by the scattering of X-rays by crystalline structures serve as a signature for the crystal that is analysed. However, broad features in a diffraction spectrum, known as non-Bragg features as a result of the absence of coherent scattering from regular and repeating structures as observed in crystals are produced by amorphous compound such as sepia melanin (Casadevall et al., 2012), (Sajjan et al., 2013).

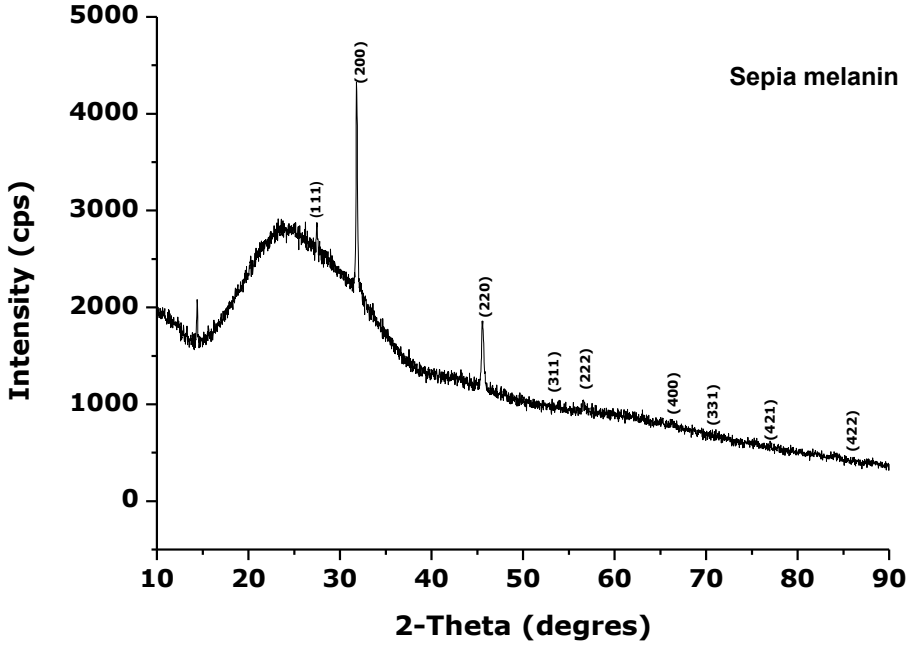


***Figure 5.24****: The XRD spectrum plotted from low data collected by* x-ray diffractometer *in measuring sepia melanin. The obtained candidate in the ICDD data base was NaCl which is among the components of sepia melanin as shown by EDS results. The sample was highly concentrated solution of sepia melanin drop coated on glass substrate (plotted from raw data). The spectrum of each is dominated by a broad non-Bragg diffraction pattern.*

The sharp diffraction peaks appearing on the spectrum (except the first peak that the used software was not able to identify) are due to NaCl molecules which have been confirmed to be the component of sepia melanin by EDS. From the peaks position of the XRD spectra shown in **figure 5.24,** it can be observed that the sepia melanin crystallographic patterns showed peaks at 2θ = 27.33, 31.69, 45.45, 53.85, 56.47, 66.22, 73.06, 75.30 and 83.97 which have the corresponding reflections (111), (200), (220), (311), (222), (400), (331), (420) and (422) respectively. The lattice parameter corresponding to this crystallographic structure is about a = 5.64020 (PDF 00-005-0628).

A broad diffraction peak (2θ=10-90º) observed on the XRD spectra of sepia melanin is showing its amorphous nature. Because of amorphous, insoluble as well as heterogeneous nature of melanins, their structures are uncertain (Sajjan et al., 2013). The utility of XRD techniques for the analysis of the structure of amorphous materials such as sepia melanin is limited. This same overall structure of sepia melanin was obtained in the literature (Subianto, 2006; Sajjan et al., 2013).

## 5.3. Optical characterization

### 5.3.1. Fourier Transform Infrared Spectra

The FTIR spectrum (**figure 5.25**) was collected at resolution of 4 $cm^{-1}$ in the transmission mode (4000–400 $cm^{-1}$) using Thermo Scientific Nicolet Is10 FTIR spectrophotometer. The broad absorption band centred about 3422 $cm^{-1}$ was observed. This broad absorption band is the characteristic of O-H or N-H stretching vibration modes. The observation of this first band is in good agreement with the report of Centeno et al. saying that a broad absorption between 3600 - 3200 $cm^{-1}$ spectral regions can be attributed to the O-H and N-H stretching vibrations of the carboxylic acid, and phenolic as well as aromatic amino functions presents in the indolic and pyrrolic systems (Centeno and Shamir, 2008). Apte et al. observed this peak at 3438 $cm^{-1}$ (Apte et al., 2013).

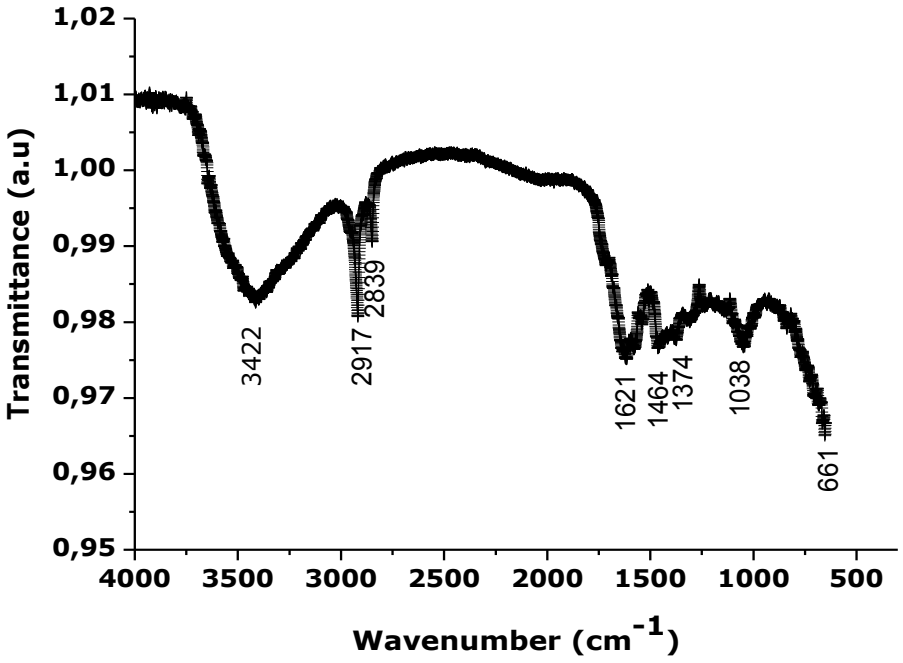


***Figure 5.25****: Room temperature IR vibrational spectra of sepia melanin spectra.*

Two absorption peaks were observed; the medium intensity band at 2917 $cm^{-1}$ and the weak one at 2839 $cm^{-1}$, and these may be assigned to the stretching vibration of aliphatic C-H group. These values are in good agreement with stretching frequencies reported in literature (Centeno and Shamir, 2008; Tarangini and Mishra, 2013). The observation of two slightly different frequencies for the CH stretching may be the result of the fact that the

hydrogen atoms in the components of sepia are located in different environments (Tarangini and Mishra, 2013).

The characteristic strong band at 1621 $cm^{-1}$ (between 1647 - 1531 $cm^{-1}$) is attributed to the bending vibrations modes of aromatic ring C=C and C=N bond of aromatic system in addition to C=O double bond (COOH) of carboxylic function. The mode between 1468 - 1330 $cm^{-1}$ can be due to aliphatic C-H groups and weak bands below 700 $cm^{-1}$ ascribed to alkene C-H substitution in the melanin pigment (Kim et al., 2012; Tarangini and Mishra, 2013). The OH bending of the phenolic and carboxylic groups that was present in the 1400-1300 $cm^{-1}$ area at the peak centered at 1374 $cm^{-1}$ indicates the Indole ring vibration/CNC stretching (Centeno and Shamir, 2008). The peak centered at 1038 $cm^{-1}$ is the indication of CH in-plane/CH out-of plane deformation. Finally the weak bands below 700 $cm^{-1}$ are assigned to the out-of-plane bending of the aromatic carbon-hydrogen bond in the sepia melanin (Magarelli, 2011).

The obtained FTIR spectrum is in agreement with the ones reported in the literature for closely related compounds, such as indole, pyrrole and substituted pyrrole. The compounds have been assigned by comparing them with other assignments for functional groups that have been published.

## 5.3.2. Raman Spectroscopy

Typical Raman spectrum collected from sepia melanin powder at room temperature using a 532 nm Argon laser to excite the sample, is shown in **figure 5.26**. It was recorded by a T64000 micro-Raman spectrometer from HORIBA scientific, Jobin Yvon Technology equipped with a triple monochromator system. Two broad bands centered at about 1344 $cm^{-1}$ and 1551 $cm^{-1}$ were observed in such Raman spectrum. The two broad bands were observed by Perna et al., and were centered at about 1400 $cm^{-1}$ and 1590 $cm^{-1}$ (Perna et al., 2013). The melanin Raman spectrum was reported to be dominated by two intense and broad peaks at about 1580 $cm^{-1}$ and 1380 $cm^{-1}$ (Huang et al., 2004). The observed bands were in agreement with two broad bands that were observed in the Raman spectrum of the commercial sepia melanin at about 1590 $cm^{-1}$ and 1360 $cm^{-1}$. The confirmation of the origin of two prominent peaks in melanin; as inelastic Raman scattering was done by measuring variety of melanin sources using multiple wavelengths (Huang et al., 2004).

The observed broad bands on Raman spectrum are related to Raman active vibrational modes involving different atoms, as carbon, oxygen, hydrogen and nitrogen, which are the main constituent of melanin. They are from the overlapping of several vibrational mode mainly; the C=C, C-N and C=N ring stretching mode of pyrrole structure as well as the C-O stretching mode and combination bands due to C-O stretching and O-H deformation of carboxylic acid (Perna et al., 2013).

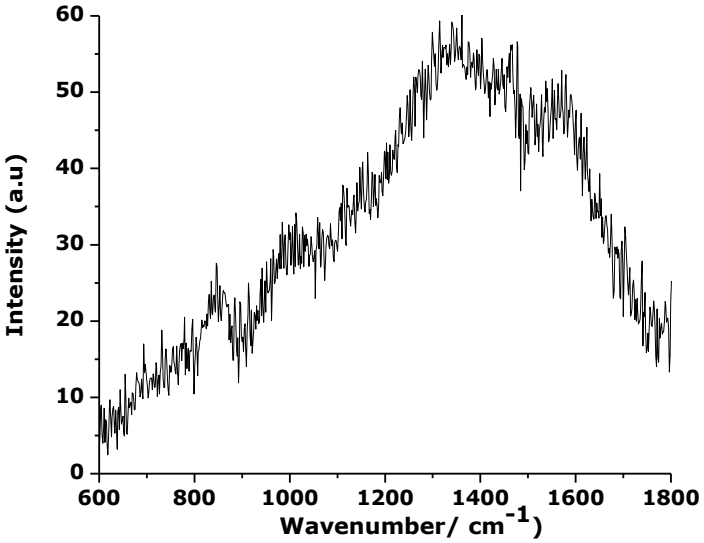


***Figure 5.26****: Typical Raman spectrum of sepia melanin.*

The sepia melanin atoms are organized according to an indolic structure having several functional groups bonded to it. The main functional groups are hydroxyl groups OH, carbonyl groups C=O, carboxylic acid COOH as well as NH groups. This melanin complexes formation results to the challenge in assigning precisely the observed Raman features of melanin to the large amount of different vibrational modes involving the many functional groups inside this biopolymer. The overall shape of the found sepia melanin Raman spectrum is similar to those reported for melanin samples about the vibration mode of melanin monomer units; and this confirms the presence of such units inside the analyzed sepia melanin sample (Huang et al., 2004; Centeno and Shamir, 2008; Perna et al., 2013).

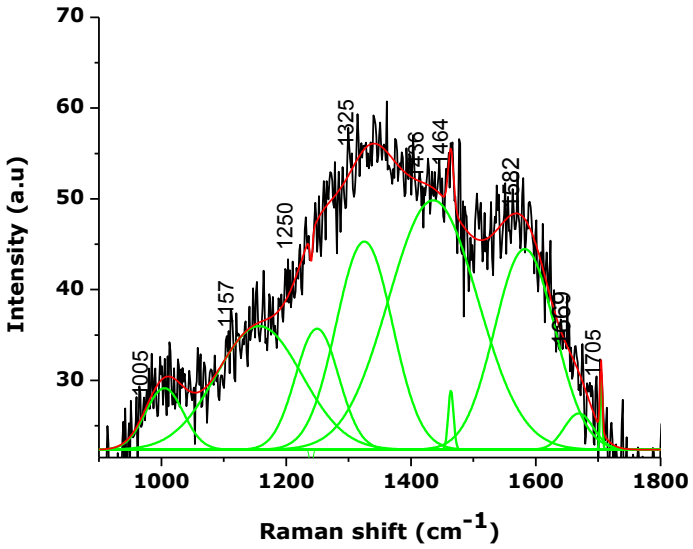


***Figure 5.27**: Fitting analysis of the experimental average Raman spectrum (black continuous line) obtained by means of Gaussian functions (green continuous lines): the sum of the Gaussian bands (red continuous line) is in good agreement with the experimental spectrum.*

The typical Raman spectrum has been analyzed by mean of Gaussian function for better analysis of the functional groups characteristic of the sepia melanin structure and to point out some spectral features which may be hidden in the experimental spectra. The results of this fitting procedure are shown as red dashed lines in **figure 5.27** and the spectral position of Raman peaks are listed in **table 5.3**. It is clearly evident that the sum of Gaussian functions (red continuous line) is well fitted to the experimental spectrum (black continuous line).

***Table 5.3**: Spectral position of Raman peaks obtained by Gaussian function fitting with their respective center positions, areas, widths, height and their corresponding assignments (**figure 5.27**).*

| Peak ($cm^{-1}$) | Center | Area | Width | Height | Assignments |
|---|---|---|---|---|---|
| 1 | 1004.95 | 515 | 60.69 | 6.78 | C-H in plane deformation |
| 2 | 1156.66 | 2343.01 | 137.24 | 13.62 | pyrrole NH in-plane deformation/ring Breathing |
| 3 | 1249.60 | 1159.05 | 69.34 | 13.33 | C-O stretching; combination of C-O stretching and O-H deformation in carboxylic acid |
| 4 | 1325.26 | 2586.54 | 89.97 | 22.93 | C-H in-plane deformation |
| 5 | 1435.63 | 4909.71 | 142.53 | 27.48 | C=C, C=N in plane vibration in pyrrole |
| 6 | 1463.99 | 68.85 | 8.42 | 6.52 | pyrrole ring stretching vibration |
| 7 | 1582.41 | 2670.77 | 96.36 | 22.11 | C=C aromatic/pyrrole ring stretching vibration |
| 8 | 1668.98 | 234.68 | 46.75 | 4 | C=C in plane vibration in pyrrole |
| 9 | 1704.71 | 55.52 | 3.63 | 7.74 | C=O stretching in COOH/Indole ring vibration |

## 5.3.3. UV-VIS-NIR spectrum

The UV-Vis spectra of the melanin samples are given in **figure 5.28.** The sepia melanin solution was measured by UV-Vis Spectrometer (HP Office Jet Pro 8000). The measurement was done on the same sample twice and it has showed great difference in absorbance. Huang et al. reported that melanin has no distinctive absorption peaks to distinguish itself from other cutaneous chromophores. Instead, melanin absorption decreases monotonically with increasing wavelengths from 300 to 1100 nm (Huang et al., 2004).

The first UV-Vis measurement was done one day after sample preparation (red line) and shows the UV-VIS-NIR absorbance in the optical range of 190 - 1100 nm (1.12 - 6.652 eV). One can distinguish 2 spectral regions; 190 - 300 nm and 300 - 1100 nm. Region 1 (190-300nm) exhibits 2 major absorbance peaks; a sharp and a broad peak centered

approximately at ~200 and ~260 nm respectively. The maximum intensity of absorption was only 41% whereas the minimum intensity of absorption was 15.1%.

Three months later, the UV-visible wavelength scan showed the absorption was highest at the UV region of 200 to 300 nm, but diminished towards the visible region. It has one sharp peak centered approximately at 220 nm and a shoulder hump at 260 nm (black line). For this sample, it was found that the maximum absorption has been increased about 2 times with the value of 78% and the minimum intensity of absorption was about 16.4%. This is because the solubility of sepia melanin in solvent increased with three months. The overall UV-Vis structure is similar to the UV-Vis spectrum of synthetized melanin nanoparticles (Kim, et al., 2012).

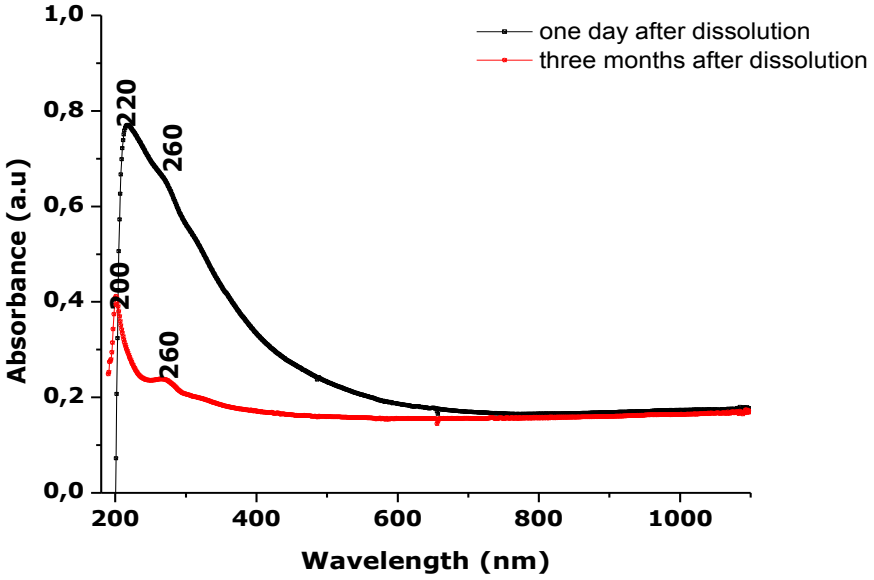


***Figure 5.28**: UV-Vis spectra of sepia melanin. The UV-Vis wavelength scan showed the absorption was highest at the UV region of 200 to 300 nm, but diminished towards the visible region.*

The spectrum of sepia melanin sample measured three months later being dissolved was similar to the spectrum of sepia melanin standard. The UV-Vis spectrum obtained showed the typical absorption profile of melanin that is characterized by a strong absorption in the UV-Vis spectral range, with a nearly featureless line shape and absorbance values monotonically decreasing from UV-Vis to NIR spectral region (Huang et al., 2004; Magarelli, 2011; Perna et al., 2013).

All spectra show a strong UV absorption in the 200 - 300 nm region that can be attributed to the $\pi \rightarrow \pi^*$ and $n \rightarrow \pi^*$ of the amino, carboxylic and aromatic moieties (Magarelli, 2011).

The UV-Blue energy transitions corresponds to the transition from the nonbonding orbital n to the antibonding orbital $\pi^*$ ($n \rightarrow \pi^*$), which occurs predominantly in carbonyl (C = O) bonds that are very abundant in the melanin. Region 2 (300 - 1100nm) displays a quasi-constant and large absorbance which certainly is the source of the black color of the sepia melanin itself. This broad and large spectral absorption is attributed to strong absorption transitions involving the orbital energy of the antibonding $\pi^*$ and the bonding $\pi$ ($\pi \rightarrow \pi^*$). This later occurs in the aromatic-unsaturated C bonds (Magarelli et al. 2010; Magarelli, 2011). The movement of delocalized electron in the sepia melanin structure and the high degree of conjugation facilitate the transitions to the antibonding $\pi^*$ orbitals. A strong absorption of sepia melanin in the red part of visible sepia melanin is mainly due to many carbonyl groups present in its indolic groups (Magarelli, 2011). This is the source of the black color of sepia melanin.

As it was reported earlier in chapter **2** (**2.3.2 subsection**), one of the criteria for a good dye sensitizer for Grätzel cell is that the dye should be “black” in the UV-Vis-NIR spectral region, with extremely high broadband absorption, preferably all the way into the near-IR in order to harvest as many incident photons as possible (Nazeeruddin et al., 2001; Sokolsky & Cirak, 2010). Therefore, the obtained UV-Vis results showed that sepia melanin exhibits a high absorption throughout UV-Vis-NIR range and this lead it to an effective candidate dye for DSSC.

## 5.3.4. Photoluminescence measurement

Photoluminescence emission spectra for the sepia melanin were recorded using Nanolog$^{TM}$ spectrofluometer. The band passes of side entrance, exit as well as first intermediate slits were 5 nm. The increment of 1.00 nm and an integration of 0.1 s were used. Spectra were automatically corrected to account for differences in pump beam power at different excitation wavelengths using a reference beam. Background scans were performed under identical instrumental conditions with the deionized water. Spectra were collected using quartz 1 cm square cuvette. There is no single wavelength that is logical for excitation of the pigment as sepia melanin has a broadband absorbance spectrum. This led to the use of different of excitation wavelengths.

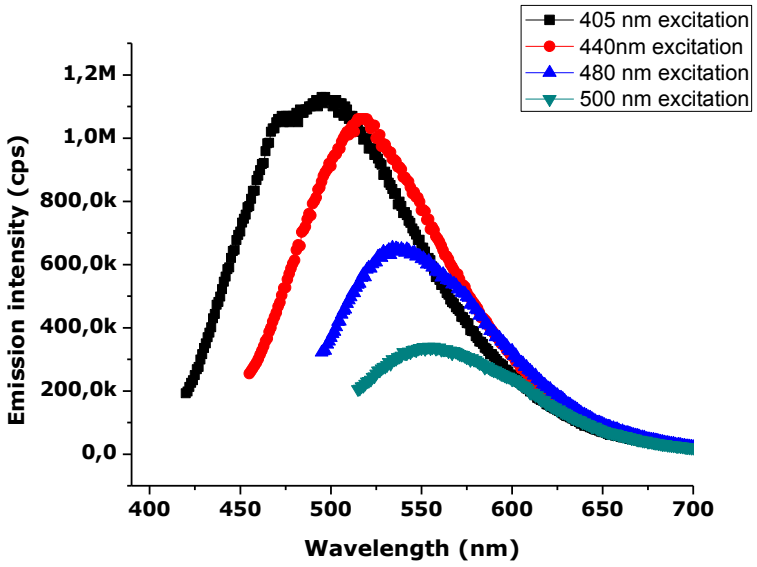


***Figure 5.29**: Emission spectra for sepia melanin solution with four excitation wavelengths (405, 440, 480, and 500 nm). The spectrum shows a broad band that shifts with excitation wavelength from left to right as the excitation wavelength increases.*

In order to obtain the best fluorescence, different excitations wavelength within the range of 400 - 700 nm were performed. The collected emission spectra of sepia melanin for a variety of excitation wavelengths are shown (**figure 5.29).** The calculated energy spectra for the different excitation wavelengths are displayed (**figure 5.30**).

The intensity of emission is reduced by the broadband absorbance spectrum of melanin that causes re-absorption and inner filter effects at all wavelengths (Riesz, 2007). In this project, it was found that sepia melanin is fluorescent. As sepia melanin showed a broad absorbance, it was good to check that it also become excited in this visible range. The excitation wavelength choice was also dependent on the reading range of the apparatus.

The corrected emission spectra of sepia melanin exhibit a peak which is red-shifted as the excitation wavelength increases. The peak position and height varies according to the pump energy. This has been speculated to be due to selective pumping of chemically distinct species within the eumelanin compound, each with different fundamental highest occupied molecular orbital (HOMO) - lowest unoccupied molecular orbital (LUMO) energy gaps (Nighswander-Rempel et al., 2005; Riesz, 2007).

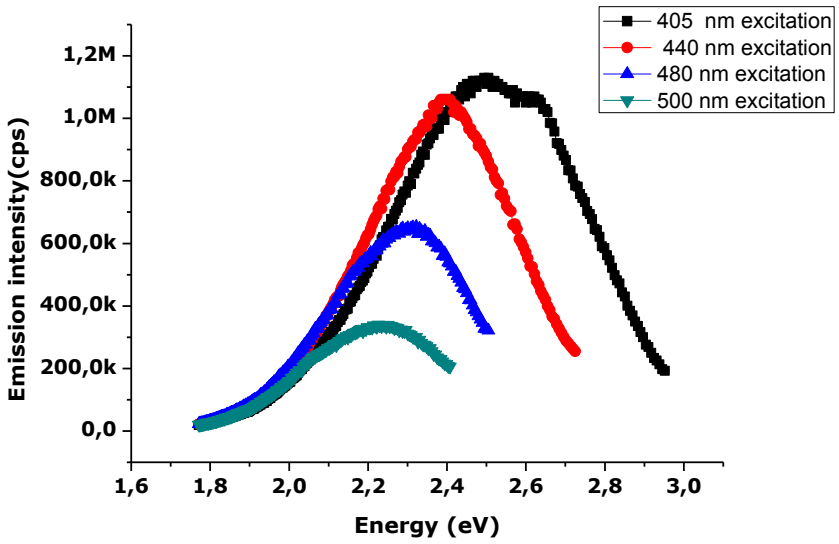


***Figure 5.30**: The emission spectra (emission vs energy) for sample 1 of a sepia melanin solution for four excitation wavelengths (405, 440, 480 and 500 nm). The spectrum shows a broad band that shifts with excitation wavelength from right to left as the excitation wavelength increases.*

The emission spectra gave the first level shows the dependence of emission spectra upon excitation wavelength. The figure above shows clearly how the emission spectrum is strongly dependent upon excitation energy (wavelength). This show that sepia melanin can be a good candidate for DSSC dye sensitizer. The **table 5.4** summarizes results obtained from PL.

***Table 5.4**: PL peaks, wavelength and calculated energies for photo-excited of sepia melanin.*

| Peaks | Excitation wavelength (nm) | The interval of scanning (nm) | Number of data point | Peak position (nm) | Energy (eV) |
|---|---|---|---|---|---|
| 1 | 405 | 420-700 | 281 | 500 | 2.47 |
| 2 | 440 | 455-700 | 246 | 520 | 2.38 |
| 3 | 480 | 495-700 | 206 | 540 | 2.29 |
| 4 | 500 | 515-700 | 371 | 570 | 2.17 |

## 5.4. Conclusion

SEM and TEM revealed that sepia melanins are formed by many aggregates agglomerated together. These aggregates are formed also by small spherical granules with different size distributions. It was found that the diameter of the aggregate is between 6 - 30 µm while that one for granules in 100 - 200 nm. The measured average diameter of aggregate was found to be about 12 µm while the average of diameter measured from two different SEM micrographs was 137 nm and 145 nm.

The high purity of the used commercial sepia melanin was revealed by Raman measurement, FTIR as well as EDS. From all these characterization techniques, it was found that there were no additional elements appearing in this material. XRD showed that the structure of sepia melanin is amorphous. UV-Vis proved that sepia melanin absorbs in a wide range of electromagnetic wave from UV to near IR. The PL result showed that sepia melanin is emitting better in the range of 370 - 700 nm.

## 5.5. References


Apte, M., Girme, G., Bankar, A., RaviKumar, A. and Zinjarde, S. (2013) '3, 4-dihydroxy-L-phenylalanine-derived melanin from Yarrowia lipolytica mediates the synthesis of silver and gold nanostructures', *Journal of Nanobiotechnology 2013*, vol. 11(2).

Bothma, J.P. (2008) *Exploring the structure-propertyrelationships in eumelanin, Masters of Philosophy Thesis*, School of Physical Science, Queensland University.

Casadevall, A., Nakouzi, A., Crippa, P.R. and Eisner, M. (2012) 'Fungal , melanins differ in planar stacking distances', *PLoS ONE*, vol. 7(2).

Centeno, A..S. and Shamir, J. (2008) 'Surface enhanced Raman scattering (SERS) and FTIR characterization of the sepia melanin pigment used in works of art', *Journal of Molecular Structure*, vol. 873, pp. 149-159.

Huang, Z., Lui, H., Chen, X.K., Alajlan, A., McLean, D.I. and Zeng, H. (2004) 'Raman spectroscopy of in vivo cutaneous melanin', *Journal of Biomedical Optics*, vol. 9(6), p. 1198–1205.

Kim, D.J., Ju, K.-Y. and Lee, J.-K. (2012) 'The synthetic melanin nanoparticles having an excellent binding capacity', *Bull. Korean Chem. Soc*, vol. 33(11), pp. 3788-3792.

Kortright, J.B. and Thompson, A.C. (2001) 'X-ray emission energies', in Thompson, A.C. and Vaughan, D. (ed.) *X-ray data booklet*, 2nd edition, Berkeley, California: Center for X-ray Optics and Advanced Light Source.

Magarelli, M. (2011) *Purification, Characterization and Photodegradation studies of modified sepia melanin (Sepia officinalis).Determination of Eumelanin content in fibers fromAlpaca (Vicugna pacos).Doctoral thesis*, University of Camerino, Departement of Chemical Sciences.

Magarelli, M., Passamonti, P. and Renieri, C. (2010) 'Purification, characterization and analysis of sepia melanin from commercial Sepia ink (Sepia officinalis)', *Rev CES Med Vet Zootec*, vol. 5(2), pp. 18-28.

Moses, D.N., Mattoni, M.A., Slack, N.L., Waite, J.H. and Zok, F.W. (2006) 'Role of melanin in mechanical properties of Glycera jaws', *Acta Biomaterialia*, vol. 2, p. 521–530.

Natalio, F., Andre, R., Pihan, S.A., Humanes, M., Weverd, R. and Treme, W. (2011) 'V2O5 nanowires with an intrinsic iodination activity leading to the formation of self-assembled melanin-like biopolymers', *Journal of Materials Chemistry*, vol. 21, p. 11923–11929.

Nighswander-Rempel, S., Riesz, J., Gilmore, J., Bothma, J. and Meredith, P. (2005) 'Quantitative fluorescence excitation spectra of synthetic eumelanin', *The journal of Physical Chemistry* , vol. 109 (43), p. 20629–20635.

Perna, G., Lasalvia, M., Gallo, C., Quartucci, G. and Capozzi, V. (2013) 'Vibrational characterization of synthetic eumelanin by means of Ramanand Surface Enhanced Raman Scattering', *The Open Surface Science Journal*, vol. 5, pp. 1-8.

Riesz, J. (2007) *The spectroscopic properties of melanin, Doctoral thesis*, The University of Queensland.

Sajjan, S.S., Anjaneya, O., Kulkarni, G.B., Nayak, A.S., Mashetty, K.B. and B., T. (2013) 'Properties and functions of melanin pigment from Klebsiella sp. GSK', *Korean Journal of Microbiology and Biotechnology*, vol. 41(1), p. 60–69.

Sokolsky, M. and Cirak, J. (2010) 'Dye-sensitized solar cells : Materials and processes', *Acta Electrotechnica et Informatica*, vol. 10(3), p. 78–81.

Subianto, S. (2006) *Electrochemical Synthesis of –Like Polyindolequinone, PhD. thesis,* Inorganic material research Program, the Queensland University of Technology.

Tarangini, K. and Mishra, S. (2013) 'Production, Characterization and Analysis of Melanin from Isolated Marine Pseudomonas sp. using Vegetable waste.', *Research Journal of Engineering Sciences*, vol. 2(5), pp. 40-46.

Watt, A.A.R., Bothma, J.P. and Meredith, P. (2009) 'The supramolecular structure of melanin', *Soft Matter*, vol. 5, p. 3754–3760.

# CHAPTER SIX: CONCLUSIONS AND FUTURE WORK

## 6.1. Conclusion

The main aim of this master dissertation has been to make comprehensive literature survey on Grätzel solar cell, its operating principle, as well as its sensitization by natural dyes focusing on sepia melanin. The objective was to investigate the morphology, chemical composition, crystalline structure as well as optical properties of sepia melanin for DSSC application.

A literature survey was successful achieved where a brief introduction and the literature review on DSSC have been provided. Different DSSC components have been discussed and DSSC operating principle. The sensitization of DSSC was also discussed and the different types of DSSC dye sensitizers. Sepia melanin as a natural dye of choice for this project was discussed further. The definition of sepia melanin; applications, general characteristics, biological functions, properties, and structure have been provided. The attractive features for sepia melanin to be attractive DSSC sensitizer compared to the use of synthetic dyes, which are not environment friendly, very expensive and their preparation requires sophisticated technique have been provided.

Sepia melanin was successful characterized by SEM and TEM in order to investigate its morphology. It was found that the purified sepia melanin powder consists of spherical nano-scaled particles with nearly double size distributions with diameter size varying 100 - 200 nm.

The discussed EDS, FTIR and Raman investigations reveal that the used sepia melanin powder samples are of a significant chemical purity. Sepia melanin has the strong interaction with the $TiO_2$ surface and photosensitization because of the hydroxyl and carboxylic functional groups. The crystalline structure characterization of sepia melanin by XRD found it to be amorphous, and this contributes to its high capacity of absorbing light in a wide range. The UV-Vis measurement proved high absorbance of sepia melanin.

The obtained results represent an important step forward in defining the structure of melanin and may prove of great interest in the production of semiconductor materials and in potential uses of melanin as photovoltaic cells especially DSSC. These results clearly show that sepia melanin can be applied as natural dye to DSSC Sepia. It is promising for

the realization of high cell performance, low-cost production, and non-toxicity. It should be emphasized here that natural dyes from food are better for human health than synthetic dyes.

## 6.2. Future work

The focus of this master's dissertation was about literature survey on DSSC and sepia melanin dye characterization for Grätzel solar cell application. To prove the obtained finding during this project, the solar cell must be fabricated to see whether the dye has higher efficiency than the other current natural dyes in the market.

The future work is to prepare a DSSC from this sepia melanin, investigate its efficiency and stability. The used sepia melanin was commercial. The synthesis of sepia melanin will be done, and then compare the finding with the commercial one.